Needle Deployment and Retraction Mechanism for Drug Injecting Swallowable Capsules

Nina Rebecca Omerovic Beccalli
Department of Mechanical Engineering
McGill University, Montreal

August 2017

A thesis submitted to McGill University in partial fulfillment of the requirements of the degree of Master of Engineering

Abstract

The gastrointestinal tract imposes a chemical and physical barrier to the oral delivery of bio-therapeutics such as insulin. As a consequence, bio-therapeutics need to be injected subcutaneously. Swallowable capsules, capable of injecting a drug directly into the intestine wall, would enable painless and convenient oral delivery of these drugs.

This thesis focuses on the development of needle deployment and retraction mechanisms to be implemented into Drug Injecting Swallowable Capsules (DISCs). The design space for the mechanisms is defined, and eleven novel designs, inspired by biological systems and macro-scale mechanisms, are proposed. One particular design, inspired by the defense mechanism of the Spanish newt, is further developed, prototyped, and tested.

The Spanish newt design consists of two concentric cylinders with needles attached to the inner cylinder. The motion of the inner cylinder, the core, is powered by two preloaded springs. This motion causes the needles to rotate with respect to their hinge point on the core, thus enabling needle deployment and retraction. The force required to achieve deployment and injection is characterized via mechanical tests, and the test results are used to select the springs from commercially-available off-the-shelf models. The final prototype is tested *in vitro* using a capsule measuring 15.9 mm in diameter and 31.5 mm in length, with a deployed needle length of 1.9 ± 0.5 mm. The mechanism successfully performs needle deployment, drug injection in 1.3 s, and needle retraction.

Résumé

Le système digestif représente une barrière chimique et physique à l'administration orale de bio-thérapeutiques tels que l'insuline. Par conséquent, ces médicaments doivent être injectés par voie sous-cutanée et non orale. Une capsule administrée oralement, capable d'injecter un médicament à travers la paroi intestinale, permettrait une administration commode et indolore de bio-thérapeutiques.

Le présent mémoire traite de la conception de mécanismes de déploiement et de rétractation d'aiguilles pour les DISCs (*Drug Injecting Swallowable Capsules*), i.e. les capsules administrées oralement, capables d'injecter un médicament à travers la paroi intestinale. L'espace de conception de ces mécanismes est établi, et douze concepts sont proposés, inspirés par des êtres vivants ou des mécanismes communs existants. Un de ces concepts, inspiré par le mécanisme de défense du triton espagnol, donne lieu au développement, à la fabrication et à l'essai d'un prototype.

Le concept du triton espagnol est composé de deux cylindres concentriques, le cylindre interne comprenant quatre courtes aiguilles. Le déplacement du cylindre interne par rapport au cylindre externe est effectué par deux ressorts précontraints. Ce mouvement provoque le basculement des aiguilles, et permet ainsi le déploiement et la rétractation de celles-ci. La force nécessaire pour réaliser le déploiement et l'injection est caractérisée par un essai mécanique. Les résultats de cet essai sont exploités afin de choisir des ressorts disponibles sur étagère. Le prototype final, mesurant 15.9 mm de diamètre et 31.5 mm de long, avec une longueur d'aiguilles déployée de 1.9 ± 0.5 mm, est testé *in vitro*. Le prototype de capsule remplit le cahier des charges, et permet de réaliser le déploiement des aiguilles, l'injection du médicament en 1.3 s, et la rétraction des aiguilles.

Acknowledgements

I am very much pleased to express my gratefulness to Dr Srikar Vengallatore, Associate Professor, Department of Mechanical Engineering, McGill University, for giving me the opportunity to work under his supervision. His insightful guidance and benevolence were essential for the success of my thesis.

I am very grateful to Professor Larry Lessard for allowing to access his machining facilities and Professor Francois Barthelat for allowing me to use the machines required to perform force tests. I would like to acknowledge Zhen Yin, fellow researcher, for teaching me how to use the testing machines, and Mathieu Beauchesne, Shop Technician, for his precious help at the workshop.

I am thankful to my fellow researchers Nicolas Ohlmann, Julieta Barroeta, Adam Smith, Caroline Collins and Linus Lehnert for the fruitful discussions, handy manufacturing tips, and precious feedback. I am also thankful to all my fellow researchers that worked at MD53A throughout my journey at McGill University, for brightening my work days at the office, and most importantly, for sweetening my Fridays.

Finally, I would like to thank my family and friends for their unconditional love and support that give me the strength, energy, and motivation to accomplish my life goals. I would specially like to thank my mother, Camila Beccalli Valenzuela, without whom I would not be where I am today.

Preface

The contributions of the author are as follows:

Chapter 1: Performed a literature review on engineered medical capsules and identified the need to develop Drug Injecting Swallowable Capsules. Further reviewed drug delivery capsules, physiological working environment, medical need, and motivation behind developing such capsules.

Chapter 2: Defined the design space for the development of needle deployment and retraction mechanisms by considering the capsule objectives, physiological requirements, and constraints from previous engineered medical capsules. Designed eleven needle deployment and retraction mechanisms to be integrated inside a small capsule of swallowable size: the maximum dimensions are 35 mm in length by 20 mm in diameter. These mechanisms were designed by seeking inspiration from both living beings and larger engineered mechanisms, and by means of cross-component analysis.

Chapter 3: Developed in detail a design inspired by the defense mechanism of the Spanish newt. Capsule development consisted of an intertwined and integrated process of analysis and manufacturing in order to determine capsule dimensions, inner core displacement, needle attachment method and assembly, piston dimensions, and component clearances, among other capsule specifications. The capsule components were manufactured and assembled. Force tests were performed on the capsule prototype to characterize the force required by the piston to deploy the needles and inject the drug. The experimental results were used to select the deployment and retraction springs.

Chapter 4: Tested the final prototype capsule ability to deploy needles, inject drug, and retract needles. Compared the prototype performance with the design requirements. Proposed methods to improve the design and manufacture of the capsule.

Chapter 5: Summarized the contributions of the thesis, and proposed future work to further develop needle deployment and retraction mechanisms for drug injecting swallowable capsules.

Contents

Abstract **i**

Résumé **ii**

Acknowledgements **iii**

Preface **iv**

1 Introduction **1**

1.1 Working environment: the gastrointestinal tract 1

1.2 State-of-the-art of engineered medical capsules 3

1.2.1 Monitoring and sensing 4

1.2.2 Visualization: Capsule Endoscopes (CEs) 5

1.2.3 Sample collection and biopsy 6

1.2.4 Active Locomotion 7

1.2.5 Drug delivery 9

Direct drug release 10

Controlled/Extended drug release 12

Drug injection 12

1.3 Drug Injecting Swallowable Capsules (DISCs) 13

1.4 Thesis objectives 15

1.5 Organization of the thesis 15

2 Needle deployment and retraction mechanisms **16**

2.1 Chapter overview 16

2.2 Design space 16

2.3 Proposed mechanism designs 19

2.3.1 Designs inspired from existing mechanisms 20
Spiked capsule 20
Portable hair brush 21
Multineedle syringe capsule 22
Diamond-column-buckling capsule 23
2.3.2 Bio-inspired designs 24
Porcupine-fish inspired design 24
Spanish newt with longitudinal actuation 26
Spanish newt with rotational actuation 27
Flower inspired design 27
2.3.3 Designs generated via cross-component analysis 28
Spiked-porcupine-fish hybrid 29
Porcupine-fish-multineedle hybrid 29
Spanish-newt-flower hybrid 30
2.4 Selected Design 31

3 Design Development: the Spanish newt with longitudinal actuation 33
3.1 Chapter overview 33
3.2 Mechanism and Components 34
3.2.1 Mechanism 34
3.2.2 Components 36
3.3 System analysis 38
3.3.1 Manufacturing considerations 38
3.3.2 Needle parameters: length, rotation angles, and displacement 40
3.3.3 Drug volume and core dimensions 41
3.3.4 Syringeability 42
3.4 Design embodiment 47
3.4.1 Core-needle interaction 47
3.4.2 Core-piston interaction 50
3.4.3 Core-case-needle interaction 52
3.4.4 Capsule manufacturing 53
3.5 Spring selection process 58

3.5.1 Force decomposition . . . 58
3.5.2 Piston force test . . . 60
Test apparatus . . . 61
Results . . . 64
Discussion . . . 66
3.5.3 Spring selection . . . 70
Deployment spring . . . 70
Retraction spring . . . 72

4 Prototype and design assessment **75**
4.1 Chapter overview . . . 75
4.2 Final prototype test . . . 75
4.2.1 Test set-up . . . 75
4.2.2 Results . . . 77
4.3 Prototype and design assessment . . . 79
4.4 Areas of improvement . . . 80
4.4.1 Manufacturing process . . . 80
4.4.2 Miniaturization opportunity . . . 81
4.4.3 Puncturing requirement and intestine wall engagement . . . 84

5 Conclusion and future work **85**

Appendix A Concept selection via quantitative analysis **90**

Appendix B Vertical piston force tests and results **93**
B.1 Testing machine specifications . . . 93
B.2 Experiments and results . . . 93

Bibliography **96**

List of Figures

1.1 Diagram of the gastrointestinal tract illustrating the location of its two extremities (mouth and the anus) and four sections (esophagus, stomach, small intestine, and large intestine). The path that the food takes along the GI tract after ingestion is highlighted by a black-dotted line [6]. 2
1.2 Pictures of commercially available capsule endoscopes. 6
1.3 Image of the biopsy capsule developed by Kong *et al.* [28]. 7
1.4 Images of the capsules with different active locomotion mechanisms. 8
1.5 Images of capsules with different drug delivery mechanisms to achieve direct-drug release. 11
1.6 Image of the extended drug delivery star-shaped capsule developed by Bellinger *et al.* [62]. 12
1.7 Images of the drug injecting capsules. 13

2.1 Images of the existing mechanisms that served as inspiration for the needle mechanism designs. 20
2.2 Diagrams of the spiked capsule design in isometric view at different stages. . 21
2.3 Diagrams of the cross-section isometric view of the portable brush inspired design at different states. 22
2.4 Sketches of the multineedle syringe capsule design at different states. 23
2.5 Sketches of the diamond-column-buckling capsule design at different states. . 24
2.6 Images of biological systems that served as inspiration for needle deployment and retraction mechanism designs. 25
2.7 Sketches of the porcupine fish capsule design at different states. 26
2.8 Sketches of the Spanish newt inspired capsule design at different states. . . . 27
2.9 Sketches of the flower inspired design at different states. 28

2.10 Sketches of the spiked-porcupine-fish hybrid design at different states. Note that at its undeployed state the metal sheet is unrolled and an enteric coating (in red) covers the needles that protrude the case. 29
2.11 Sketches of the porcupine-fish-multineedle hybrid design at different states. The piston plates (in green) have the same curvature as the needle plates. The compression washer (in blue) is used to retract the needles. 30
2.12 Sketches of the spanish-newt-flower hybrid design at different states. Note the increased length of the case compared to the Spanish newt design. This increased length allows the over-displacement of the core inside the case, which induces the retraction of the needles. 31

3.1 Schematic of the Spanish newt mechanism at its deployed state (before injection) in isometric view. The case is shown transparent to illustrate the interior of the capsule. The needles are hinged to the core and pass through holes in the case. When deployed, the core is in the up position, and the needles are normal to the wall of the capsule. 35
3.2 Schematics of the kinematics of the Spanish newt mechanism. The cross-section views shows the capsule at four different stages: undeployed, deployed before injection, deployed after injection, and retracted. Notice the displacement of the core, piston, and needles during deployment (from (A) to (B)), injection (from (B) to (C)), and retraction (from (C) to (D)). 35
3.3 Exploded view diagram of the mechanism in real scale. The capsule has ten parts, each of which is labeled: (a) deployment cap, (b) deployment spring, (c) piston, (d) core, (e) needles, (f) case, (g) retraction pusher, (h) retraction spring, and (i) retraction cap. Note that the two retention pins and the sleeve are not shown here. 36

3.4 Schematic of the cross-section view of the capsule at the needle attachment point, simultaneously showing the undeployed and deployed core-case hole alignment (illustrated independently by the inset). The holes of the core are filled with a flexible material (silicone rubber seal) that acts as a hinge for the needle (shown in yellow). The needles rotate by the hinge point H, located at the outer diameter of the core, and they are pushed by the case's outer diameter. The core needs to travel a distance d to rotate the needles by α, and deploy the needles by L_{dep} out of the case. 41
3.5 Schematic of the core with the needles and the piston assembled. The core's inner diameter D_{in} and the volume of drug inside the core V_{req} determine core length L_{req}. The total length of the core L_{core} considers L_{req}, the piston head height h_p, and the needle clearance L_c. 42
3.6 Schematic of the cross-section view of the capsule showing the core, piston, and needles with the relevant parameters to determine syringeability force. The numerical values of these parameters are given in Table 3.1. 43
3.7 Image of the $\sim$ 6 mm needles with different blobs. Blobs are made from instant adhesive or cold-weld-two-part epoxy, and are placed at the end or offset from the end of the needle. From left to right the blobs material-location are: no-blob (standard needle), adhesive-offset, epoxy-offset, adhesive-offset, epoxy-end, and adhesive-end. 48
3.8 Image of the three combinations of core-material and needle attachment, which achieved watertightness and allowed needle rotation between 0° and 60°. From left to right: silicone rubber tube with tight-fit needles, flexible photopolymer with glued needles, and polycarbonate tubing with needles on silicone rubber hinges. 49
3.9 (A) Diagram of the core-case-needle assembly illustrating the location and function of the sleeve in the mechanism. The holes of the sleeve are not covered with the silicone rubber sealant (yellow). The holes provide a clearance for the needles to connect with the inside of the core and not to interfere with the displacement of the piston. (B) Image of the sleeve installed inside the core and cut to the final dimension. Notice the tight fit of the sleeve in the core. . 50

3.10 Schematic of the piston head (on the left) and O-ring (on the right) with the relevant design parameters to calculate the squeeze ratio W/F and the stretch $S = d_p/d_{or}$. 51
3.11 Images of a successful core-piston watertightness tests at (A) $t = 0$ s and (B) $t > 0$ s. Water jets come out of the needles in (B) and no water leaks were observed behind the head of the piston. 52
3.12 Image of the capsule components. From left to right: piston, deployment cap, retraction pusher, retraction cap, core (with sleeve), and case. These components were assembled to build the complete capsule. 54
3.13 Image of the finished capsule assembly. The capsule is filled with water, used for the prototype test, and tinted blue, to facilitate its visualization. 54
3.14 Images of the three sub-assemblies that compose the capsule. The parts that compose each sub-assembly are described in each image. 55
3.15 Images of the final assembly process of the capsule. Each image describes a particular action taken during the assembly process. 56
3.16 Images illustrating manufacturing challenges faced when prototyping the capsule. The images illustrate (A) the need of a widget to hold the cylinders when drilling, (B) the dimension variability of the needles, and (C) the amplification of small machining inaccuracies of components when assembled. 57
3.17 Images illustrating the core-case-needle assembly challenges. The images show two steps performed during needle installation. 57
3.18 (A) Diagram of a cross-section view of the capsule showing the four phenomena inducing piston force: core-case friction and hinge force during deployment (left), and piston-core friction and syringeability during injection (right). (B) Diagram of a cross-section view of the capsule showing the reference frame for the piston displacement x with respect to the case, where x_0 is the initial position, x_1 corresponds to the end of deployment and the beginning of injection, and x_2 corresponds to the end of injection. 59

3.19 Diagram of the expected measured piston force profile. Piston force is plotted in the vertical axis, and displacement of the piston in the horizontal axis. During needle deployment (from x_0 to x_1), piston force is composed of core-case friction (constant), and hinge force. Hinge force is expected to be linear, zero at the end of deployment, and opposed to core-case friction during deployment. During injection (between x_1 and x_2), piston force corresponds to piston-core friction (constant and greater than core-case friction). Note that syringeability is not measured in this test. 60
3.20 Images of the horizontal force measuring equipment. The top image highlights the apparatus components. The middle image shows a closer view of the testing bed of the machine. It shows the capsule prototype, installed with the testing widget, onto the moving and static base platforms of the machine. The bottom image shows a closer view of the capsule prototype. The testing widget, composed of the piston holder and the capsule holder, is glued to the platform of the testing machine. The capsule prototype is directly mounted onto the testing widget. The alignment of the capsule with the piston is calibrated before the test. 62
3.21 Image of the capsule prototype mounted on the testing widget. On the left, the piston is installed in the piston holder. On the right, the core-case-needle assembly (upside-down) is installed in the capsule holder. 63
3.22 Graph of force versus displacement showing piston force curves (in grey), and the minimum and maximum piston force curves (in black). These extremes curves form an envelope in which all piston force curves are contained. The relevant observed values of the piston force curve are annotated: maximum peak force (in red), injection force range (in blue), and maximum deployment force (in magenta). 65
3.23 Plot of experimental piston force versus displacement from tests listed in Table 3.4, colored by setup number. 67
3.24 Plot of experimental piston force versus displacement from tests listed in Table 3.4, colored by testing speed. Additionally, measurements obtained using the vertical testing machine at 0.2 mm/s and 2 mm/s are also shown. 68

3.25 Plot of force versus piston displacement showing the theoretical force profiles of deployment springs from Table 3.7 (in blue), and the experimental piston force envelope (in black). The chosen spring (in red) is selected because it provides the highest force at the end of injection. 72
3.26 Plot of force versus piston displacement showing the theoretical force profiles of retraction springs from Table 3.8 (in green), and the minimum retraction spring force boundary (in blue). The minimum retraction spring force boundary is composed of the core-case friction force, the hinge force, and the resistance imposed by the deployment spring. Spring 2 (in red) is selected because it provides the smallest sufficient force at the end of retraction. . . . 74

4.1 Image of the final prototype test set-up. The capsule is held by a clamping vice at its two extremes, the deployment and the retraction caps. The two pins, holding the deployment and retraction springs in place, are shown in light-blue. (Note that the prototype shown here is the older prototyped version with six needles). 76
4.2 Images of the relevant frames extracted from the final prototype test recording. The images are labeled with their respective frame number and show the prototype at different stages. Note that the core, piston, and needles, are traced in black, red, and burgundy dashed-lines, respectively, to better visualize their position at every stage. 77
4.3 Image of the final prototype test at frame #4, fully deployed and injecting. The image shows the deployed needle length and angle. The blue arrow indicates the location of the observed leak. 79
4.4 Diagram of the cross-section view of the capsule design. The volume contribution of each component is sectioned, labeled, and shown in a distinct color. The total volume of the capsule is 6.3 mL. Individual volume contributions of components are listed in Table 4.3. 82

5.1 Schematic of the kinematics of the modified Spanish newt design with a single-actuation mechanism. The cross-section views show the capsule at four different stages. This design consists of having a two-step inner diameter core, and a back spring. When the piston is pushed by the deployment spring, it travels with the core in the case ((A) to (B)). When the core reaches the end of its displacement, the needles are deployed (B). The piston then continues traveling inside the core. When the piston reaches the wider diameter of the core (end of injection), it disengages from the core (C). The force of the back spring is then capable of pushing the core back to its initial position (D). . . 88

B.1 Image of the vertical force measuring equipment. The image highlights the apparatus components (left), and zooms into the testing bed of the machine (right) to show the prototyped capsule body installed, with the testing widget, onto the moving and static base platforms of the machine. The testing widget, composed of the piston holder and the capsule holder, is tightened to the clamps of the testing machine. The capsule prototype is directly mounted onto the testing widget. The alignment of the capsule with the piston is calibrated before the test. 94

B.2 Plot of experimental piston force versus displacement from tests listed in Table B.1 (speeds of 0.2 and 2 mm/s), colored by testing speed. Moreover, two sample force curves, from experiments performed in the horizontal testing machine at 0.05 mm/s and 0.1 mm/s, are also shown for reference. 95

List of Tables

1.1 Gastrointestinal tract characteristics [4]. 3
1.2 Physiological properties of the small intestine. 4

3.1 Numerical values used for syringeability calculations. 46
3.2 Values of Reynolds number Re and syringeability force F_{syr} obtained for various values of injection time t_{inj}. The injection times considered range between the maximum allowed injection time (5 s), and a tenth of this time. Note that the Reynolds number is smaller than the critical value (2.1e3) for all injection times considered here, meaning that the flow is laminar inside the needles, and that Eq. 3.6 is valid. 46
3.3 Morphological chart for the design of the needle-core interaction. Any combination (with one design option per parameter) is *a priori* possible. 47
3.4 Piston force test matrix. In order to assess the repeatability of the measurements, the prototype and the test apparatus are disassembled and reassembled three times during the testing process. This defines the three different setups. 64
3.5 Summary of relevant values gathered from the piston force tests. 66
3.6 Injection force range for all curves, setup 1, setup 2, and setup 3. 67
3.7 Springs from D.R. Templeman Co.® that meet the geometrical requirements for the deployment spring. The selected deployment spring is in bold font. . 71
3.8 Springs from D.R. Templeman Co.® that meet the geometrical requirements for the retraction spring. The selected retraction spring is in bold font. . . . 73

4.1 Time characterization of the final prototype. 77
4.2 Final prototype performance overview with respect to the mechanism requirements from Section 2.2. 80
4.3 Absolute and relative volume contributions of the capsule components. . . . 81

4.4 Volume contribution of capsule prototype and ideal minimum volume contribution of the design. 83

A.1 Evaluation criteria 91
A.2 Concept evaluation 92

B.1 Piston force test matrix of the vertical tests. 94

Chapter 1

Introduction

Engineered medical swallowable capsules were introduced in the 1950s with the development of a capsule capable of measuring the internal body temperature [1]. Since then, and thanks to technological advancements, the functional landscape of these capsules has expanded [2]. Today, engineered medical capsules can achieve multiple and more complex functions such as monitoring, visualizing, sampling, and delivering drugs inside the gastrointestinal tract. The need to develop a Drug Injecting Swallowable Capsule (DISC) was recognized from performing a thorough literature review of the state-of-the-art of medical capsules. The field of drug injecting capsules is underdeveloped compared to other functional capabilities of capsules. In this context, developing a capsule capable of injecting a drug directly into the intestine wall would enable the oral delivery of drugs that are currently subcutaneously injected [3]. In the following section, Section 1.1, the gastrointestinal tract is reviewed in order to better understand the working environment of medical swallowable capsules. Section 1.2 describes the state-of-the-art of these capsules, and Section 1.3 expands on drug delivery capsules and explains the need for developing a capsule capable of injecting a drug directly into the intestine wall.

1.1 Working environment: the gastrointestinal tract

The gastrointestinal (GI) tract is the working environment of medical capsules. It is 8 m to 9 m long from the mouth to the anus. Between these two extremities, the tract is segmented into four sections: (1) esophagus, (2) stomach, (3) small intestine, and (4) large

intestine. Figure 1.1 illustrates the anatomy of the gastrointestinal tract. The small intestine is the longest segment of the GI tract measuring between 6.7 m and 7.6 m, and it is further segmented into 3 sections: (1) duodenum, (2) jejunum, and (3) ileum. The narrowest passage along the GI tract is at the pylorus [4]. This sphincter measures 2 cm in diameter, which sets the maximum allowable diameter for swallowable capsules. The pylorus controls the passage of the chyme (partially digested food) from the stomach to the intestine [5].

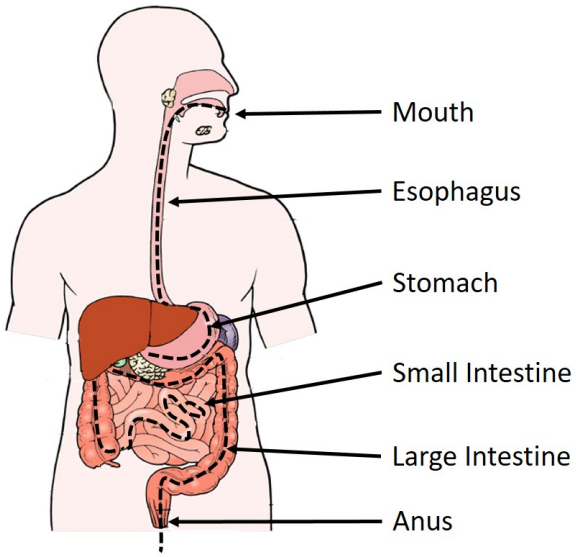

FIGURE 1.1: Diagram of the gastrointestinal tract illustrating the location of its two extremities (mouth and the anus) and four sections (esophagus, stomach, small intestine, and large intestine). The path that the food takes along the GI tract after ingestion is highlighted by a black-dotted line [6].

The pH along the GI tract greatly varies depending on the section. At the level of the esophagus, the pH is between 6.5 and 7.5, at the stomach the pH lowers to an acidic range of 1.5 to 4, which helps with the decomposition of proteins in the presence of proteases. The pH ranges between 8.5 and 4 at the intestines: between 7 and 8.5 at the duodenum, and between 4 and 7 along the rest (including the large intestine). The temperature also varies along the GI tract depending on the section. Table 1.1, extracted from [4], provides a brief definition of the organs, their dimensions, pH, and chyme transit times.

The small intestine has a surface area of 200 m^2, which is about a hundred times the surface of the skin [5]. This large surface area is created by the villi and micro-villi, hair like

TABLE 1.1: Gastrointestinal tract characteristics [4].

Organ	Description	Dimension (cm)	pH	Transit time
Esophagus	Hollow and muscular tube	Diameter: 2, length: ∼25	6.5-7.5 (Saliva)	∼10 s
Stomach	Large and elastic sac, lined with mucous membrane	Diameter: 2 (at the pylorus)	1.5-6.5	∼1 hr
Small intestine	Long and elastic lumen with many curves. Internal surface coated with villi	Diameter: 2.5-4, length: 670-760	4-8.5	∼4 hrs
Large intestine	Elastic lumen with two main flexures	Diameter: 3-6, length: ∼150	4-7	∼5 hrs

structures, in the internal wall of the small intestine. Circular folds in the lumen of the small intestine help slow down the chyme by making it travel spirally rather than in a straight line. Absorption of nutrients occurs primarily in the small intestine.

The small intestine features two modes of motility: segmentation and peristalsis. Segmentation helps with the mixing and digestion of chyme, and occurs 8 to 12 times per minute, until most nutrients are fully absorbed. Peristalsis helps the chyme advance along the intestine. After 90 to 120 minutes, all the chyme has exited the duodenum, and in 3 to 5 hours, the small intestine [5].

Table 1.2 summarizes some of the physiological properties of the small intestine that are relevant for the development of medical capsules.

1.2 State-of-the-art of engineered medical capsules

The concept of engineered medical swallowable capsules was introduced in the 1950s thanks to the invention of the transistor that allowed the integration of temperature, pressure, and

TABLE 1.2: Physiological properties of the small intestine.

Physiological Property	Value(s)	Unit	Ref.
Duodenum length	25.4	cm	[5]
Duodenum pH	$7 - 8.5$	pH	[4]
Chyme transit time at duodenum	$90 - 120$	min	[5]
Segmentation frequency	$8 - 12$	min^{-1}	[5]
Intestine wall thickness	1.6 ± 0.3	mm	[5]
Peristaltic wave propagation speed	$0.08 - 2$	cm/s	[7]
Intestine needle puncturing force	2.30 ± 0.83	N	[8]
Circumferential peristaltic force	720.8	mN	[9]
Interstitial hydrostatic pressure	(-8) - 6	mmHg	[10]
Maximum safe voltage level	3	V	[11]
Maximum safe current intensity	2	mA	[11]

pH sensory capabilities inside small capsules. Later, in the 2000s, the development of complementary metal-oxide silicon (CMOS) image sensors, application-specific integrated circuit (ASIC) devices, and white-light emitting diode (LED) illumination opened the doors for the development of wireless capsule endoscopes [2]. Following the success of these capsules, research has focused on further developing these and other functional domains for medical capsules, such as sample and biopsy collection, locomotion, and drug delivery [2]. The following subsections provide a review of capsules that have been developed for monitoring and sensing (Section 1.2.1), visualization (Section 1.2.2), sample collection and biopsy (Section 1.2.3), active locomotion (Section 1.2.4), and drug delivery (Section 1.2.5).

1.2.1 Monitoring and sensing

In 1957, Mackay and Jacobson [1] developed a medical capsule capable of transmitting pH information using a radio-transmitter and pH sensitive materials.

In the 1980s at the John Hopkins University, the Thermometer Pill was developed and commercialized [12]. This capsule was designed to monitor the internal temperature of astronauts when working in high temperature environments and hostile conditions. The Thermometer Pill used a single cell nickel-cadmium battery and transmitted information through radio-frequencies [13]. Other commercial capsules, such as CorTemp® by NASA

[14] and VitalSense® by Philips® [15], were developed shortly after the Thermometer Pill to monitor the temperature of football players, soldiers, and medical patients.

1.2.2 Visualization: Capsule Endoscopes (CEs)

Capsule endoscopes (CEs) allow visualization and imaging of the gastrointestinal tract [2]. They were developed in order to replace standard endoscopy (or colonoscopy) procedures, and today they are considered the gold standard procedure for small bowel evaluation in patients with inflammatory bowel disease, suspected small bowel neoplastic lesions, and obscure GI bleeding. Traditional endoscopic procedures explore the GI tract with a long wire that holds a camera at its end, inserted through the mouth (or anus) of patients, and moved into and along the GI tract to visualize the site of interest. With these endoscopic procedures, patients need to undergo air insufflation and sedation, suffering from risks of infection and perforation of the GI tract. CEs, on the other hand, integrate a camera, a light source, a transmitter, and batteries [2], and allow the visualization and examination of the GI tract wirelessly, granting access to the previously-inaccessible small-bowel, and reducing the risks of sedation, perforation, and infection [12], [16].

In the year 2000, Given Imaging® commercialized one of the first capsule endoscopes. Clinical trials were presented in 2001 and the company's capsule, M2A (Mouth to Anus), was awarded FDA approval the same year [17]. The M2A measured 11 mm in diameter and 25 mm in length, and it was passively propelled by peristalsis along the GI tract. The M2A was further improved, and its name was changed to PillCam®. Given Imaging® then created the PillCam® series, targeting specific exploration sites: the PillCam® ESO (Figure 1.2a) for the esophagus, PillCam® SB for the small intestine, and PillCam® COLON for the large intestine [18]. The PillCam® series encompasses 95% of the CE market, and it has been used in over 1.7 million procedures worldwide and in more than 1900 clinical studies [17].

Other CEs such as OMOM® by Jinshan Science & Technology® [19], EC-10® by Olympus® [20] (Figure 1.2b), MiroCam® by IntroMedic® [21], and CapsoCam® by CapsoVision® [22] are also available in the market [17], [23].

(A) PillCam® by Given Imaging® [18].

(B) EC-10® by Olympus® [20].

FIGURE 1.2: Pictures of commercially available capsule endoscopes.

1.2.3 Sample collection and biopsy

Sample collection capsules are those that collect free-flowing fluid and matter from the GI tract so it can be analyzed after capsule retrieval. In 1996, Gu and Gu [24] patented a suction collection method. The capsule has an inner space in vacuum and it suctions fluids when the enteric coating that blocks the opening dissolves in the intestine. In 2006, Meindert *et al.* [25] patented a capsule that uses capillarity forces to suction sample fluid in the gastrointestinal tract. In 2014, Amoako-Tuffour *et al.* [26] proposed a two-part-casing capsule that rotates to align holes and let fluid into the capsule, and rotates back to lock-in the sample, thereby avoiding contamination during body evacuation.

Biopsy capsules collect tissue extracted from a live organ so that it can be later examined. The first biopsy capsule was designed in the early stages of medical capsule development in the 1950s by Crosby and Krugler [27]. The capsule used suction and a knife to perform the biopsy. The capsule suctioned the inner wall of the intestine and cut the sucked-in skin with a rotatory knife powered by a torsion spring. In 2005, Kong *et al.* [28] proposed a similar concept consisting of a rotational tissue-cutting razor powered by a torsion spring, and triggered by the melting of a paraffin block (Figure 1.3). In 2011, Shalabi [4] proposed a capsule equipped with tweezers that travel along a guided cam. The tweezers deploy and retract radially and the mechanism is actuated by a torsion spring. In 2010, Simi *et al.* [29] developed a biopsy mechanism based on a magneto-mechanical elastic torsion spring that

was driven by an external magnetic field. Stabilization, anchoring, and sufficient torque was achieved using an external handheld magnet to obtain a biopsy on porcine intestines.

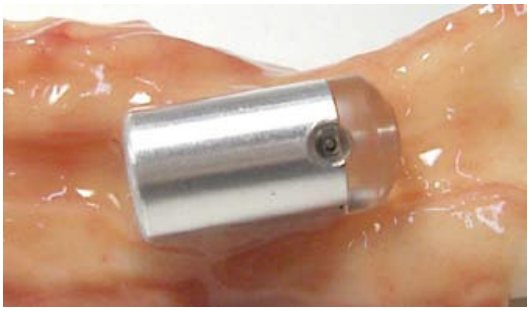

FIGURE 1.3: Image of the biopsy capsule developed by Kong *et al.* [28].

1.2.4 Active Locomotion

Active locomotion of medical capsules refers to their ability to resist peristalsis (to anchor themselves at a particular site), to reorient themselves, or to actively displace themselves inside the GI tract, as opposed to using peristalsis to passively move within the gastrointestinal tract. Peristalsis is a complex event of five contractile patterns that impacts the speed, positioning, and orientation of capsules with passive locomotion [30]. The need for active locomotion became clear after the commercialization of capsule endoscopes [31].

Mechanical structures such as hooks that grip onto the gut wall, propellers enabling a gliding motion through the gut, and inflatable balloons that imitate an inch-worm movement are some of the mechanisms that have been investigated to provide the control and steering capabilities for capsule endoscopes envisioned by doctors [32]. Figure 1.4 shows some of the capsules with active locomotion capabilities described below.

(A) Quirini *et al.*: 4-legged capsule [33].

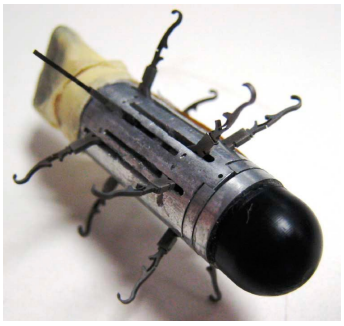

(B) Valdastri *et al.*: 12-legged capsule [34].

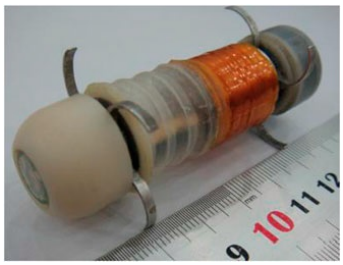

(C) Chen *et al.*: capsule with balloons and spiral legs [35].

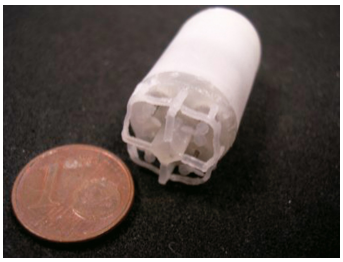

(D) Tortora *et al.*: Capsule with four propellers [36].

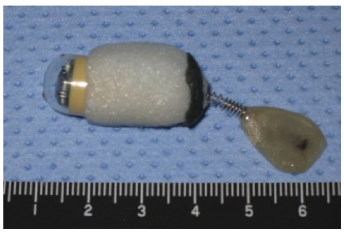

(E) Morita *et al.*: Tail-shaped propeller capsule [37].

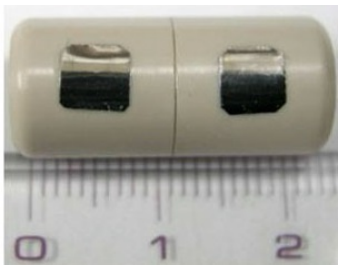

(F) Woo *et al.*: capsule with electric stimulation [38].

FIGURE 1.4: Images of the capsules with different active locomotion mechanisms.

Legged capsules with 4, 8, and 12 legs have been proposed by Menciassi *et al.* [39], Quirini *et al.* [33] (Figure 1.4a), and Valdastri *et al.* [34] (Figure 1.4b). The legs of the capsule move either simultaneously or alternately to advance along the GI tract [40].

Several variations of legged capsules have been proposed, such as micro-legs with and without high friction adhesive pads [41], [42], mucoadhesive patches [43], and tissue collapsing mechanisms [44]. Lin *et al.* [45] proposed an inch-worm-legged hybrid mechanism, where the capsule used 3 legs to anchor itself to the GI wall while moving through an inch-worm crawling motion. Chen *et al.* [35], [46] proposed a similar capsule that uses air-balloons and spiral legs, instead of regular legs, to increase safety from puncturing the GI tract (Figure 1.4c). Kim *et al.* [47], [48] developed micro-hooks biomimicking those of an insect made out of shape memory allow (SMA) and paddling members. Kósa *et al.* [49], [50], proposed a swimming capsule consisting of three tails powered by the electromagnetic field generated by

a magnetic resonance imaging (MRI) system. Capsules with propellers have been proposed by Tortora *et al.* [36], who integrated four propellers into a capsule that were controlled with a joystick (Figure 1.4d), and Morita *et al.* [37], who combined a tail-shaped propeller with magnetic resonance power source to control the capsule velocity and orientation (Figure 1.4e).

Electrical stimulus as a mean of locomotion was introduced by Woo *et al.* [38], [51] (Figure 1.4f). Electric pulses were sent out to momentarily contract the wall of the intestine and move the capsule along the GI tract [52]. Further studies showed that electric stimulation caused damage to electrically sensitive organs, such as the liver, and disturbed natural peristalsis [51].

None of the aforementioned mechanical locomotion systems started clinical trials because of the hazard associated with their external locomotive members. Conversely, magnetically actuated locomotion mechanisms have been furthered developed, introduced in capsule endoscopes and undergone human trials [40], [53].

1.2.5 Drug delivery

The delivery of some drugs using standard medical capsules features several drawbacks, including poor treatment adherence, gastrointestinal drug intolerance, drug denaturation due to stomach acidity, and poor drug absorbability in the intestine. Engineered medical capsules for drug delivery are designed to address the aforementioned problems. These capsules measure between 21 mm and 35 mm in length, and between 11 mm and 20 mm in diameter, and are capable of delivering between 60 µL and 1 mL of drug in the form of liquid, solid, gel, or powder. Drug delivery mechanisms, actuation, and triggers differ from capsule to capsule. Drug delivery capsules can be classified into three groups with respect to their functional capability: direct drug release, controlled/extended drug release, and drug injection.

Direct drug release

Direct drug release capsules are capable of releasing drug passively or actively without controlling the delivery rate or the amount of drug being released.

In 1991, Lambert *et al.* [54] developed a capsule capable of delivering 1 mL of drug in the GI tract. The mechanism consists of a flexible latex reservoir that is pressure-filled with drug. An opening of the reservoir is blocked by a piston. The piston is actuated by a compressed spring and when the piston moves, it opens the outlet, letting the drug out as the latex reservoir compresses to its original state. The capsule is activated using external magnets and a thermo-mechanical method (melting a nylon wire that retains a compressed spring). This capsule is also equipped with a cogwheel that acts as a mechanical location detector.

In 2005, Phaeton Research Limited® received FDA approval for the Enterion Capsule® (Figure 1.5a) [52]. This capsule actively delivers 1 mL of liquid, powder, or solid drug by pushing it out with a spring loaded piston. The drug is expelled the moment the pressure generated by the piston is large enough to open the cap of the capsule, and the spring is activated by the aforementioned thermo-mechanical method. Capsule motion through the GI tract is passive. The simplicity and effectiveness of this capsule has played in its favor; by 2009, over 3000 capsules had been dispensed, and the capsules were used in more than 100 clinical studies over a 5-year period [52].

Innovative Devices® developed two drug delivery capsules: the InteliSite® and the InteliSite Companion® that can deliver 0.8 mL and 1 mL of drug, respectively. InteliSite® consists of an inner and outer casing that rotate relative to each other to align two openings from where the drug can escape the capsule [55]. The InteliSite Companion® consists of an outer casing, and an inner cage that is released into the GI lumen upon activation (Figure 1.5b). The capsule is externally activated via radio-frequency, which induces the deformation of a shape-memory alloy (SMA) that keeps a compressed spring in place [56].

In 2015, Le *et al.* [57] used two ring-type soft magnets and a plastic hinge to build a drug delivery capsule that opens along its short axis when a magnetic field is applied (Figure 1.5c). The capsule is capable of delivering a volume of drug of up to 0.234 mL.

In the same year, Goffredo *et al.* [11], [58] developed an electrolysis based micro-pump that pushes drug through a nozzle when an elastic membrane between the drug and the electrolytic solution reservoirs gets pressurized (Figure 1.5d). The capsule is powered by an on-board battery and it is capable of delivering 60 µL of drug. The capsule is also capable of measuring tissue impedance; the pump is activated when it reads a preprogrammed impedance value.

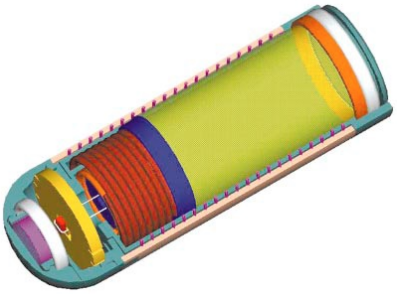

(A) Schematic of the Enterion Capsule® by Phaeton Research Limited® [52].

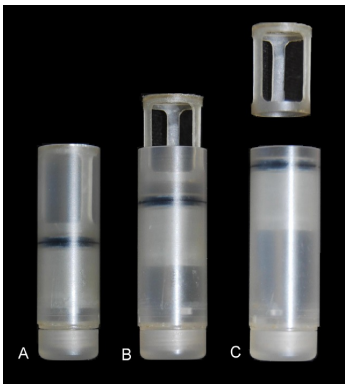

(B) Picture of the InteliSite Companion® by Innovative Devices®. From left to right, drug cage is undeployed, deploying, and deployed. [56].

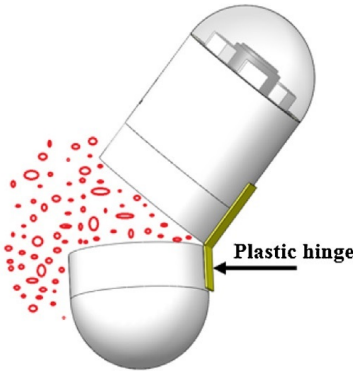

(C) Schematic of the capsule by Le *et al.* releasing drug. The two parts of the capsules are held together by a plastic hinge [57].

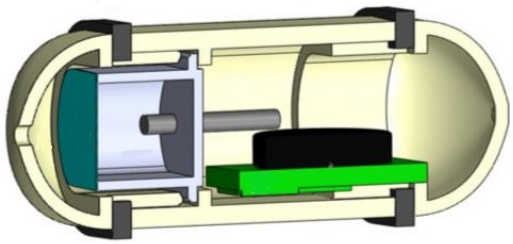

(D) Schematic of the capsule by Goffredo *et al.* equipped with an electrolysis based micro-pump [11].

FIGURE 1.5: Images of capsules with different drug delivery mechanisms to achieve direct-drug release.

Controlled/Extended drug release

Controlled or extended drug release capsules can control the amount or rate of drug delivery.

Medimetrics® developed the IntelliCap® drug delivery capsule that controls the drug delivery time profile and can achieve burst release, progressive release, or multilocation dosing using a micro-pump. The capsule is controlled via radio-frequencies, a temperature sensor, and a pH sensor [59], [60]. In 2016, Beccani *et al.* [61] developed a capsule based on a coil-magnetic-piston mechanism. The capsule is capable of delivering 0.2 mL of drug in controlled doses over time with a scheduler. In 2016, Bellinger *et al.* [62] proposed a star shaped capsule, initially compacted into an oval shape (Figure 1.6). The capsule is designed to stay in the stomach for 14 days to deliver drug through diffusion, and has the objective of increasing treatment adherence.

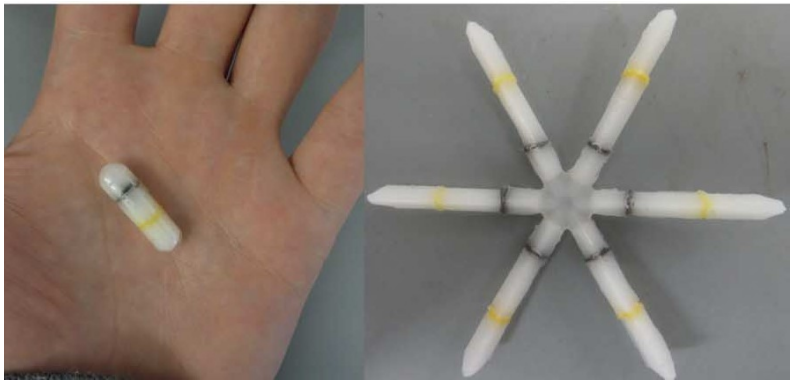

FIGURE 1.6: Image of the extended drug delivery star-shaped capsule developed by Bellinger *et al.* [62].

Drug injection

Drug injecting capsules can inject a drug through the intestine wall. Two swallowable capsules that inject drug in the intestine have been proposed by Woods and Constandinou [9], and Rani-Therapeutics® [63].

In 2013, Woods and Constandinou developed a capsule with localized drug delivery and anchoring capabilities (Figure 1.7a). This capsules can deliver 1 mL of drug through a needle that protrudes from the capsule by 1.5 mm and can be deployed in 1.8 s. The

needle deployment mechanism consists of a micro-motor, a spring, and a cam. The needle is equipped with a driving peg, and as the cam rotates, it pushes the needles out of the capsule. The drug is ejected using a piston and a compressed conical spring capable of delivering a maximum load of 0.59 N. The spring is released by the thermo-mechanical method, powered by a lithium coin battery [9], [10].

In late 2016, Imran was granted a patent for a drug injecting capsule: the Auto-Pill® (Figure 1.7b). This capsule consists of a balloon-like structure and dissolvable needles infused with solid drug. The drug is released after the needles are injected and dissolved inside the intestine wall. The balloon inflates due to a chemical reaction and provides enough force to inject the needles into the intestine wall. The balloon and the needles are assembled in an enteric coated (pH sensitive coating that dissolve in the small intestine) cellulose capsule [63].

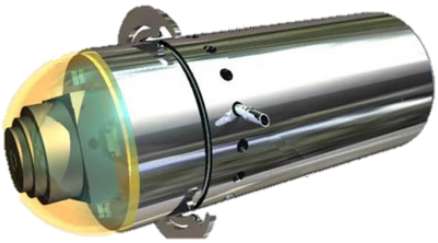

(A) Woods and Constandinou's capsule with the needles at the deployed state [9].

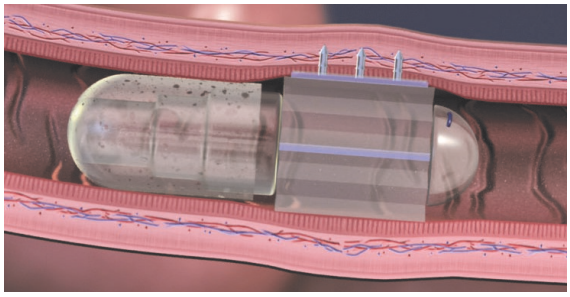

(B) Auto-Pill® by Rani-Therapeutics® with the needles deployed and engaging into the intestine wall [63].

FIGURE 1.7: Images of the drug injecting capsules.

1.3 Drug Injecting Swallowable Capsules (DISCs)

Drug injecting swallowable capsules (DISCs), like the ones developed by Woods and Constandinou, and Rani-Therapeutics®, are medical engineered capsules capable of injecting bio-therapeutics directly inside the small intestine wall. The development of these capsules has the objective of replacing the need for subcutaneous or intramuscular injections when delivering bio-therapeutics.

The development of bio-therapeutics is growing worldwide, and in 2016 in the US nearly 60 % of drugs in clinical trials were bio-therapeutics [64]. Bio-therapeutics (biologics, peptides, and antibodies) are medications that help control chronic diseases such as arthritis, diabetes, multiple sclerosis, plaque psoriasis, Crohn's disease, and ulcerative colitis among others [63]. Insulin is an example of a bio-therapeutic that helps control blood glucose level. People who suffer from diabetes, in particular those with type 1 diabetes, need to inject themselves with insulin two to four times a day. In the US alone, nearly 30 million people have been diagnosed with diabetes and 1.25 million of them are type 1 [65]. Worldwide, about 442 million adults are diabetic, which is equivalent to 1 in 11 adults in the world [66].

The delivery of bio-therapeutics into the systemic circulation of the body is only achievable through parental routes (non-oral means), typically through subcutaneous injections. If bio-therapeutics were orally swallowed, they would denature with the acidity of the stomach, and if passed safely to the intestine, they would not permeate the mucosa of the small intestine wall, where molecules are normally absorbed. Thus, even if oral administration is the preferred route to deliver medications, injections remain necessary when delivering bio-therapeutics [67].

In 2014, Traverso *et al.* [3] recognized the opportunity for the development of orally ingested devices that could inject drug from inside the intestine. Traverso *et al.* performed endoscopic and subcutaneous injections in swine, and proved that injecting drugs from inside the intestine provides a higher bioavailability, and faster absorption, compared to injections in the stomach, colon, and skin [3]. Traverso *et al.* also showed that it is safe to evacuate (in swines) a capsule with a series of needles of gauge G25 protruding by 5 mm from a capsule without causing any damage along its path in the GI tract.

The intestine is a highly vascularized and insensate organ. A direct injection in the intestine would be painless for patients, and the drug would be rapidly and directly absorbed into the systemic circulation, bypassing the pH and enzymatic effects of the stomach and physically overcoming the mucosa and epithelial wall barrier of the intestine [3].

Only two swallowable capsules that inject a drug from inside the intestine have been proposed (the capsule by Woods and Constandinou, and the Auto-Pill® by Rani-Therapeutics®, both described in Section 1.2.5) and only the capsule by Rani-Therapeutics® (backed up by

Google Ventures®) is in clinical trial stages. Nevertheless, the Auto-Pill® has the limitation of needing to modify the drug being injected to manufacture its drug-infused needles, has a maximum load of 3 mg to 5 mg of drug, and it is not yet available in the market. The need for a universal capsule that is capable of injecting any drug, without chemical modification, from inside the intestine has still not been met. To make progress towards this goal, it is necessary to design and develop miniaturized mechanisms for deploying and retracting needles that can be implemented inside drug injecting swallowable capsules.

1.4 Thesis objectives

The objective of this thesis is to contribute to the development of drug injecting swallowable capsules by (1) defining the design space for needle deployment and retraction mechanisms that can be implemented inside these capsules, (2) proposing novel designs for needle deployment and retraction mechanisms, and (3) developing, prototyping, and testing one of the proposed designs to assess its feasibility.

1.5 Organization of the thesis

This thesis is organized into five chapters. Chapter 2 develops the design space for needle deployment and retraction mechanisms and describes the eleven novel designs proposed. Chapter 3 describes in detail the development and prototyping of one of the suggested designs. Chapter 4 describes the experimental results and assesses the performance of the prototype. Chapter 5 summarizes the thesis and suggests future work for the development of drug injecting swallowable capsules.

Chapter 2

Needle deployment and retraction mechanisms

2.1 Chapter overview

The objective of this chapter is to define the design space for needle deployment and retraction mechanisms of drug injecting swallowable capsules (Section 2.2) and to propose eleven novel mechanism designs (Section 2.3). One design is selected (Section 2.4) and further developed in the following chapters. Note that the development of DISCs is divided into two main components: the needle deployment and retraction mechanism on the one hand, and the activation mechanism on the other hand. The development of the activation mechanisms is out of the scope of this project, therefore a manual trigger will be considered when designing the needle mechanism. The mechanism should achieve needle deployment, drug injection, and needle retraction.

2.2 Design space

The design space of the needle deployment and retraction mechanism is linked to the requirements of DISCs and the working environment of the capsule. The main objective of the capsule is to inject drug from inside the GI tract into the intestine wall. Keeping this in mind, the needle deployment and retraction mechanism should (1) fit inside the drug

injecting swallowable capsule, (2) deploy needles outside the capsule, (3) inject drug into the intestine wall, (4) fully retract the needles before passively evacuating the body, and (4) store the energy it needs to actuate deployment, injection, and retraction.

The narrowest path along the gastrointestinal tract is at the pyloric sphincter, which measures 20 mm in diameter. This sets the maximum diameter allowed for DISCs so they can pass through the gastrointestinal tract. The largest capsule developed in literature measures 35 mm in length. Therefore, a DISC prototype should measure maximum 35 mm in length and 20 mm in diameter.

The amount of drug the capsule should contain depends on the drug type, patient, and particular situation. Moreover, since intestinal injections increase the bioavailability of drugs, the required dose would be lower than the dose of subcutaneous injections. Nonetheless, and to be conservative, the drug volume was chosen by using standard insulin syringe sizes as proxies. Insulin is typically injected in volumes ranging from 0.3 mL to 1 mL, and injections over 0.5 mL need to be injected in two steps [68]. Additionally, most vaccine dosages consist of volumes of 0.5 mL. Therefore, 0.5 mL is chosen as the drug load requirement for a DISC.

The drug needs to be injected while the needles are inserted inside the wall of the intestine. Needle insertion into the intestine wall is assumed to occur during the segmentation motion of the intestine. During this motion, the intestine contracts 12 times per minute to mix the chyme, before initiating the peristalsis motion, which moves the chyme down the tract. Therefore, the intestine remains in a contracted state in blocks of 5 seconds, time within which the drug should be completely injected.

Needle deployment is required to take place at the duodenum, which is the first segment of the small intestine, and main site of absorption of nutrients and other molecules. The chyme takes 90 to 120 minutes to travel through the duodenum and the displacement motion only starts after nutrients have been absorbed. Therefore, needle deployment is required to take place within 90 minutes once the capsule has passed the pylorus (located at the start of the duodenum). From literature review, it was found that needles should protrude between 1 to 2 mm out of the capsule [9], and radially outwards, perpendicular to the capsule.

The capsule should be equipped with at least one needle, and needle distribution on the capsule should ensure needle engagement with the wall of the intestine. Given the oval and

elongated aspect ratio of capsules, and the already narrow intestinal tract (30 mm) at its relaxed state, the capsule can be assumed to travel along the intestinal tract with its axis parallel to that of the intestine. Thus, the needles should be positioned around the perimeter of the cylindrical portion of the capsule.

The needle size used in the prototype is of gauge 25. This needle size was proven safe to pass through the GI tract by Traverso *et al.* [3]. Smaller needles can be used in further design iterations of the capsule. The needles should be hinged to the capsule so they can deploy and retract in and out of the capsule. The needles must also be connected with the drug reservoir so the drug can evacuate the capsule through the needles.

After the injection is completed, the needles should fully retract back into the capsule, leaving no needle in the gastrointestinal tract, nor partially protruding outside of the capsule. The retraction of the needles can occur directly after injection or before evacuating the body (within ~ 9 hrs).

The energy needed to actuate the deployment, injection, and retraction needs to be contained on-board of the capsule, instead of having external magnetic-fields or radio-frequencies as energy sources. Literature review demonstrates that preloaded compression springs are an effective and simple means of storing energy mechanically inside a capsule. Thus, springs are used as actuators for the mechanism designs. The amount of energy stored in springs should be sufficiently high to achieve the desired capsule behaviour.

To the extent possible, the capsule should be simple in design and easy to manufacture. The mechanisms should not depend on batteries or motors to accomplish their task. According to the literature, capsules that received FDA approval and enjoyed commercial success (such as the Enterion Capsule®) are those based on the simplest designs. Moreover, if DISCs succeed in replacing injections of bio-therapeutics, they would be used by the millions every day [66], and the use of batteries and motors would be environmentally and economically unsustainable.

Overall, the functional and non-functional requirements of needle deployment and retraction mechanisms can be summarized in the following two lists:

Functional Requirements:

1. Deploy needles (at least one) by 1 to 2 mm perpendicular to the capsule.
2. Inject $V_{drug} = 0.5$ mL of drug in less than $t_{inj} = 5$ s.
3. Fully retract the needles after injection.

Non-functional requirements:

1. Needles must be distributed along the perimeter of the capsule.
2. Capsule must measure at most 35 mm in length and 20 mm in diameter.
3. Energy source should be sufficient, small, and originated from preloaded springs.
4. Drug reservoir must be watertight.
5. Needle mechanism should be as simple as possible.
6. Capsule should not use motors or batteries.
7. Capsule should be easy to manufacture.

Note that a manual trigger is considered as the activation method for needle mechanisms. Capsule activation is a separate development module of DISCs, and it is out of the scope of this project. Nonetheless, the manual activation method of the proposed designs could be adapted to include activation mechanisms.

2.3 Proposed mechanism designs

Eleven needle mechanisms are proposed and separated into three sections. Section 2.3.1 contains designs inspired by everyday macro-scale mechanisms that have been miniaturized and adapted to fit the capsule size and requirements. Section 2.3.2 contains novel mechanisms inspired by biological systems. Section 2.3.3 contains designs developed by cross-component analysis of designs proposed in Sections 2.3.1 and 2.3.2. Note that all eleven mechanisms are integrated inside an enteric coated capsule shell in order to protect the capsule and its components from the stomach acidity.

2.3.1 Designs inspired from existing mechanisms

Four needle mechanisms were inspired by large-scale existing mechanisms: a portable hair brush [69] and a needle threader [70]. Figure 2.1 shows images of the two sources of inspiration.

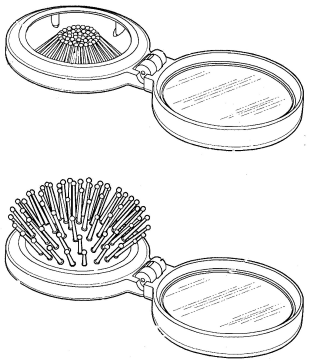

(A) Deployed (bottom) and retracted (top) portable hair brush image taken from a patent application [69].

(B) Needle threader [70] with a flexible diamond-shaped wire frame.

FIGURE 2.1: Images of the existing mechanisms that served as inspiration for the needle mechanism designs.

Spiked capsule

The spiked capsule consists of a hollow capsule body with needles fixed on the outside, protruding by 2 mm. A *spring-piston mechanism* is built inside the capsule, which consists of a preloaded compression spring and a piston. When the spring is released, it pushes on the piston, making it travel inside the capsule, resulting in drug injection. The needles on the capsule are arranged symmetrically around and along the capsule. The needles *deploy* by dissolution of the enteric capsule shell, exposing the needles inside the GI lumen at the duodenum. Figure 2.2 shows diagrams of this design. Note that the spiked capsule design does not have a mechanical retraction mechanism, but needles can be designed of dissolvable materials that would dissolve inside the gastrointestinal tract before evacuation.

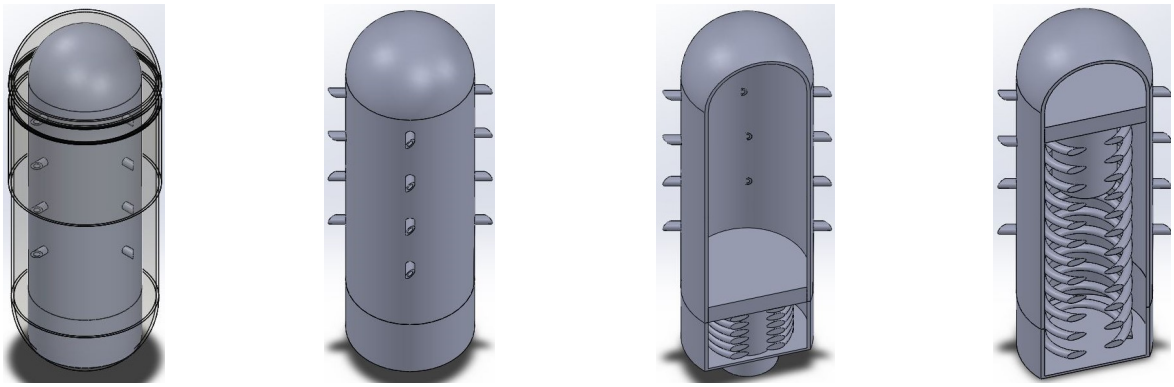

(A) Undeployed. (B) Deployed. (C) Deployed (cross-section). (D) After injection (cross-section).

FIGURE 2.2: Diagrams of the spiked capsule design in isometric view at different stages.

Portable hair brush

The portable hair brush (Figure 2.1a) consists of a deformable membrane that has two stable positions, bulging outwards and inwards, in relation to its bristles. When the membrane is bulging outwards (deployed), the bristles point away from the center of the membrane. When the membrane is bulged inwards (retracted), the bristles point inwards, towards the center of the membrane.

The analogous mechanism design consists of a deformable membrane with needles integrated at the end of a spring-piston capsule (Figure 2.3). When the spring is actuated, the piston exerts a pressure on the drug, consequently on the membrane, thus forcing it to bulge outward. The needles on the membrane are deployed when the membrane is bulged outwards. The retraction mechanism consists of detaching the membrane from the capsule. This causes the membrane to curl into a half-sphere with the needles pointing inwards. The capsule evacuates the body in two components, the membrane, in the form of a half-sphere, and the capsule body. The piston of the capsule, at its deployed state, acts as a cap for the open end of the capsule.

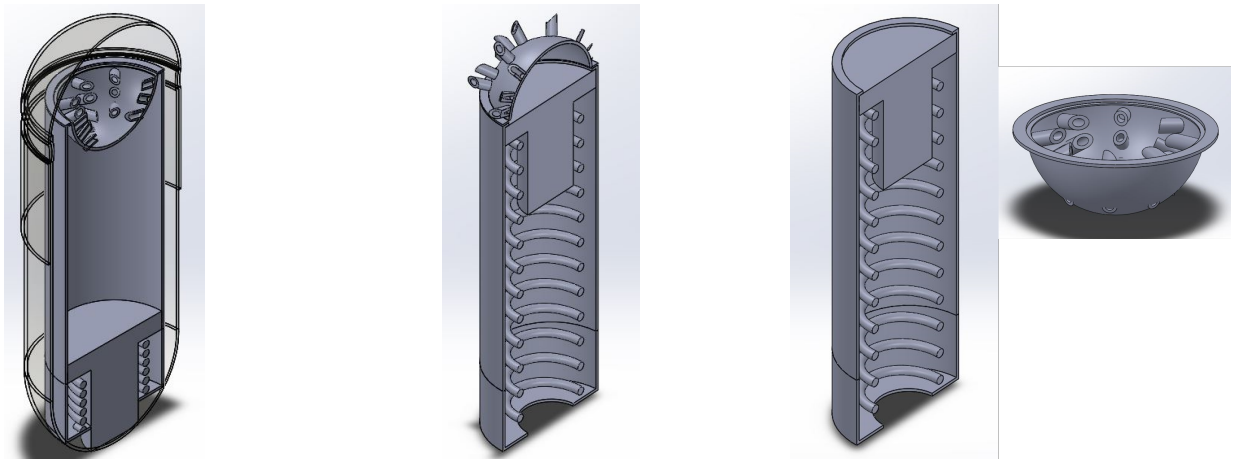

(A) Undeployed. (B) Deployed (after injection). (C) Retracted.

FIGURE 2.3: Diagrams of the cross-section isometric view of the portable brush inspired design at different states.

Multineedle syringe capsule

The multineedle syringe capsule is a variation of the portable hair brush design. This capsule is equipped with a spring-piston mechanism and a movable disk (instead of a flexible membrane) offset from one end of the capsule body. The movable disk has needles that point outwards and the drug is contained between the piston and the disk. When the spring is actuated, the piston exerts a pressure on the drug, consequently on the disk, thus causing it to advance and protrude the needles outside the capsule. Once the needles are deployed, the piston continues to advance inside the capsule to inject the drug. A back spring at the end of the capsule pushes back the disk once injection is completed. Figure 2.4 shows sketches of this capsule at its undeployed, deployed, and retracted states.

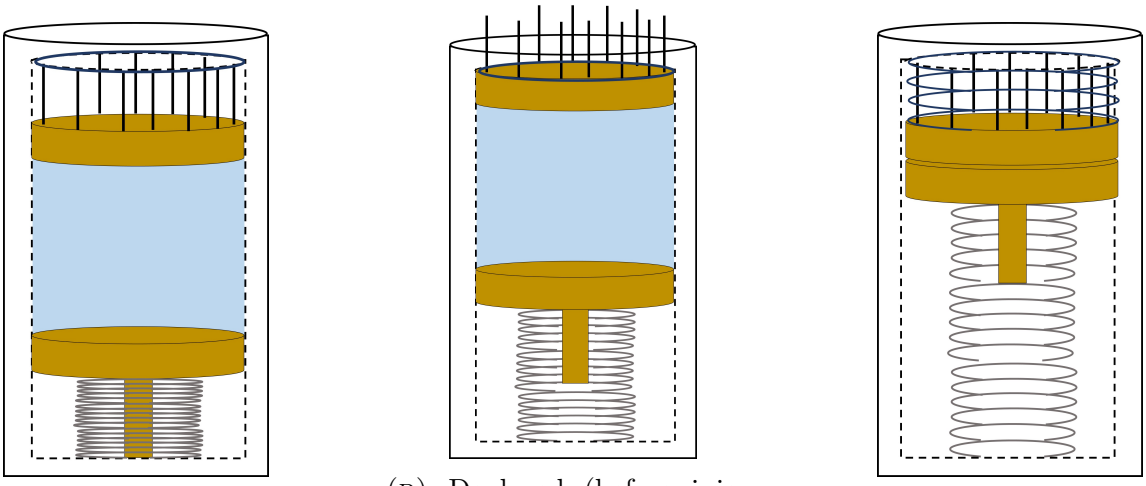

(A) Undeployed. (B) Deployed (before injection). (C) Retracted.

FIGURE 2.4: Sketches of the multineedle syringe capsule design at different states.

Diamond-column-buckling capsule

The diamond-column-buckling design is inspired by the shape and flexibility of a needle threader (Figure 2.1b). This design consists of two diamond-shaped deformable structures (that form an octahedron frame) assembled inside a spring-piston capsule. The structure is assembled inside the drug reservoir. The end points of the structure are supported on one end of the capsule, on one side, and on the piston, on the other (Figure 2.5a). One needle is attached at each middle vertex of the diamond structures pointing towards the capsule wall. When the piston advances inside the drug reservoir, it compresses the diamond-shaped structures, causing them to deform and increase their length radial to the capsule (Figure 2.5b). The needles are aligned with holes on the capsule wall that are sealed with a flexible material. When the needles advance towards the wall, they perforate a hole through this material and deploy out of the capsule. Retraction of the needles originates from an over-deformation of the diamond-shaped structures as the piston continues to travel inside the capsule, causing an inversion of the structures onto a pyramid-shaped frame (Figure 2.5c). Note that drug injection takes place throughout deployment and retraction. Figure 2.5 shows sketches of this capsule at its undeployed, deployed, and retracted states.

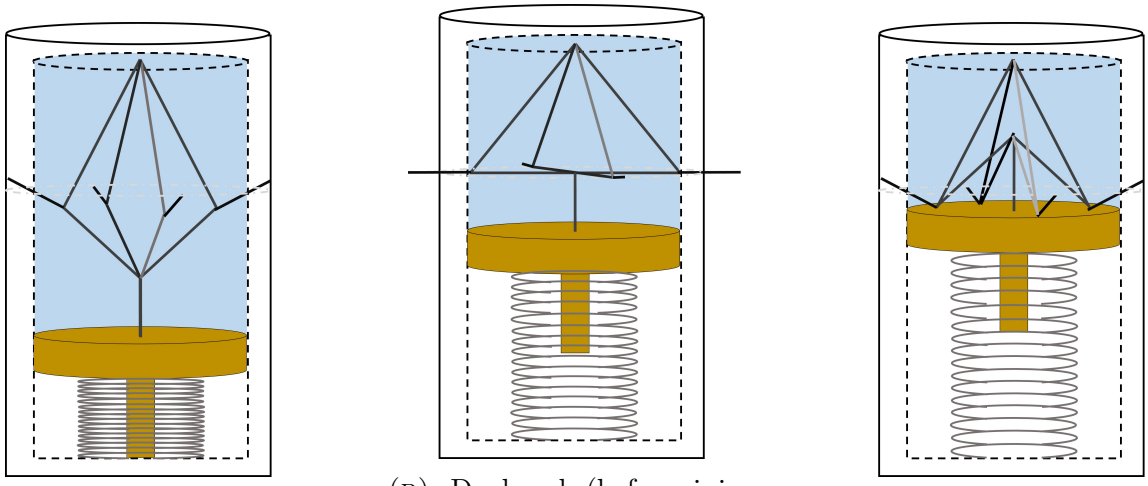

(A) Undeployed. (B) Deployed (before injection). (C) Retracted.

FIGURE 2.5: Sketches of the diamond-column-buckling capsule design at different states.

2.3.2 Bio-inspired designs

In nature, spikes are typically used as defense mechanisms to hurt predators or inject venom. The defense mechanisms of the porcupine-fish and the Spanish newt are used as inspiration for needle mechanism designs. Additionally, the blossoming motion of a flower is used as inspiration for another design. Figure 2.6 shows these sources of inspiration.

Porcupine-fish inspired design

The porcupine fish has the ability to deploy needles on its skin by inflating its body. In a relaxed state, the porcupine fish is small and smooth; when inflated, it transforms into a big spiked fish. Figure 2.6a shows this fish at its relaxed and distressed states. The porcupine fish inspired design integrates the concept of body expansion as a needle deployment mechanism.

The porcupine-fish design consists of a metal sheet with needles. The metal sheet is rolled with the needles pointing outwards and placed inside a hollow capsule with holes along the body (Figure 2.7a). The needles align with the holes of the capsule, which are sealed with a

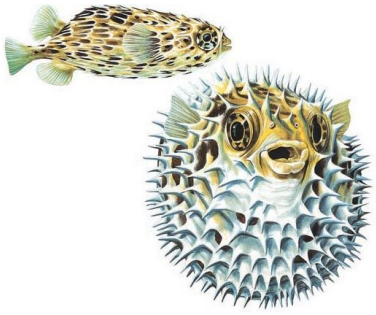

(A) Porcupine fish at its relaxed (top-left) and distressed (bottom-right) states. [71].

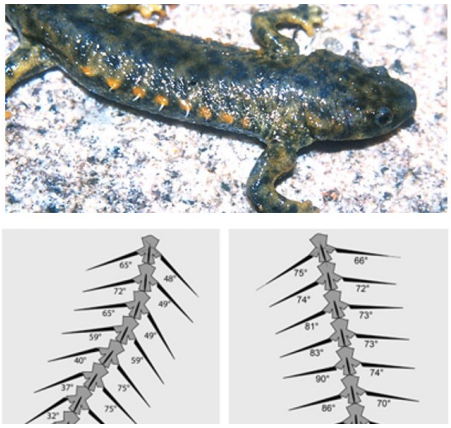

(B) Spanish newt image at the top, and sketches of the vertebral column of the newt at its relaxed (bottom-left) and distressed (bottom-right) states. [72].

(C) Lily blossomed flower (right) and flower bud (left) [73].

FIGURE 2.6: Images of biological systems that served as inspiration for needle deployment and retraction mechanism designs.

flexible material. Needle deployment consists of increasing the diameter of the rolled sheet, so the needles puncture through the flexible seal and protrude outside of the capsule (Figure 2.7b). Needle retraction consists of decreasing the diameter of the sheet, rolling back the sheet to its initial position (Figure 2.7d). Injection is done by a spring-piston mechanism that is integrated inside the capsule. The piston travels inside the metal sheet, once the needles are deployed, to inject the drug. The piston travels until the end of the capsule, clearing the way to roll back the metal sheet. Figure 2.7 shows sketches of this capsule at its undeployed, deployed before injection, injecting, and retracted states.

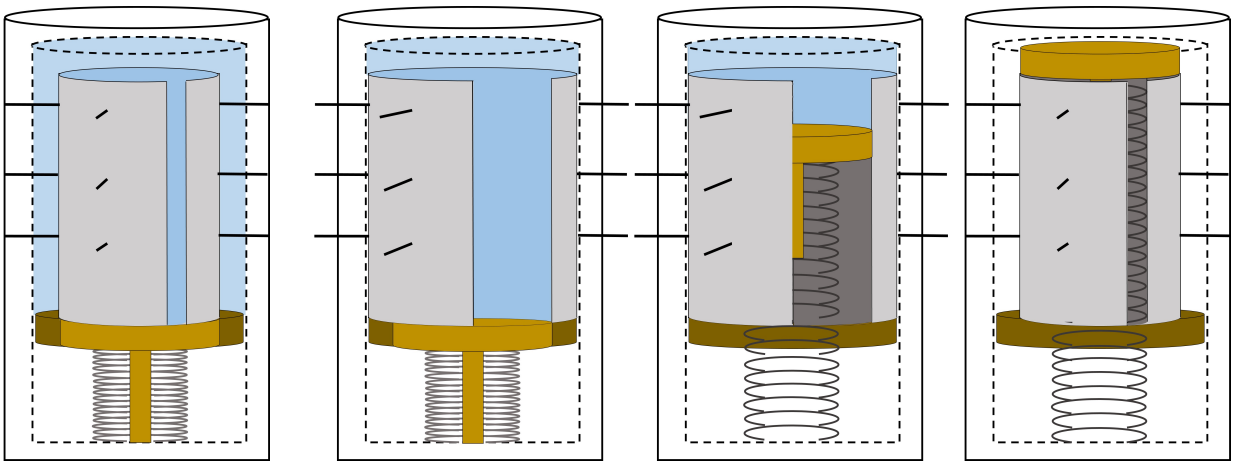

(A) Undeployed. (B) Deployed (before injection). (C) Deployed and injecting. (D) Retracted.

FIGURE 2.7: Sketches of the porcupine fish capsule design at different states.

Spanish newt with longitudinal actuation

The Spanish newt transforms its ribs into spikes when under distress. This amphibian changes the angle of its ribs with respect to its vertebral column, forcing them out of its body. The ribs break through the skin and protrude out of the body [72]. Figure 2.6b shows an image of this amphibian and drawings of its vertebral column at its relaxed and distressed states. The design inspired by the defense mechanism of the Spanish newt consists of using the concept of needle rotation as a deployment mechanism.

The Spanish newt capsule design uses the relative motion of two concentric cylinders. Needles hinged to the inner cylinder, the core, are aligned with holes on the outer cylinder, the case. The relative motion between the core and the case results in the tilt of the needles, thus protruding them out of the case. Deployment is achieved by advancing the core inside the case, and retraction is achieved by reversing the deployment motion. The needle-core connection allows the needles to rotate, and the drug to flow from within the core of the capsule. The motion of the core is powered by two preloaded compression springs, one for deployment and one for retraction. The deployment spring actuates needle deployment and drug injection, in one continuous motion. The retraction spring, activated once injection is over, counteracts the deployment spring and brings the core and needles back to their initial

position. Figure 2.8 shows this capsule in its undeployed, deployed, injecting, and retracted states.

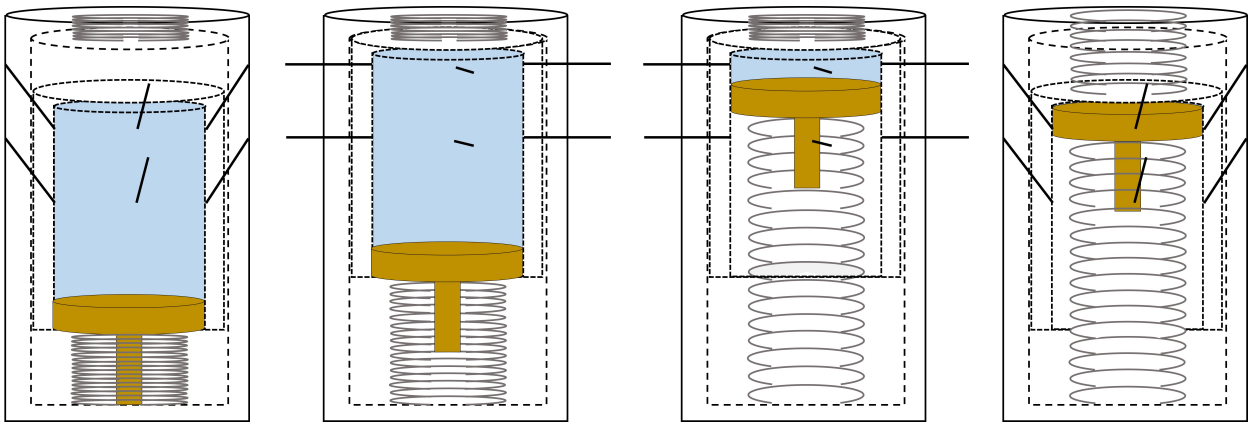

(A) Undeployed. (B) Deployed (before injection). (C) Deployed and injecting. (D) Retracted.

FIGURE 2.8: Sketches of the Spanish newt inspired capsule design at different states.

Spanish newt with rotational actuation

A variation of the Spanish newt inspired design uses the concept of rotation of the inner cylinder with respect to the outer one (as opposed to a longitudinal relative motion). The fundamental concept of needle deployment is the same as in the longitudinal design. The difference arises at the actuation mechanism. Deployment and retraction are both actuated by one torsion spring activated at two separate instances, before injection to deploy the needles, and after injection, to retract the needles. Injection is also activated separately as it is powered by the preloaded compression spring of the spring-piston mechanism.

Flower inspired design

The flower inspired design consists of a spring-piston mechanism with a custom piston. The custom piston consists of a tube extension added onto the front face of a standard piston. The needles are hinged to the tube and are allowed to rotate by their hinge point. The

needles, on one end, are attached to the tube of the piston, and on the other end, they are aligned with holes in the capsule. The holes in the capsule are sealed with a flexible material that allows the needles to pierce through it, and simultaneously, provides a watertight seal for the capsule. Needle deployment imitates the movement of a blossoming flower. When the piston advances, it induces the rotation of the needles and their protrusion through the capsule wall. After a certain displacement of the piston, the needles are normal to the capsule wall, achieving full deployment. Needle retraction is achieved by further advancement of the piston, over-rotating the needles to mirror deployment. Injection of the drug occurs throughout the deployment and retraction motion. Figure 2.9 shows sketches of this capsule at its undeployed, deployed, and retracted states.

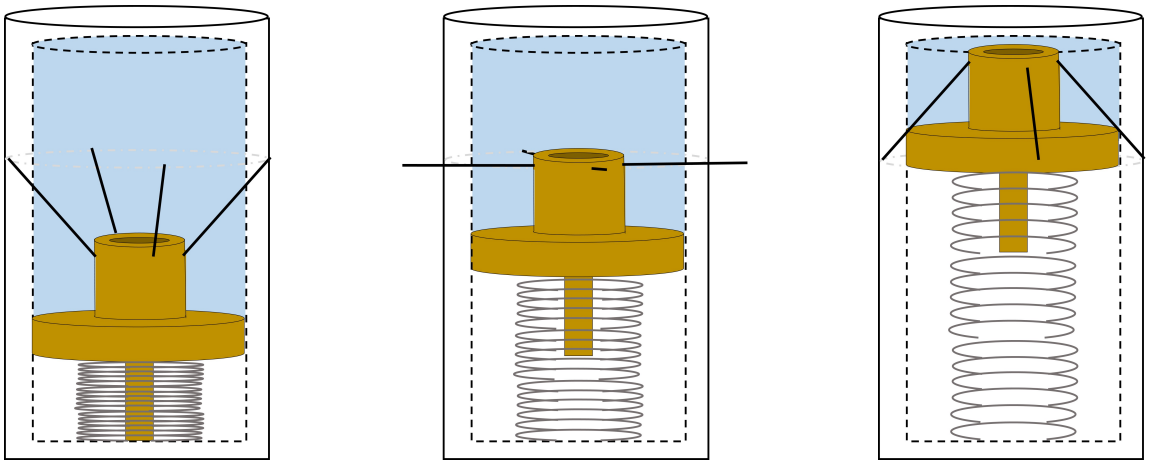

(A) Undeployed. (B) Deployed. (C) Retracted.

FIGURE 2.9: Sketches of the flower inspired design at different states.

2.3.3 Designs generated via cross-component analysis

A cross-component analysis was used to further populate the design pool. Combinations of designs from Sections 2.3.1 and 2.3.2 were considered. Three designs were selected from this analysis: the spiked-porcupine-fish hybrid, the porcupine-fish-multineedle hybrid, and the Spanish-newt-flower hybrid.

Spiked-porcupine-fish hybrid

The spiked-porcupine-fish hybrid design combines the needle deployment of the spiked capsule, and the body and retraction mechanism of the porcupine-fish. The capsule resembles mostly the porcupine-fish capsule, and instead of starting at its undeployed state (with the metal sheet rolled up) it starts with the needles protruding out of the capsule body. The needles are protected by the enteric capsule shell, as in the spiked design (Figure 2.10a). This combined design adds a mechanical retraction mechanism to the spiked capsule and simplifies the needle mechanism of the original porcupine-fish design. Figure 2.10 shows sketches of this capsule at its undeployed, deployed before injection, injecting, and retracted states.

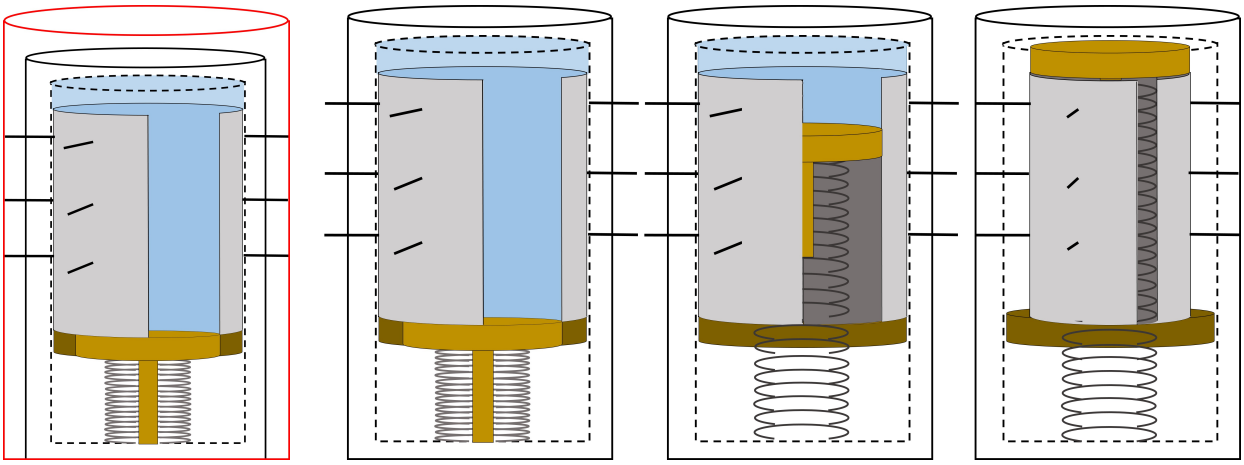

(A) Undeployed. (B) Deployed (before injection). (C) Deployed and injecting. (D) Retracted.

FIGURE 2.10: Sketches of the spiked-porcupine-fish hybrid design at different states. Note that at its undeployed state the metal sheet is unrolled and an enteric coating (in red) covers the needles that protrude the case.

Porcupine-fish-multineedle hybrid

The porcupine-fish-multineedle hybrid design combines the multineedle disk into the porcupine-fish design. The rolled metal sheet of the porcupine-fish design is replaced by two solid long curved plates with needles, inspired by the solid disk of the multineedle syringe mechanism.

The piston consists of two long curved plates (same curvature as the needle plates). The drug is contained between the piston and the needle plate. The two piston plates are assembled together holding a compressed spring in between. When the spring is released, the piston plates push on the drug, and consequently on the needle plates, thus causing them to advance and the needles to deploy. Retraction is carried out via a compression washer fitted into the capsule wall. When released, the compression washer pushes the needle plates back to their initial position, retracting the needless. Figure 2.11 shows sketches of this capsule at its undeployed, injecting, and retracted states.

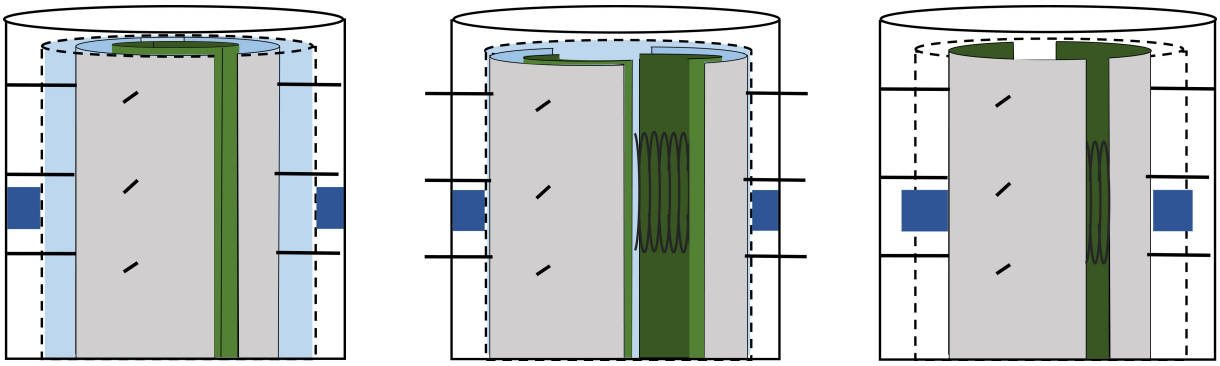

(A) Undeployed. (B) Deployed and injecting. (C) Retracted.

FIGURE 2.11: Sketches of the porcupine-fish-multineedle hybrid design at different states. The piston plates (in green) have the same curvature as the needle plates. The compression washer (in blue) is used to retract the needles.

Spanish-newt-flower hybrid

The Spanish-newt-flower hybrid design integrates the ability of the flower design (to retract needles by moving the piston/core in the same direction of deployment) into the Spanish-newt design. The deployment and injection of the Spanish-newt remain the same, but the retraction is a result of further displacement of the core along the case. This allows to perform deployment, injection, and retraction in one single motion. The motion is actuated by a single preloaded compression spring. Figure 2.12 shows this capsule at its undeployed, deployed, injecting, and retracted states.

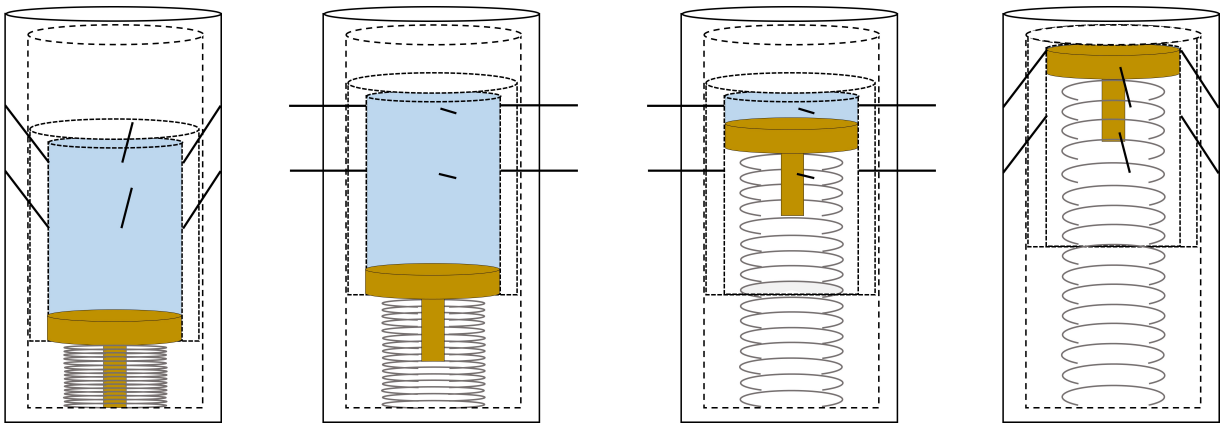

(A) Undeployed. (B) Deployed (before injection). (C) Deployed and injecting. (D) Retracted.

FIGURE 2.12: Sketches of the spanish-newt-flower hybrid design at different states. Note the increased length of the case compared to the Spanish newt design. This increased length allows the over-displacement of the core inside the case, which induces the retraction of the needles.

2.4 Selected Design

From the designs proposed in Section 2.3, the Spanish newt design with longitudinal actuation is chosen to be further developed and prototyped. Quantitative analysis (Appendix A) demonstrates that this design best meets the non-functional requirements of needle deployment and retraction mechanism. In particular:

- deployment and injection are achieved through one continuous motion and a single actuating spring;
- manufacturing of the deployment/injection and retraction mechanisms can be separated into two steps, facilitating the manufacturing and assembly process of the prototype;
- injection can be designed to start after deployment, and retraction after injection– unlike in other designs, where injection intrinsically takes place during deployment and retraction; and

- the needles are distributed around the circumference of the capsule as desired, and the number of needles that can be implemented is flexible.

Chapter 3

Design Development: the Spanish newt with longitudinal actuation

3.1 Chapter overview

This chapter, which describes the detailed development of the Spanish newt inspired design, is divided into five sections. In Section 3.2, the kinematics of the mechanism are explained, and the components of the capsules, and respective considerations, are described. Then, a preliminary analysis is performed in Section 3.3. The analysis investigates needle parameters, such as needle length and required rotation angle; core dimensions, in order to hold 0.5 mL of drug inside the core; and syringeability considerations. Section 3.4 covers the embodiment of the design, and investigates three interactions of components: needle-core interaction, which develops the needle attachment method; piston-core interaction, where the piston dimensions are determined; and core-case-needle interaction, which further determines the case specifications and the assembly of the core, case, and needles. Manufacturing and assembly of the capsule, including the discussion of manufacturing challenges, are also covered in Section 3.4. Finally, the springs are selected in Section 3.5 by performing mechanical tests to characterize the piston force required to achieve deployment and injection. The force curves are used to select the corresponding springs.

3.2 Mechanism and Components

3.2.1 Mechanism

The Spanish newt mechanism is showed in Figure 3.1. It consists of two concentric cylinders: the inner cylinder is called *core*, while the outer cylinder is called *case*. Four metallic needles are distributed around the perimeter of the capsule. The needles are attached to the core via flexible hinges and pass through holes in the case. The tilting motion of the needles, allowed by the flexible hinges, is referred to as *needle rotation* in the following. The needles are deployed when they are perpendicular to the capsule body, defined as the 0° position. The deployed needles protrude by 1 to 2 mm out of the case. The needles are in the retracted position when they rotate by 60° from the deployed position. When retracted, the needles are completely contained inside the wall of the case. Needle rotation is driven by the longitudinal displacement of the core relatively to the case.

Figure 3.2 illustrates the kinematics of the Spanish newt mechanism. The actuation of the mechanism relies on two preloaded springs, one for needle deployment and drug injection, and one for needle retraction. The capsule is initially undeployed (Figure 3.2a). The deployment spring is triggered first, pushing on the piston. At first, static friction between the piston and the core makes the core slide through the case with the piston, thus deploying the needles. The core stops when the needles are deployed (Figure 3.2b). The piston then continues advancing, now through the static core, which provokes injection of the drug through the needles. When injection is complete (Figure 3.2c), the retraction spring is triggered, pushing the core back to its initial position, and partially recompressing the deployment spring. This displacement provokes the retraction of the needles (Figure 3.2d).

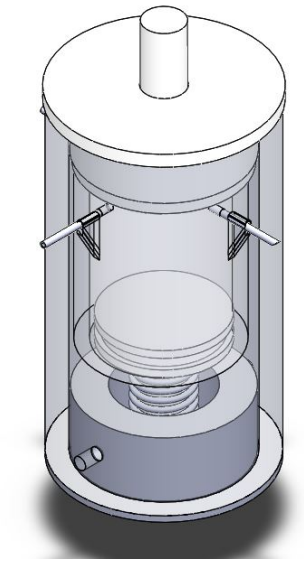

FIGURE 3.1: Schematic of the Spanish newt mechanism at its deployed state (before injection) in isometric view. The case is shown transparent to illustrate the interior of the capsule. The needles are hinged to the core and pass through holes in the case. When deployed, the core is in the up position, and the needles are normal to the wall of the capsule.

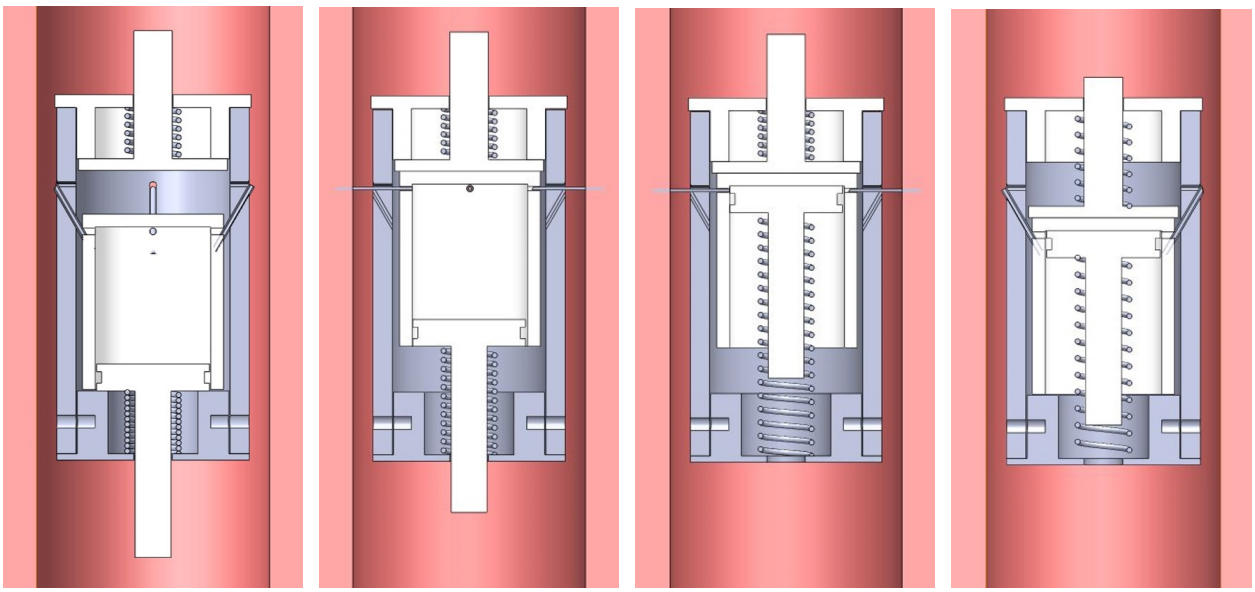

(A) Undeployed. (B) Deployed before injection. (C) Deployed after injection. (D) Retracted.

FIGURE 3.2: Schematics of the kinematics of the Spanish newt mechanism. The cross-section views shows the capsule at four different stages: undeployed, deployed before injection, deployed after injection, and retracted. Notice the displacement of the core, piston, and needles during deployment (from (A) to (B)), injection (from (B) to (C)), and retraction (from (C) to (D)).

3.2.2 Components

The Spanish newt mechanism breaks down into ten parts. Figure 3.3 shows an exploded view of the capsule. The components and their design considerations are described below:

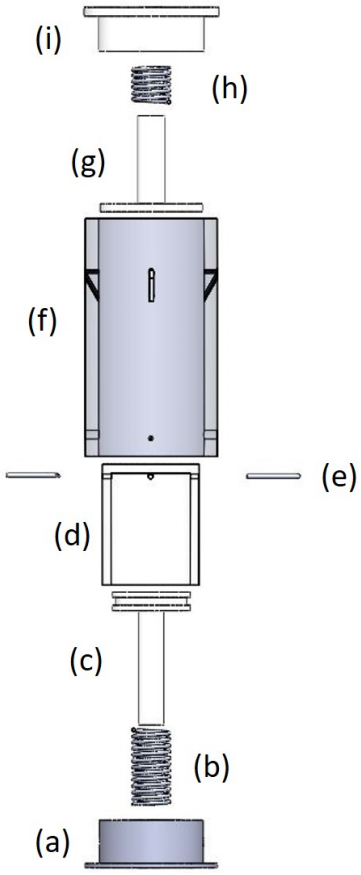

FIGURE 3.3: Exploded view diagram of the mechanism in real scale. The capsule has ten parts, each of which is labeled: (a) deployment cap, (b) deployment spring, (c) piston, (d) core, (e) needles, (f) case, (g) retraction pusher, (h) retraction spring, and (i) retraction cap. Note that the two retention pins and the sleeve are not shown here.

- **Needles**: metallic needles of gauge 25 (outer diameter of 0.5 mm and inner diameter of 0.3 mm) are used. The needles should protrude by 2 mm from the capsule wall when deployed and be fully retractable. The distribution of the needles, i.e. their number and location on the capsule's exterior surface, is important to ensure the engagement

of all needles with the intestine wall. Several configurations should be tested *in vitro* in intestine models to determine the most effective needle distribution strategy. In order to make the mechanism relatively easy to manufacture, it was chosen to use four needles on a single row around the perimeter of the case. The needles are attached towards one end of the core so that the piston displacement does not cover the needle attachment points.

- **Core**: the core is the inner cylinder that contains 0.5 mL of drug and bears the needles on flexible hinges. The hinges between the core and the needles should allow the needles to rotate by 60° (from the undeployed position to the deployed position and to the retracted position) as described in Section 3.2.1. The needles should be connected with the inside of the core to allow the drug to flow out. However, they should not protrude inside the core, in order to avoid interfering with the piston. The flexible hinges should ensure watertightness to prevent the drug from leaking out of the capsule.
- **Case**: the case is the outer cylinder that houses the whole mechanism. Its inner diameter is slightly larger than the outer diameter of the core. However, their clearance should be as small as possible, to prevent the core from moving laterally inside the case. The case completely houses the needles when they are retracted. This implies a geometrical constraint: the thickness of the case should be larger than the radial projection of the undeployed needles. In the deployed position, the holes in the case, where the needles pass, are aligned with the holes in the core, where the needles are attached. The holes in the case are non-cylindrical in order to account for needle rotation, forming a V-shaped hole, narrower outside the case and wider inside.
- **Deployment cap and retraction cap**: the caps close the case on both ends (and are attached to the case via screws). The deployment cap bears the piston and the deployment spring. The retraction cap bears the retraction pusher and the retraction spring. The shafts of the piston and of the retraction pusher extend past the caps to enable the manual activation mechanism of the springs. Pins lock the piston shaft and the retraction pusher shaft, holding the springs in their preloaded positions.
- **Piston**: the piston travels with the core during deployment and relatively to it during

injection. The head of the piston is equipped with a rubber O-ring for watertightness. The piston is pushed by the deployment spring. Its shaft is locked onto the deployment cap by a pin that can be manually removed to trigger deployment and injection.

- **Retraction pusher**: the retraction pusher displaces the core back to its initial position after injection, which causes the needles to retract. The head of the retraction pusher has the same diameter as the core. Like the piston, the shaft of the retraction pusher is locked by a pin outside the retraction cap that can be manually removed to trigger retraction.
- **Deployment spring and retraction spring**: the deployment spring actuates between the deployment cap and the piston. It should provide sufficient force to deploy the needles and inject the drug. The retraction spring actuates between the retraction cap and the retraction pusher. It should provide enough force to push the core back, partially recompressing the deployment spring and retracting the needles.
- **Sleeve**: the sleeve is an extra piece of tubing inserted inside the core. The sleeve is not shown in Figures 3.1 to 3.3, and its functions and characteristics are described in Section 3.4.1.

3.3 System analysis

The preliminary analysis of the capsule is segmented into four subsections: manufacturing considerations (Section 3.3.1), needle parameters determination (Section 3.3.2), core dimensions determination (Section 3.3.3), and syringeability requirements and considerations (Section 3.3.4). Note that the work presented here is part of an integrated and iterative process, and the calculations done in this section use information and values that emerge during the embodiment and manufacturing of the capsule, presented in later sections.

3.3.1 Manufacturing considerations

Any orally administered capsule is desired to be as small as possible to minimize the discomfort of patients who swallow it. The maximum target dimension of the prototype are 35

mm in length by 20 mm in diameter, as specified in Section 2.2.

Manufacturing capabilities and limitations need to be considered when designing a small mechanism. The two manufacturing methods considered for this capsule are machining off-the-shelf components and 3D printing.

All the capsule components (with the exception of the piston and the retraction pusher) were machined from off-the-shelf stock materials. When manufacturing simple shapes (i.e. cylinders with holes that would only require cutting, grinding, milling, and drilling) it is more convenient to machine the components from off-the-shelf materials over 3D printing. This is especially true during embodiment stages, since machining allows for a progressive, inexpensive, and dynamic design process. Note that this was in part because the aforementioned machining tools were easily accessible during this work; moreover, 3D printed cylinders had undesired internal printing supports. Nevertheless, some drawbacks to consider when machining include inaccuracies when machining small scale features using large equipment, and dimension limitations of available stock materials. In this work, the core and the case of the prototype are made of polycarbonate stock tubes that best fit the capsule requirements. For the case, a tube with an outer diameter of 15.9 mm (5/8") and wall thickness of 1.5 mm (1/16") was used. For the core, a tube with an outer diameter of 12.7 mm (1/2") and wall thickness of 1.5 mm (1/16") was used.

3D printing was used to manufacture the piston and retraction pusher. The FORM2 resin printer was selected over other 3D printers for its superior printing resolution and surface finish. The piston and retraction pusher were printed with the FORM2's Clear Photoreactive Resin. 3D printing proved cheaper and more dynamic than machining when manufacturing complex shapes (i.e. requiring a lathe if machined), and especially when repeatedly manufacturing complex shapes with slight dimension modifications. Some drawbacks to consider when 3D printing include: delays imposed by 3D printing services, printer specific build requirements (i.e. supports and printing orientation), and undesirable dimensional changes due to shrinkage or expansion of materials.

3.3.2 Needle parameters: length, rotation angles, and displacement

The objective of this section is to determine L_n, the total needle length, α, the needles' retracted angle, and d, the required core displacement to achieve needle deployment. Case thickness t_{case} and core thickness t_{core} are set to 1.5 mm, as explained in Section 3.3.1. The clearance l_c between the case and the core is 0.5 mm, and the clearance of the needles inside the core l_{in}, which ensure the needles are connected to the interior of the core, is set to 0.5 mm.

Figure 3.4 illustrates the kinematics of the core-case-needle motion and defines the relevant geometrical parameters. In the undeployed position, the needles are contained within the thickness of the case. The needle holes in the core and in the case are V-shaped, narrower on the outside and wider on the inside. Therefore, the needles are assumed to rotate about a hinge point H, located on the core's outer diameter. The contact point between the needles and the case is located on the outer diameter of the case. The needle's free length L_f refers to the length of the needle that is free to rotate, from the hinge point to the contact point with the case. Simple geometrical considerations based on Figure 3.4 yield the following expressions:

$$L_n = L_f + t_{core} + l_{in} = L_{dep} + t_{case} + l_c + t_{core} + l_{in} \tag{3.1}$$

$$d = \sqrt{L_f^2 - (t_{case} + l_c)^2} \tag{3.2}$$

$$\alpha = \sin^{-1}\left(\frac{d}{L_f}\right) \tag{3.3}$$

Using the numerical values of L_{dep}, t_{case}, l_c, t_{core}, and l_{in}, Eq. (3.1), (3.2), and (3.3) yield: $L_n = 6$ mm, $d = 3.5$ mm, and $\alpha = 60°$. Note that further into the manufacturing process, the interior of the case had to be ground down to $t_{case} = 1.1$ mm to obtain adequate clearance with the core. With this core thickness, the calculated values are $d = 3.1$ mm,

$\alpha = 64°$, and $L_n = 5.5$ mm. However, the resulting discrepancies are small and below relevant manufacturing tolerances. Therefore the initially calculated values were kept in the remaining of the work when manufacturing the capsule.

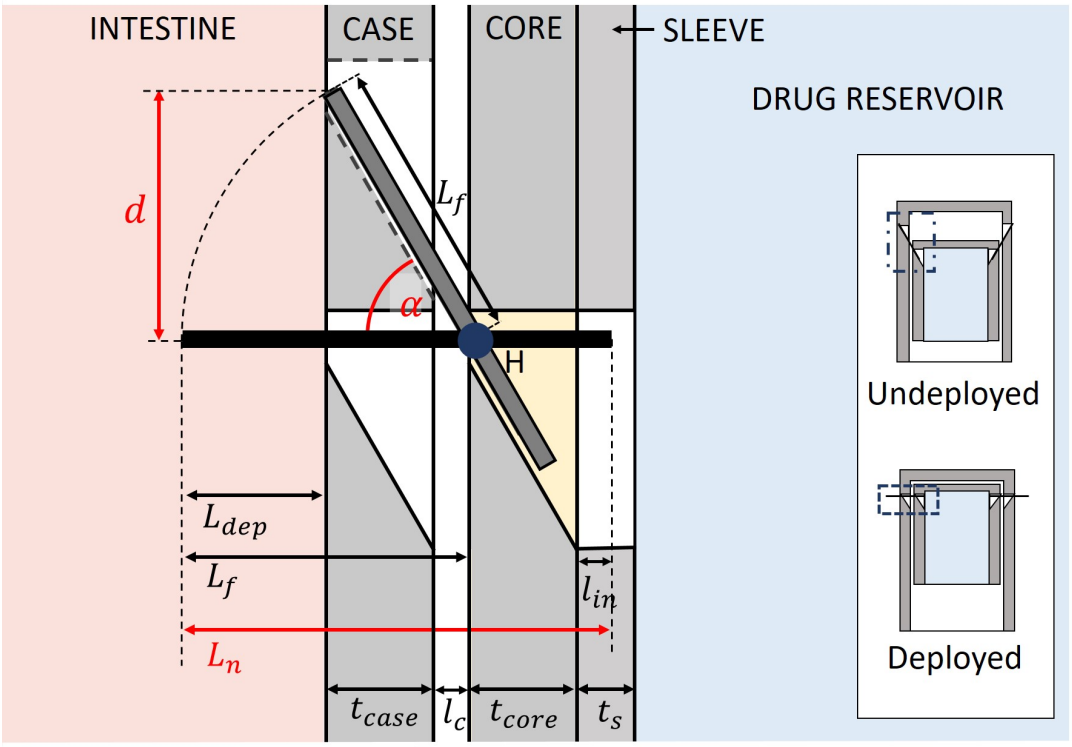

FIGURE 3.4: Schematic of the cross-section view of the capsule at the needle attachment point, simultaneously showing the undeployed and deployed core-case hole alignment (illustrated independently by the inset). The holes of the core are filled with a flexible material (silicone rubber seal) that acts as a hinge for the needle (shown in yellow). The needles rotate by the hinge point H, located at the outer diameter of the core, and they are pushed by the case's outer diameter. The core needs to travel a distance d to rotate the needles by α, and deploy the needles by L_{dep} out of the case.

3.3.3 Drug volume and core dimensions

The volume of drug to be injected is 0.5 mL. The dimensions of the core, which acts as the drug reservoir, are determined by this volume requirement. The outer and inner diameters of the core are also determined by the case dimensions and available materials. The core

length L_{req} is thus defined by its inner diameter D_{in} and its volume requirements V_{req} (Eq. (3.4)). The core's total length L_{core} is shown in Figure 3.5. It takes into account the piston head height h_p, and the clearance L_c provided for the needles attached at the end of the core, which is equivalent to the needles' outer diameter.

$$L_{req} = \frac{4V_{req}}{\pi D_{in}^2} \tag{3.4}$$

$$L_{core} = h_p + L_{req} + L_c \tag{3.5}$$

With $V_{req} = 0.5$ mL, $D_{in} = 7.9$ mm (5/16"), $h_p = 3.4$ mm, and $L_c = 0.5$ mm, the obtained core lengths are $L_{req} = 10.1$ mm, and $L_{core} = 14$ mm.

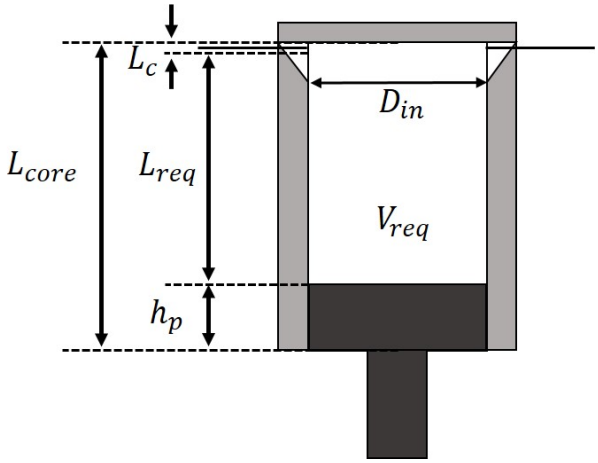

FIGURE 3.5: Schematic of the core with the needles and the piston assembled. The core's inner diameter D_{in} and the volume of drug inside the core V_{req} determine core length L_{req}. The total length of the core L_{core} considers L_{req}, the piston head height h_p, and the needle clearance L_c.

3.3.4 Syringeability

Injecting the required volume of drug through the needles in a given time requires to overcome the viscous friction of the fluid inside the needles. The resulting force on the piston is called

syringeability. Syringeability needs to be estimated in order to select the deployment spring accordingly.

In this section, it is assumed that the piston travels at constant speed during injection. This assumption is made because solving the complete equation of motion of the piston would require to know accurately the friction force between the piston and the core. Since this friction force is difficult to model, it is measured experimentally later in the thesis (Section 3.5.2). The objective of the present section is to estimate the value of the syringeability force, in order to compare it to the measured piston-core friction force. Syringeability is a speed-dependent force. Several values of injection time (which influences piston speed) are therefore considered. Figure 3.6 shows the framework of the calculations and the notations used.

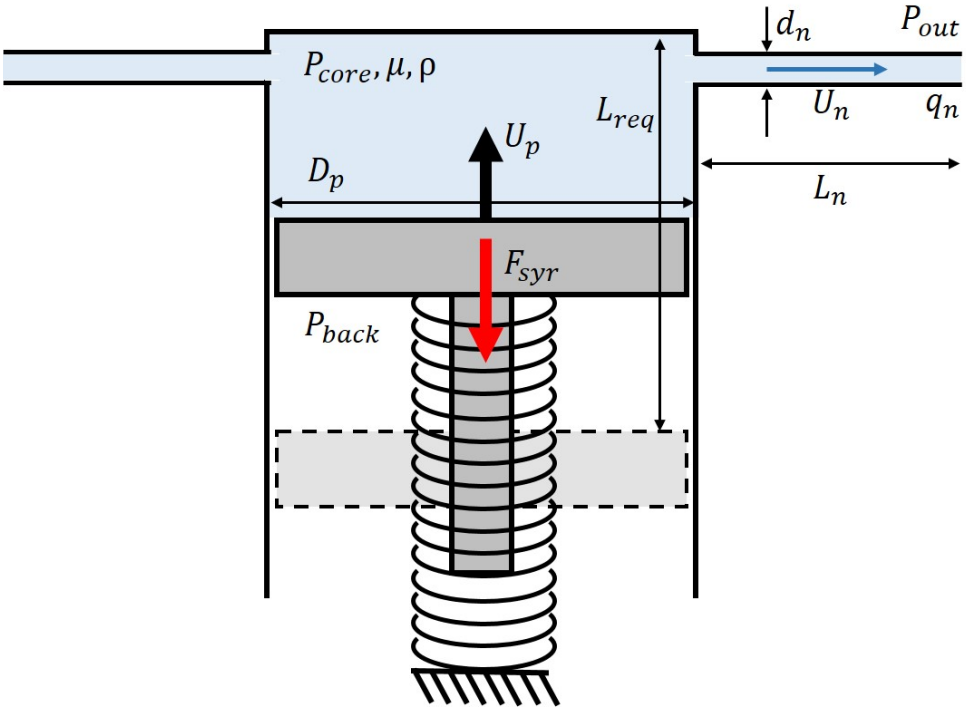

FIGURE 3.6: Schematic of the cross-section view of the capsule showing the core, piston, and needles with the relevant parameters to determine syringeability force. The numerical values of these parameters are given in Table 3.1.

If the flow inside the needles is laminar, the pressure drop in the needles due to fluid viscosity can be described by the Hagen-Poiseuille equation [74]:

$$P_{core} - P_{out} = \frac{128 \mu L_n q_n}{\pi d_n^4}, \tag{3.6}$$

where P_{core} is the pressure inside the core, P_{out} is the pressure at the end of the needle, q_n is the volume flow rate in one needle, d_n is the inner diameter of the needle, L_n is the needle length, and μ is the dynamic viscosity of the fluid.

The Hagen-Poiseuille equation provides a good approximation of the forces when the fluid is Newtonian and the flow is laminar. Flow laminarity is characterized by the Reynolds number, which is given by [74]:

$$Re = \frac{\rho d_n U_n}{\mu}, \tag{3.7}$$

where ρ is the density of the drug, and U_n is the characteristic flow velocity in the needles. The characteristic velocity U_n in each needle is obtained by conservation of mass flow between the piston and the needles:

$$U_n = \frac{V_{req}}{\frac{\pi}{4} N d_n^2 t_{inj}}, \tag{3.8}$$

where V_{req} is the total volume of drug, t_{inj} is the injection time, and N is the number of needles.

The Reynolds number is calculated for different values of the injection time t_{inj}, ranging from 0.5 s to 5 s, the maximum allowed injection time. The fluid properties that are used are those of water at 36°C. The numerical values used in this section are shown in Table 3.1, and the obtained values of Re are given in Table 3.2. Laminar Poiseuille flow is stable for $Re < 2100$ [74]. It can be seen from Table 3.2 that the calculated Reynolds number, for all the injection times considered, are smaller than this critical value. Thus, the Hagen-Poiseuille equation (Eq. 3.6) is valid.

The conservation of total flow rate through the needles and through the piston yields:

$$\frac{\pi}{4} D_p^2 U_p = N q_n, \tag{3.9}$$

where D_p is the piston diameter, U_p is the piston velocity relatively to the core (assumed constant), and N is the total number of needles. The piston velocity can be expressed as core length divided by injection time:

$$U_p = \frac{L_{req}}{t_{inj}} \tag{3.10}$$

The syringeability force F_{syr} is defined as the resultant of pressure forces on the piston. This force is generated by the pressure drop inside the needles, due to the viscosity of the drug, and described by the Hagen-Poiseuille equation (Eq. 3.6). The syringeability force is, by definition:

$$F_{syr} = \frac{\pi}{4} D_p^2 (P_{core} - P_{back}), \tag{3.11}$$

where P_{back} is the pressure behing the piston. Finally, it is assumed that $P_{out} = P_{back}$, since a large hole is drilled into the deployment cap in order to allow fluid to fill the core underneath the piston. By combining Eq. (3.6), (3.9), (3.10), and (3.11), the expression of the syringeability force is obtained as:

$$F_{syr} = \frac{8\pi}{N} \left(\frac{D_p}{d_n} \right)^4 \frac{\mu L_n L_{req}}{t_{inj}} \tag{3.12}$$

TABLE 3.1: Numerical values used for syringeability calculations.

Parameter	Symbol	Units	Value
Fluid dynamic viscosity	μ	Pa s	0.7e−3
Fluid density	ρ	kg/m^3	9.9e2
Needle length	L_n	mm	6.0
Needle inner diameter	d_n	mm	0.3
Piston travel length	L_{req}	mm	10.1
Volume of drug	V_{req}	mL	0.5
Piston diameter	D_p	mm	7.9
Number of needles	N		4

TABLE 3.2: Values of Reynolds number Re and syringeability force F_{syr} obtained for various values of injection time t_{inj}. The injection times considered range between the maximum allowed injection time (5 s), and a tenth of this time. Note that the Reynolds number is smaller than the critical value (2.1e3) for all injection times considered here, meaning that the flow is laminar inside the needles, and that Eq. 3.6 is valid.

Symbol	Units	Values		
t_{inj}	s	0.50	1.0	5.0
Re	-	1.5e3	7.5e2	1.5e2
F_{syr}	N	0.26	0.13	0.03

Table 3.2 shows the obtained values of syringeability force for different injection times. Syringeability increases when injection time decreases. Indeed, reducing the injection time implies increasing fluid velocity in the needles, which induces higher viscosity effects. It should be reminded that the speed of the piston is assumed to be constant; the values of F_{syr} shown in Table 3.2 only indicate an order of magnitude. The obtained approximations of the syringeability force will be compared to the piston-core friction force, which is measured in Section 3.5.2.

3.4 Design embodiment

This section contains the three main design embodiment considerations for the capsule design (Sections 3.4.1 to 3.4.3) and the manufacturing process of the capsule (Section 3.4.4). The design embodiment is segmented into: core-needle interaction (Section 3.4.1), core-piston interaction (Section 3.4.2), and core-case-needle interaction (Section 3.4.3). Note that the design embodiment is a process intertwined with analysis and manufacturing, and some decisions were made due to manufacturing reasons. Additionally, the embodiment of one part influences decisions taken in another. This section is organized by embodiment considerations, and not in the chronological order in which decisions were made.

3.4.1 Core-needle interaction

The objective of this module is to design the core-needle flexible hinge that allows the needle to rotate from a 0° to a 60° angular position, and minimizes the required forces needed to achieve this rotation. Moreover, the core-needle hinge should be watertight, the needles should not get obstructed during manufacturing, assembly, or operation of the capsule, and the needles should not interfere with the displacement of the piston head.

The relevant design variables are: core material, attachment type, hole properties of the core, and needle properties at the attachment point. Table 3.3 was used to find the best combination of options. Each option and combination was carefully analyzed and tested when necessary, in order to determine the best solution.

TABLE 3.3: Morphological chart for the design of the needle-core interaction. Any combination (with one design option per parameter) is *a priori* possible.

Parameters	Design options		
Core material	50A Silicone rubber tube	Flexible Photopolymer	Polycarbonate tubing
Needle hinge type	Tight-fit	Direct bonding using instant adhesive	20A Silicone rubber sealant hinge
Hole property	Straight	Chamfered	With tentacles
Needle-end property	Standard needle	Needle with blob directly on one end	Needle with blob offset from one end

The three needle hinge types considered were (1) tight-fit, which consists of puncturing the core material directly with the needle without predrilling any hole, (2) direct bonding, which consists of using an instant adhesive to glue the needle to a hole of same or slightly larger diameter on the core, and (3) a silicone rubber hinge. This last option consists of filling a hole in the core of at least twice the needle diameter with a silicone rubber seal and inserting the needle through it once dry. The silicone rubber then acts as a flexible, watertight hinge between the needle and the core. Note that the silicone rubber sealant (Elmer's® Silicone Rubber Sealant, equivalent to Durometer 20A) is a distinct and softer material than the silicone rubber tube from (McMaster-Carr®, Durometer 50A). In terms of hole properties, the tentacles option consists of extending the needle-attachment support area. Finally, the blobs added to some needles that to modify the needle-end properties act as an obstacle to prevent the needle from sliding in or out of its position. These blobs are made from two adhesives capable of holding onto stainless steel: instant bonding adhesive (Loctite® 401) and cold-weld-two-part epoxy (J-B Weld® Twine Tube). The blobs were made by using another needle to add a fraction of a drop of adhesive to the end of the needle that bears the blob. Figure 3.7 shows different needle-end properties considered.

FIGURE 3.7: Image of the $\sim$ 6 mm needles with different blobs. Blobs are made from instant adhesive or cold-weld-two-part epoxy, and are placed at the end or offset from the end of the needle. From left to right the blobs material-location are: no-blob (standard needle), adhesive-offset, epoxy-offset, adhesive-offset, epoxy-end, and adhesive-end.

Three combinations of core material and needle attachment achieved both, watertightness and needle rotation from 0° to 60°: the silicone rubber tube with tight fit needles, the flexible

photopolymer with needles directly glued to the core, and the polycarbonate tubing with the silicone rubber hinges. Figure 3.8 shows the three combinations.

FIGURE 3.8: Image of the three combinations of core-material and needle attachment, which achieved watertightness and allowed needle rotation between 0° and 60°. From left to right: silicone rubber tube with tight-fit needles, flexible photopolymer with glued needles, and polycarbonate tubing with needles on silicone rubber hinges.

The polycarbonate solid tube with silicone rubber hinges performs better than the other two options in several aspects. It features a lower resistance to needle rotation, and polycarbonate is easier to machine than the silicone rubber tube and the photopolymer. The needles used are standard, since adding blobs caused two undesired effects: it risks obstructing the needles, and it interferes with the needle assembly on the silicone rubber seal. This last effect is a result of the blobs being neither small enough, nor consistently at the same position on the needles. The holes in the core, which are filled with silicone rubber sealant, are V-shaped, adapted to the path of the rotating needle.

Another component introduced while studying the core-needle interaction is the sleeve. The sleeve is a FEP (Fluorinated Ethylene Propylene) clear tube inserted inside the core, which acts as an extension of the core's thickness. The sleeve has holes aligned with those of the core, but that are larger and not covered with silicone rubber. The sleeve has two purposes: (1) introduce a clearance between the piston and the needles, and (2) allow the needles to protrude out of the silicone rubber seal, ensuring the orifice of the needle is open for drug flow. Figure 3.9a illustrates how the sleeve addresses its two purposes. Figure 3.9b shows an image of the sleeve installed inside the core; notice how the sleeve's outer diameter is the

same as the inner diameter of the core, which results in a tight fit of the sleeve in the core, and a watertight sleeve-core interface.

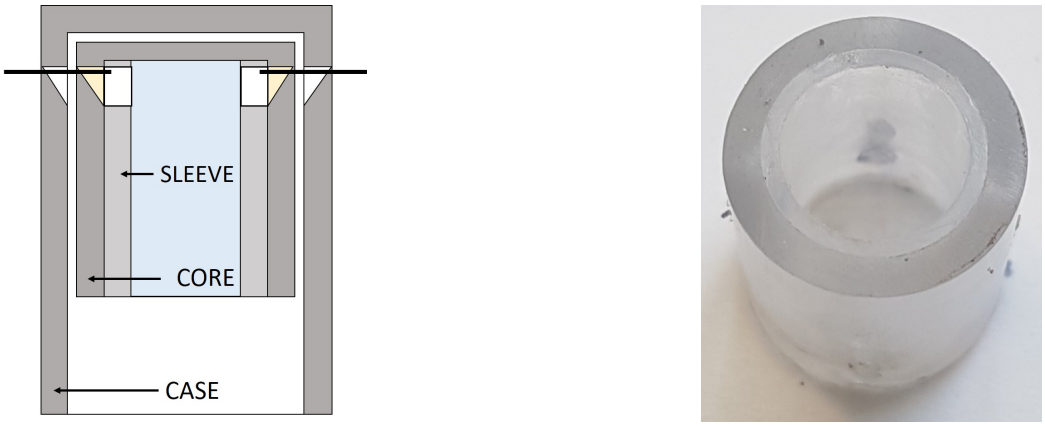

(A) (B)

FIGURE 3.9: (A) Diagram of the core-case-needle assembly illustrating the location and function of the sleeve in the mechanism. The holes of the sleeve are not covered with the silicone rubber sealant (yellow). The holes provide a clearance for the needles to connect with the inside of the core and not to interfere with the displacement of the piston. (B) Image of the sleeve installed inside the core and cut to the final dimension. Notice the tight fit of the sleeve in the core.

3.4.2 Core-piston interaction

The objective of this module is to design a piston that travels inside the core (and the sleeve), in order to inject the drug through the needles. The design should achieve low friction and watertightness. Moreover, the piston head needs to be as short as possible, in order to minimize the total length of the capsule.

A rubber O-ring is used to achieve watertightness. The design variables for the O-ring are its outer diameter D_{or}, cross-section width W, and cross-section shape. The narrowest off-the-shelf O-ring that fits the sleeve's inner diameter d_s is selected and purchased from McMaster-Carr®. It features an outer diameter of 7.9 mm (5/16"), and a circular cross-section with a width of 1.8 mm (0.07"). The piston is designed for this specific O-ring.

The piston design parameters are the dimensions of the head (height h_p and diameter D_p), the dimensions of the groove for the O-ring (width G and O-ring clearance F), and the thickness h_f of the flange. The thickness of the flange is only defined by the minimum thickness that can be 3D printed, which is roughly 0.9 mm. The value of h_f impacts the height of the piston head. Figure 3.10 shows the diagram of the piston and O-ring, with their relevant dimensions.

Manufacturing handbooks [75] specify suitable piston and groove dimensions depending on the diameter of the traveling tube, the O-ring's dimensions, and its material hardness. Usually, design rules state the groove width should be $G = 1.5W$, and that the squeeze ratio W/F should be between 10% and 20%. The stretch $S = d_p/d_{or}$ should be at most 5%.

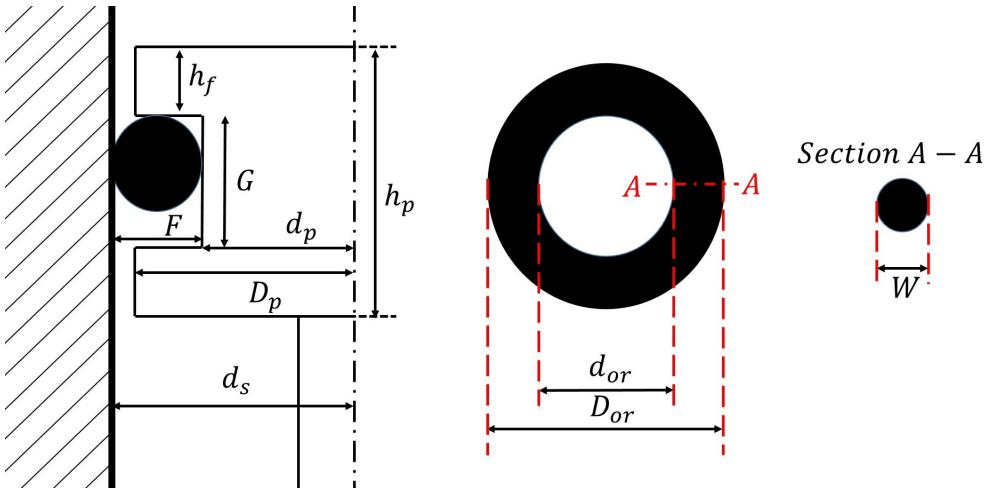

FIGURE 3.10: Schematic of the piston head (on the left) and O-ring (on the right) with the relevant design parameters to calculate the squeeze ratio W/F and the stretch $S = d_p/d_{or}$.

The handbook specification are guidelines for traditional engineering applications with high pressure and force exertions. It was noticed that following these guidelines resulted in high friction force between the piston and the sleeve.

Several pistons were 3D printed and tested for watertightness and friction force. Watertightness was tested by putting water in a core-sleeve assembly, manually pushing the piston, and inspecting for leaks. Figure 3.11 shows two snapshots of this process. The friction forces

experienced by the piston were roughly estimated using the deployment spring. All the pistons were lubricated with silicone paste, and the spring was used to advance the piston in the core. The piston that traveled the furthest was identified as the one featuring the lowest resistance to travel, and therefore the lowest friction force. The selected piston was the one that achieved the lowest friction force without any leak.

The final dimensions of the piston head are $d_p = 4.1$ mm, $D_p = 7$ mm, $G = 1.7$ mm, and $h_p = 3.4$ mm. The piston dimensions induce, for the O-ring, $G = 0.96W$, a 92% squeeze ratio, and a 92% stretch. The piston shaft measures 3 mm in diameter and 25 mm in length.

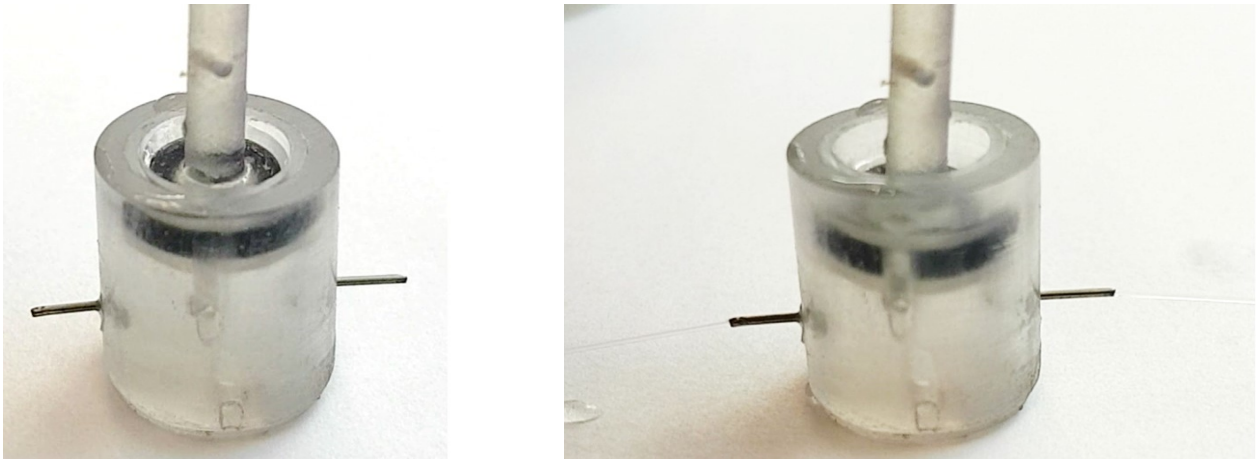

(A) $t = 0$ s (B) $t > 0$ s

FIGURE 3.11: Images of a successful core-piston watertightness tests at (A) $t = 0$ s and (B) $t > 0$ s. Water jets come out of the needles in (B) and no water leaks were observed behind the head of the piston.

3.4.3 Core-case-needle interaction

The objective of this section is to address the integration of the core-needle assembly developed in Section 3.4.1 into the case. The objectives are to achieve: low friction between the case and the core, no lateral movement of the core inside the case, and needle rotation from 0° to 60° as required.

The inner diameter of the case should have a small clearance with the core to achieve low friction force and no lateral movement of the core. The datasheets of the off-the-shelf

polycarbonate tubings specify the inner diameter of the case and the outer diameter of the core to be both 12.7 mm (1/2"). In practice, the two parts interfere with each other, so drilling and sanding inside the case is needed in order to obtain a low friction force. The inner diameter of the case is considered to be appropriate when the core is let go vertically on one end of the case, and it can free fall through and out of the case on the other end. The inner diameter of the case that met this requirement was 13.7 mm. The clearance between the core and the case is therefore $l_c = 0.5$ mm.

The holes of the case are designed to be V-shaped (drawing the path of the needle rotation), and with the same dimensions as the holes of the core. The assembly method for the core-case-needle system consists of (1) fully inserting the needles in the core, leaving the core's surface clear from protruding needles, (2) inserting the core into the case and aligning the holes of the core with those of the case, and (3) pushing out the needles from the core so they protrude through the holes of the case (Figure 3.17 in the following section–Section 3.4.4–shows pictures of the assembly process of the core, case, and needles). This method protects the silicone rubber hinge from detaching when installing the needles, and ensures the needles are properly connected with the inside of the core. Note that the rest position of the core-case assembly is with the needles deployed, at 0°.

3.4.4 Capsule manufacturing

The manufacturing process consists of machining some components, and 3D printing others. The piston and retraction pusher were 3D printed with the FORM2 printer. The needles, screws, and springs are off-the-shelf components. The core, case, sleeve, deployment cap, and retraction cap were machined as individual parts, though several machining steps were performed in assembly mode to obtain proper fitting of the machined components. Figure 3.12 shows the components before assembly and Figure 3.13 shows the assembled capsule.

FIGURE 3.12: Image of the capsule components. From left to right: piston, deployment cap, retraction pusher, retraction cap, core (with sleeve), and case. These components were assembled to build the complete capsule.

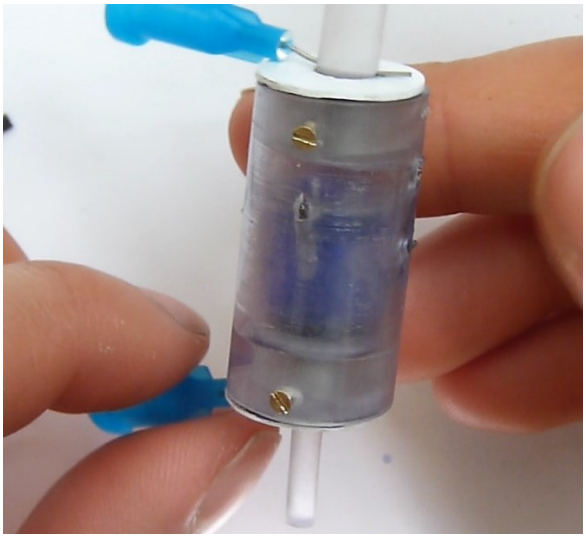

FIGURE 3.13: Image of the finished capsule assembly. The capsule is filled with water, used for the prototype test, and tinted blue, to facilitate its visualization.

The capsule was assembled by joining three sub-assemblies: the deployment cap sub-assembly, the retraction cap sub-assembly, and the core-case-needle sub-assembly (which includes the sleeve). Figure 3.14 shows these three sub-assemblies.

(A) Deployment cap sub-assembly: piston, deployment cap, and deployment spring.

(B) Retraction cap sub-assembly: retraction pusher, retraction cap, and retraction spring.

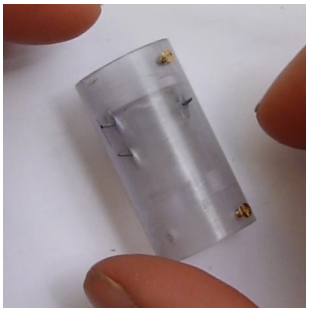

(C) Core-case-needle sub-assembly: core with sleeve, case, and needles.

FIGURE 3.14: Images of the three sub-assemblies that compose the capsule. The parts that compose each sub-assembly are described in each image.

The assembly steps of the complete capsule are shown in Figure 3.15. The first step consists of putting the core-case-needle sub-assembly into the retracted position (Figure 3.15a), and loading the capsule with blue inked water (used for the prototype test) with the help of a syringe (Figure 3.15b). The deployment cap sub-assembly is added next, by inserting the piston inside the core and screwing the deployment cap in place (Figure 3.15c). The core is held in the retracted position by friction with the piston. Finally, the retraction cap sub-assembly is added on the other end of the capsule and screwed into place (Figure 3.15d). At this stage, the capsule is ready for the final prototype test.

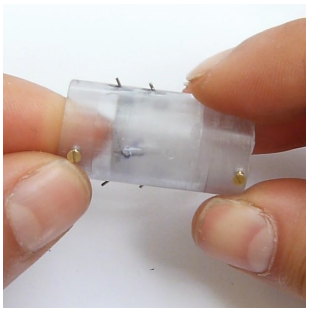

(A) Pushing the core to a retracted position.

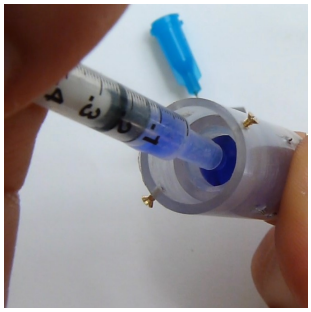

(B) Loading the capsule with inked water.

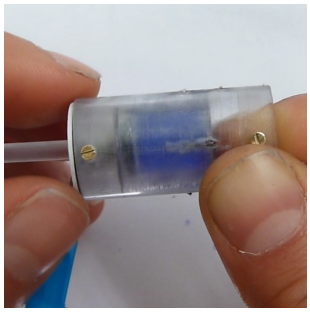

(C) Installing the deployment cap subassembly.

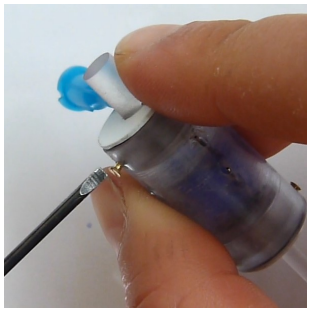

(D) Screwing the retraction cap subassembly.

FIGURE 3.15: Images of the final assembly process of the capsule. Each image describes a particular action taken during the assembly process.

Manufacturing and assembling a small capsule with different moving parts and a working fluid is very challenging. In terms of manufacturing, any small deviation from designed dimensions results in large discrepancies, which can be observed during assembly (see Figure 3.16c). Machining small features and handling small parts with standard machining tools require practice and training. Notwithstanding, vibrations of machines and deflection of cutting tools introduce unavoidable errors. Figure 3.16 illustrates some of these challenges.

In terms of assembly, the main challenge is the attachment of the needles with the core, which needs to be done while the core is in the case, and without pushing the silicone rubber seal inside the core. The needle assembly method involves prepiercing into the silicone rubber seal with a needle using a solid support inside the core. Additionally, when putting the capsule in the retracted position, some needles tend to get pulled out of the core. This can be solved by readjusting the placement of the needles as shown in Figure 3.17b.

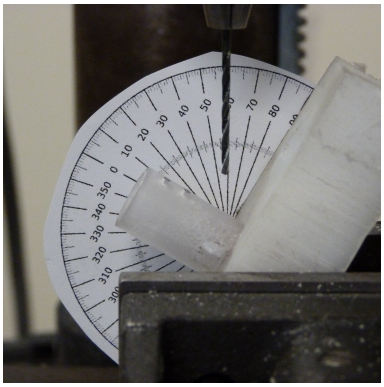

(A) Custom widget to help drill holes at 60° on curved surfaces.

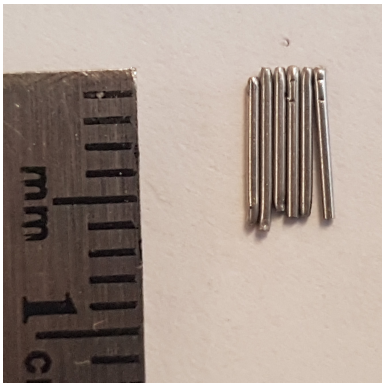

(B) Needles cut to ∼ 6 mm.

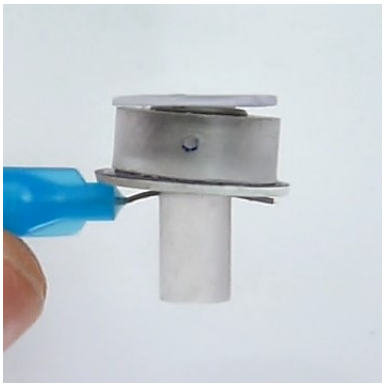

(C) Tilted retraction pusher in the retraction cap sub-assembly.

FIGURE 3.16: Images illustrating manufacturing challenges faced when prototyping the capsule. The images illustrate (A) the need of a widget to hold the cylinders when drilling, (B) the dimension variability of the needles, and (C) the amplification of small machining inaccuracies of components when assembled.

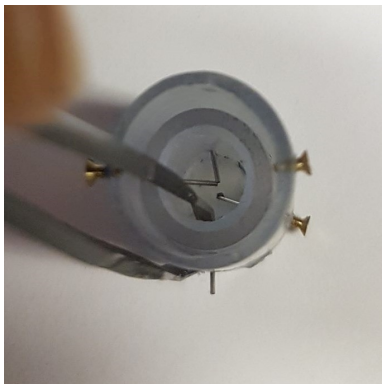

(A) Pushing needles out from inside the core.

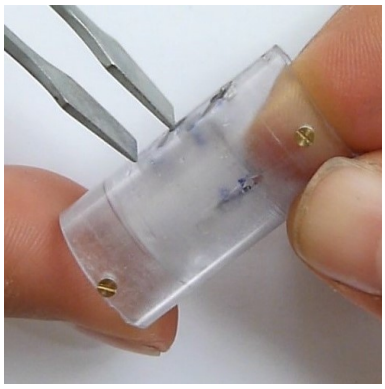

(B) Adjusting the needles after pushing down the core to its retracted position.

FIGURE 3.17: Images illustrating the core-case-needle assembly challenges. The images show two steps performed during needle installation.

3.5 Spring selection process

The objective of the spring selection process is to choose off-the-shelf springs to actuate the deployment motion and the retraction motion of the capsule. The deployment spring must be capable of deploying the needles and injecting the drug out of the capsule. The retraction spring must be capable of pushing the core back to its original position, thereby of partially recompressing the deployment spring.

The force requirements for the deployment spring need to be understood in order to select a spring that deploys the needles and injects the drug successfully, within a maximum injection time of 5 seconds. Mechanical testing is performed to obtain the force versus displacement profile of the piston throughout deployment and injection. The test is performed without any working fluid. This allows for a simpler test apparatus, since there is no need to fill the capsule with fluid at every test repetition. Therefore, this test measures all the deployment forces, except syringeability. Syringeability has been estimated in Section 3.3.4, thus its effect can be subsequently integrated and considered when selecting the deployment spring.

Section 3.5.1 decomposes the forces involved during capsule deployment, and anticipates the different force components to be experienced by the spring. Section 3.5.2 covers in detail the performed tests, in order to understand and characterize the force profile of the piston during deployment. Finally, Section 3.5.3 synthesizes the spring requirements, and justifies the selection of a deployment and a retraction spring.

3.5.1 Force decomposition

The force experienced by the deployment spring, called *piston force* in the following, is caused by four phenomena: core-case friction, hinge force (due to elastic deformation of rubber hinges), piston-core friction, and syringeability. The first two components occur during deployment and the last two during injection. Figure 3.18(a) shows where the forces originate from, during deployment and injection. The piston displacement with respect to the case is noted x. x_0 is the initial piston position, x_1 corresponds to the end of deployment and beginning of injection, and x_2 corresponds to the end of injection (Figure 3.18(b)).

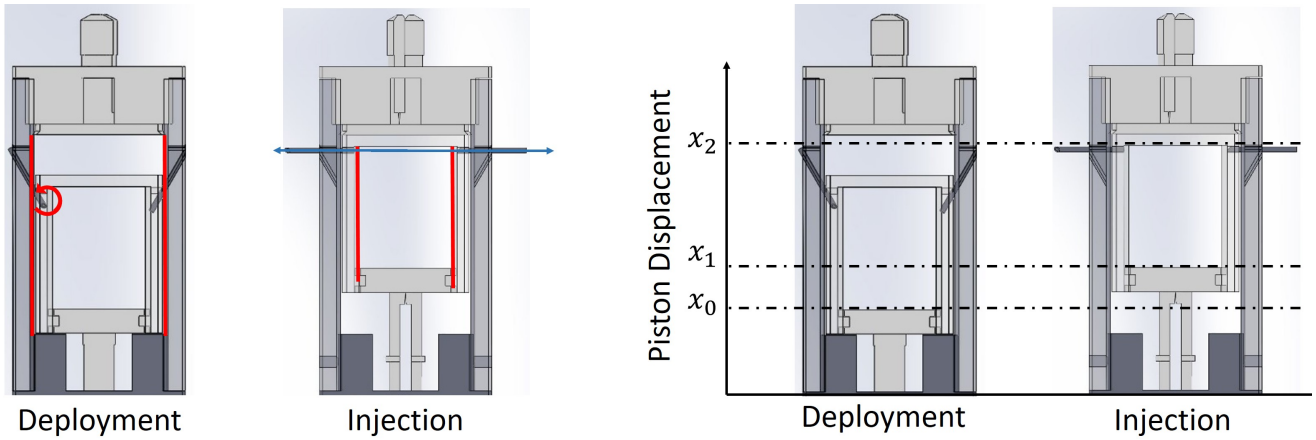

(A) (B)

FIGURE 3.18: (A) Diagram of a cross-section view of the capsule showing the four phenomena inducing piston force: core-case friction and hinge force during deployment (left), and piston-core friction and syringeability during injection (right). (B) Diagram of a cross-section view of the capsule showing the reference frame for the piston displacement x with respect to the case, where x_0 is the initial position, x_1 corresponds to the end of deployment and the beginning of injection, and x_2 corresponds to the end of injection.

During needle deployment, the piston force is expected to be the sum of core-case friction force and hinge force. Core-case friction is expected to be approximately constant from the beginning to the end of deployment (between x_0 and x_1). Hinge force is caused by the elastic deformation of the silicone rubber hinges, it can thus be expected to be approximately linear. The silicone rubber hinges are assembled with the needles in the deployed position (as explained in Section 3.4.3). Therefore, the hinge force is expected to be zero when the needles are deployed (at x_1), and opposed to core-case friction during deployment (i.e. negative from x_0 to x_1).

During injection, the piston force is expected to be the sum of the piston-core friction force and the syringeability force. Piston-core friction force is expected to be approximately constant, since it is due to solid friction. Its value should be higher than the maximum force required for full deployment, to ensure deployment occurs before injection. Syringeability forces are not measured in this test, since the measurements are performed without any working fluid, as stated earlier.

Figure 3.19 shows the expected piston force profile of the mechanical test.

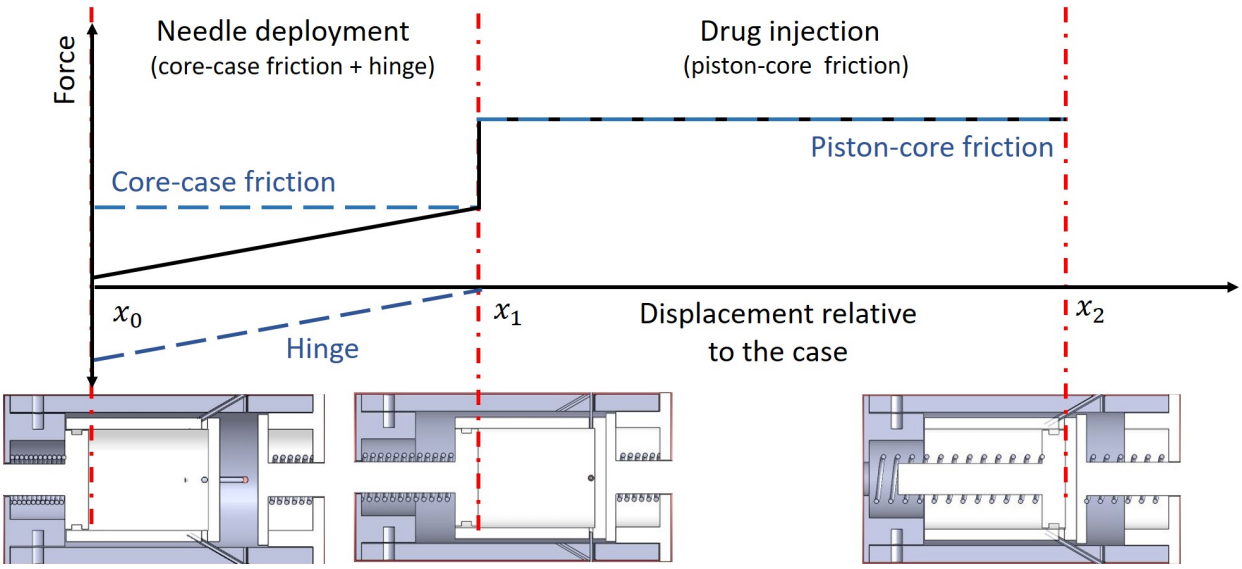

FIGURE 3.19: Diagram of the expected measured piston force profile. Piston force is plotted in the vertical axis, and displacement of the piston in the horizontal axis. During needle deployment (from x_0 to x_1), piston force is composed of core-case friction (constant), and hinge force. Hinge force is expected to be linear, zero at the end of deployment, and opposed to core-case friction during deployment. During injection (between x_1 and x_2), piston force corresponds to piston-core friction (constant and greater than core-case friction). Note that syringeability is not measured in this test.

3.5.2 Piston force test

The piston force test is a force-displacement test, controlled by piston-case displacement x. The test is performed between x_0 (undeployed position) and x_2 (fully deployed and injected position), at constant velocity. Piston force is measured by a load cell, and the obtained force profile is called *piston force profile*. The final version (without the springs) of the prototype was tested in this experiment.

To ensure reliability of the recorded data, and show independence of the results with respect to the speed used to advance the piston, the tests are performed at speeds varying from 0.05 mm/s to 2 mm/s. Additionally, in order to investigate the variability of the results

due to the assembly, the test apparatus and the capsule are completely disassembled and reassembled three times. The three resulting sets of tests are called *setups* in the following.

Test apparatus

Instruments The test apparatus is shown in Figure 3.20. It consists of a mechanical testing machine, a PC-based controller, and a computer. The mechanical testing machine and controller are manufactured by ADMET®. The mechanical testing machine has a horizontal loading setup, which consists of a static and a moving base. The static base is instrumented with a 500 lb load cell (ADMET® 300 Series Micro Test System) and the maximum speed of the moving base is 0.1 mm/s. Higher speed tests, i.e. 0.2 mm/s and 2 mm/s, are performed with a vertical testing machine, detailed in Appendix B. The sampling rate of the tests is set to 20 samples/second. The controller, MTESTQuattro®, is connected to a PC-based application program, the MTESTQuattro® Controller Firmware (Version MTQ 3.12.02).

Widget installation A testing widget was manufactured to clamp the prototype onto the testing machine. The widget consists of two parts: the piston holder and the capsule holder. The piston is assembled onto the piston holder as shown in Figure 3.21. A lateral screw holds the piston shaft in position. The core-case-needle assembly is assembled onto the capsule holder also shown in Figure 3.21. The capsule holder features a tube of equal diameter and length as the retraction cap. This tube is installed in the case, where the retraction cap would normally be installed. Each holder is glued onto a base of the testing machine. The capsule holder is glued first. Then, the piston holder is glued with the piston fully inserted inside the core to ensure the proper alignment of the piston with the core. The capsule and widget, installed on the testing machine, are shown on the bottom image of Figure 3.20.

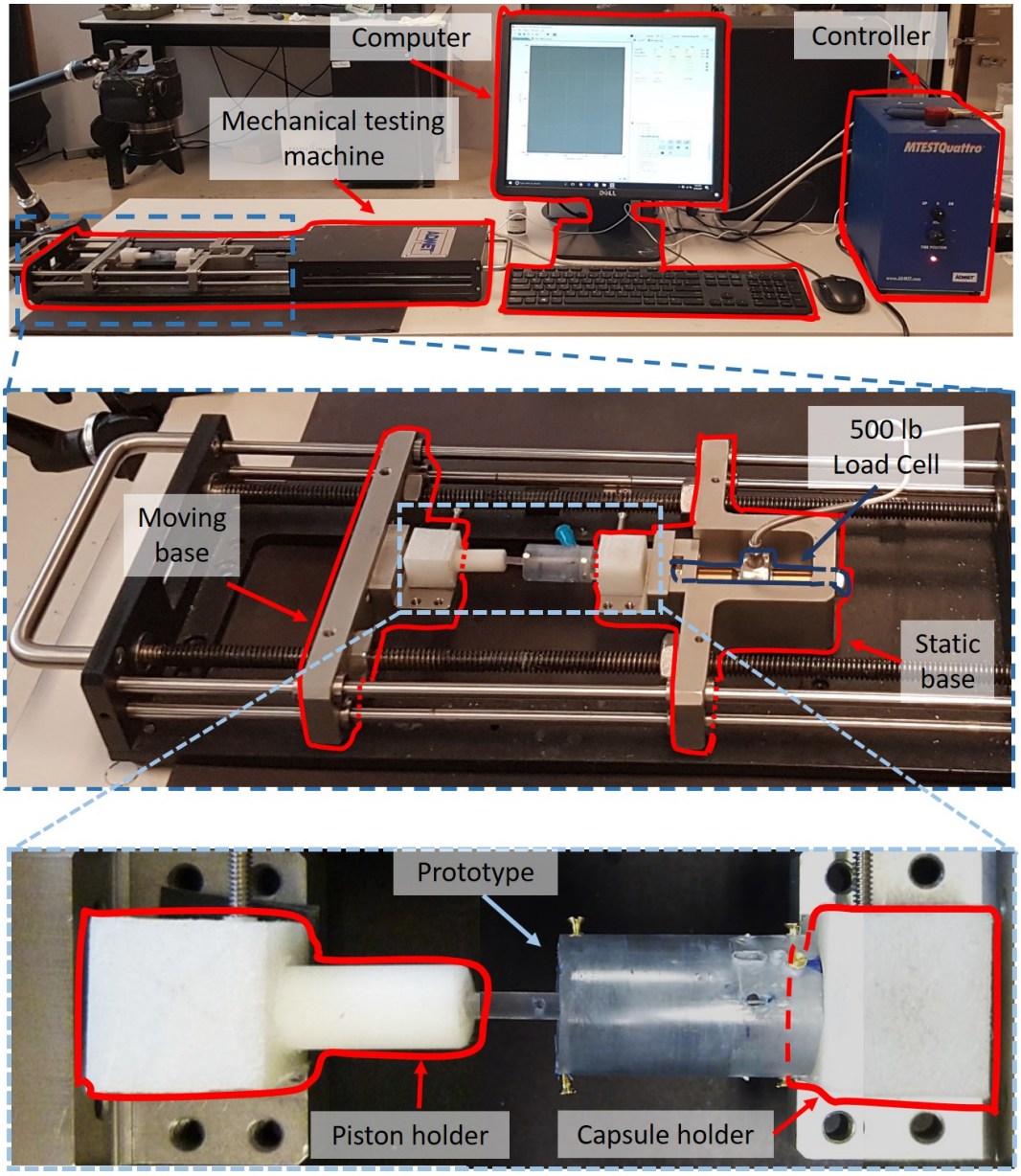

FIGURE 3.20: Images of the horizontal force measuring equipment. The top image highlights the apparatus components. The middle image shows a closer view of the testing bed of the machine. It shows the capsule prototype, installed with the testing widget, onto the moving and static base platforms of the machine. The bottom image shows a closer view of the capsule prototype. The testing widget, composed of the piston holder and the capsule holder, is glued to the platform of the testing machine. The capsule prototype is directly mounted onto the testing widget. The alignment of the capsule with the piston is calibrated before the test.

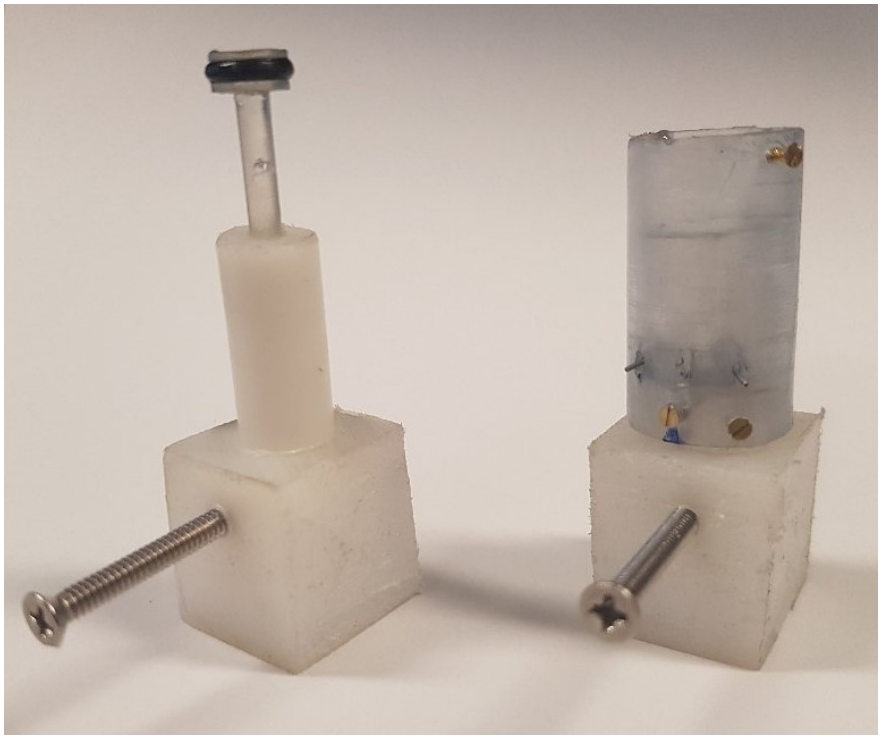

FIGURE 3.21: Image of the capsule prototype mounted on the testing widget. On the left, the piston is installed in the piston holder. On the right, the core-case-needle assembly (upside-down) is installed in the capsule holder.

Before the first test, the setup needs to be adjusted to ensure that the widget, the tube holding the piston and the capsule, are properly aligned. The piston is moved out using the controllers until it just exists the core. The required alignment adjustments are visible when the piston is at the entry point of the core. Once adjusted, the piston is fully pushed in and out, to let the system settle in place. This procedure is repeated until there are no visible improvements required.

Test Matrix Table 3.4 details the conditions of the ten performed tests. This test matrix allows to investigate the dependency of the piston force profiles on both test speed and setup number. The number of test speeds per setup is not uniform because the needles detached from the capsule after multiple deployment and retraction cycles. A complete reassembly of the capsule was thus necessary before the scheduled number of test was finished.

TABLE 3.4: Piston force test matrix. In order to assess the repeatability of the measurements, the prototype and the test apparatus are disassembled and reassembled three times during the testing process. This defines the three different setups.

Test number	Setup number	Speed (mm/s)
1	1	0.1
2	1	0.1
3	2	0.1
4	2	0.05
5	2	0.05
6	3	0.1
7	3	0.1
8	3	0.1
9	3	0.1
10	3	0.05

Results

Figure 3.22 shows the piston force profiles obtained from tests described in Table 3.4. Piston force is plotted on the vertical axis, and piston-case displacement on the horizontal axis. The *maximum and minimum boundaries* (in black), respectively, correspond to the maximum and minimum overall forces experienced among all the measurements (in grey). These boundaries form an envelope in which piston force is contained for all the measurements.

The set of observed force profile can be separated into four stages. Each of these four stages corresponds to the observation of a specific motion between the capsule's components:

- a force increase from $x_0 = 0$ mm to $x_1 = 3.5$ mm, corresponding to needle deployment;
- a peak force F_{peak}, located between $x_1 = 3.5$ mm and $x_1' = 3.8$ mm, corresponding to the end of needle deployment and the beginning of injection. The position of the peak is slightly different for each test. x_1 and x_1' are defined by the extreme positions of the force peaks F_{peak}, observed in all tests;

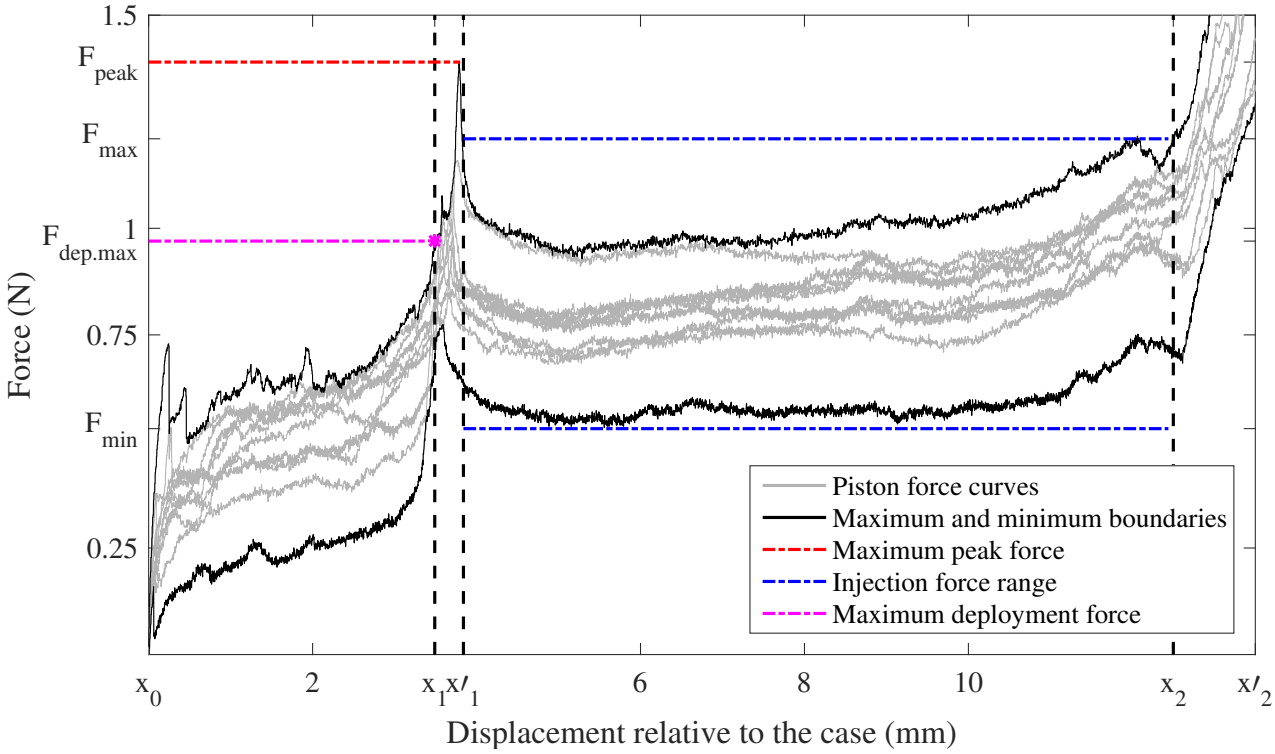

FIGURE 3.22: Graph of force versus displacement showing piston force curves (in grey), and the minimum and maximum piston force curves (in black). These extremes curves form an envelope in which all piston force curves are contained. The relevant observed values of the piston force curve are annotated: maximum peak force (in red), injection force range (in blue), and maximum deployment force (in magenta).

- a plateau from $x_1' = 3.8$ mm to $x_2 = 12.5$ mm, corresponding to the injection motion. x_2 is defined by the piston position where the O-ring just begins to interact with the needle holes; and
- a final force shoot up from $x_2 = 12.5$ mm to $x_2' = 13.6$ mm, when the piston reaches the needle holes and the end of the core. x_2' corresponds to when the piston reaches the end of the core.

The capsule behaves as designed: needle deployment occurs before injection, and a clear distinction between needle deployment (from x_0 to x_1) and injection (from x_1' to x_2) is

identified. The maximum force at x_1 is called *maximum deployment force*, and is denoted by $F_{dep.max}$. A force peak is observed at the transition between needle deployment and injection (from x_1 and x_1'), and is denoted by F_{peak}. During injection (from x_1' to x_2), the global maximum force observed among all tests is called F_{max}, and the global minimum force observed during injection among all tests is called F_{min}. The minimum and maximum injection forces define the *injection force range* $[F_{min}, F_{max}]$.

Figure 3.22 shows the important parameters of the force profile, and Table 3.5 gathers the corresponding values.

TABLE 3.5: Summary of relevant values gathered from the piston force tests.

Parameter of interest	Units	Minimum	Maximum
Maximum force at x_1, $F_{dep.max}$	N	-	0.97
Peak force magnitude F_{peak}	N	0.83	1.39
Peak force position (x_1 and x_1')	mm	3.5	3.8
Maximum injection force F_{max}	N	-	1.21
Minimum injection force F_{min}	N	0.53	-

Discussion

This section first considers the repeatability of the tests, characterized by test dependence on setup and speed. Then it discusses the piston force profiles and their implications.

Setup dependence Figure 3.23 shows the test curves from Table 3.4, colored by setup number. All the observed force profiles are contained within the injection force range [F_{min}, F_{max}]. The injection force ranges for all tests, setup 1, 2, and 3, are given in Table 3.6. The force ranges among setups greatly overlap, and the variation among the recorded force profiles shows no particular setup-dependent trend. Thus, Figure 3.23 suggests that there is no significant effect of setup on the measured piston force.

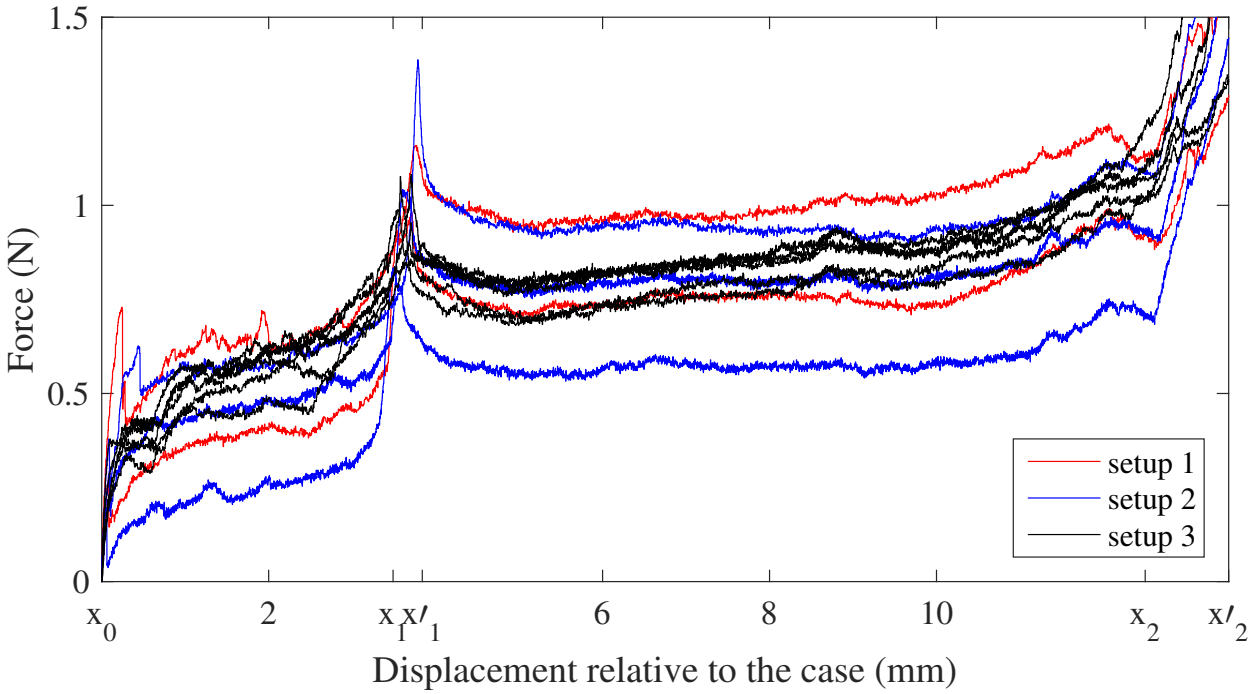

FIGURE 3.23: Plot of experimental piston force versus displacement from tests listed in Table 3.4, colored by setup number.

TABLE 3.6: Injection force range for all curves, setup 1, setup 2, and setup 3.

Set of curves	$[F_{min}$ - $F_{max}]$ (N)
All	0.53 - 1.21
Setup 1	0.70 - 1.21
Setup 2	0.53 - 1.12
Setup 3	0.68 - 1.21

Test speed dependence The capsule is designed to operate with a piston speed of at least 2 mm/s. If the injection is performed in 5 seconds, the average piston speed is 2 mm/s. Higher piston speeds could be obtained if injection was shorter. It is therefore important to understand the effect of speed on the measured piston force profile.

Figure 3.24 shows test curves from Table 3.4, colored by speed. Note that the two sample curves added at 0.2 mm/s and 2 mm/s were obtained with a vertical testing machine (as described in Appendix A). The maximum test speed of the vertical machine is 8.4 mm/s, while that of the horizontal machine is 0.1 mm/s. The data obtained from the vertical machine suffers from a low signal-to-noise ratio. Thus, only one sample curve of the 0.2 mm/s and 2 mm/s tests are plotted in Figure 3.24 to show the observed trends and magnitudes. The results shown in Fig. 3.24 suggest that there is no significant effect of speed on the measured piston force, within the limits of variability observed for the different setups.

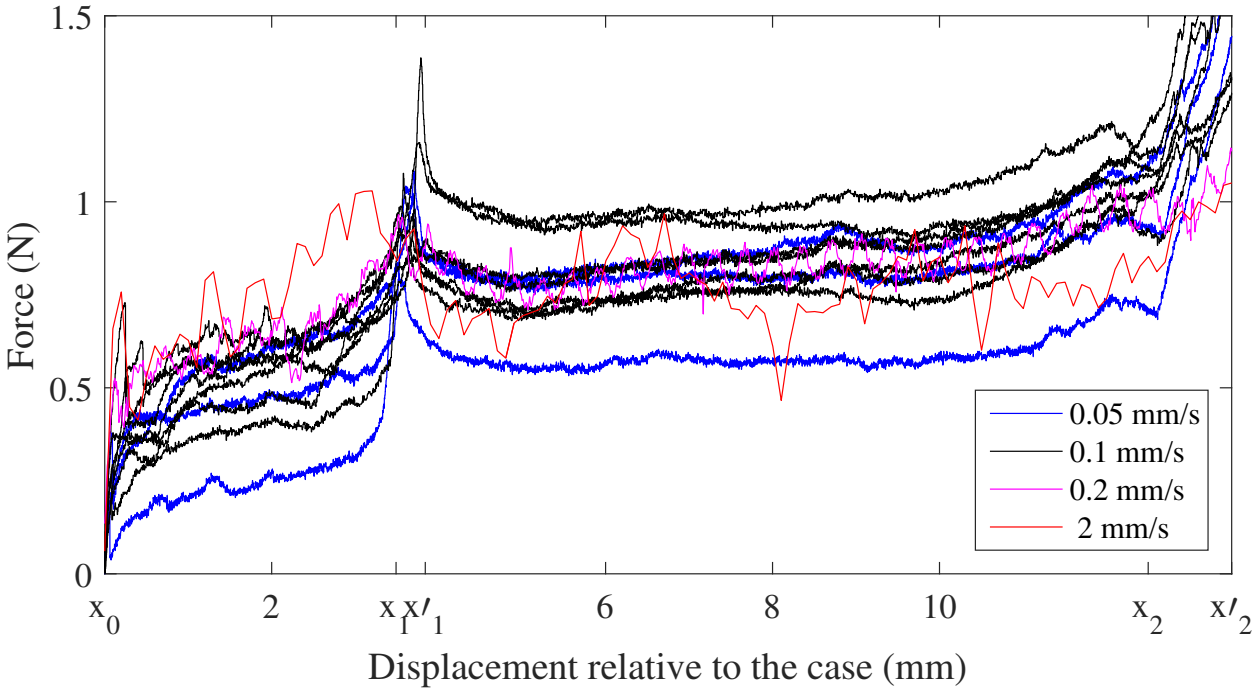

FIGURE 3.24: Plot of experimental piston force versus displacement from tests listed in Table 3.4, colored by testing speed. Additionally, measurements obtained using the vertical testing machine at 0.2 mm/s and 2 mm/s are also shown.

Model for core-case friction and hinge force The piston force measured during deployment is not linear. However, it follows the expected increasing trend (shown in Figure

3.19). A linear model, calibrated on the measured deployment force, is useful for the selection of the springs. This calibration is performed on the highest experimental curve (i.e. the maximum boundary); the obtained model is thus conservative. During deployment, between x_0 and x_1, the piston force $F_{dep}(x)$ can be modeled as the sum of the constant core-case friction force F_{c-c} and the linear hinge force F_h:

$$F_{dep}(x) = F_{c-c} + F_h(x) \tag{3.13}$$

Additionally, it is assumed that hinge force is zero at x_1, where the silicone rubber hinges are in their natural position. By evaluating Eq. (3.13) at x_1, since hinge force is then zero, the value of core-case friction is obtained: $F_{c-c} = 0.97$ N. By evaluating Eq. (3.13) at x_0, the maximum value of hinge force is obtained:

$$F_h(x_0) = F_{dep}(x_0) - F_{c-c}(x_0) = -0.97 \text{ N} \tag{3.14}$$

This conservative linear trend for the deployment force profile is used later, during the retraction spring selection process.

Static piston-core friction The peak force observed from x_1 to x_1' can be inferred to be caused by static friction between the piston and the core. The force peak coincides with the moment where deployment ends and the piston starts traveling inside the core. The static friction force was not initially modelled, but is observed consistently in all tests. This force peak is desired, as it separates deployment from injection. The static friction prevents the piston from sliding prematurely into the core before needle deployment is completed. Additionally, the static friction is also desired to prevent the hinges from displacing the core upwards, which would deploy the needles before activation.

Kinetic piston-core friction The plateau observed from x_1' to x_2 can be inferred to be caused by the kinetic friction between the piston and the core. It is contained within the injection force range $[F_{min}, F_{max}]$. The injection force range is of particular interest, since the

spring provides the lowest force at the end of injection. Therefore, F_{max} at x_2 is a limiting factor to consider when selecting the deployment spring.

3.5.3 Spring selection

Deployment spring

The deployment spring should provide sufficient force to push the piston until the end of the core within the required injection time $t_{inj} = 5$ s. It should overcome the forces measured in the mechanical test, plus syringeability, the only speed-dependent force of the system.

At the maximum desired injection time $t_{inj} = 5$ s, the average estimated syringeability force is $F_{syr} = 0.03$ N (from Section 3.3.4), which corresponds to 2% of the maximum piston force measured during injection $F_{max} = 1.21$ N. For simplicity, during the spring selection process, only piston-core friction force is considered in the injection phase. This assumption is valid since a spring capable of providing enough force to overcome piston-core friction at the end of injection (x_2), provides a higher force throughout capsule deployment (from x_0 to x_2). This ensures that piston speed is higher than the required average speed (in this case, 2 mm/s to achieve $t_{inj} = 5$ s) during most of the injection.

At the end of piston displacement, the spring should have a force equal to or greater than $F_{max} = 1.21$ N, which is the maximum recorded piston force at x_2. Figure 3.25 shows the minimum and maximum force boundaries of the piston force, and their intersection with x_2, to illustrate this force requirement.

The size of the capsule imposes geometrical constraints on the deployment spring's outer diameter D_o and compressed length x_c. D_o is determined by the sleeve's inner diameter (7.9 mm), since the spring needs to travel inside the core with the piston. The spring's compressed length x_c should be as small as possible to avoid any inefficient use of volume. An arbitrary maximum $x_c = 5$ mm, corresponding to 16% of the effective capsule length (31.5 mm), is set.

Table 3.7 lists all the off-the-shelf springs available at D.R. Templeman Co.® that meet the geometrical constraints of the capsule. The parameters defining each spring are their

stiffness k and their free length x_f, which determine the spring force versus displacement profile. All the springs from Table 3.7 provide a higher force than the static friction force at x_1, however they all fall within the force envelope at x_2.

TABLE 3.7: Springs from D.R. Templeman Co.® that meet the geometrical requirements for the deployment spring. The selected deployment spring is in bold font.

Spring number	D_o [mm]	x_f [mm]	x_c [mm]	k [N/m]	$(x_f - x_c)$ [mm]	Force at x_2 [N]
1	**6.1**	**19.1**	**3.2**	**280**	**15.8**	**0.93**
2	6.1	20.6	4.2	210	16.5	0.83
3	6.1	20.6	5.0	245	15.6	0.76
4	6.1	20.6	5.2	297	15.4	0.87

Spring 1 is selected because it features the lowest compressed length, and the highest force at x_2. Note that a custom spring with enough force to achieve full injection and that meets the geometry requirements could be designed. However, spring 1 is sufficient to demonstrate the proof of concept of the mechanism.

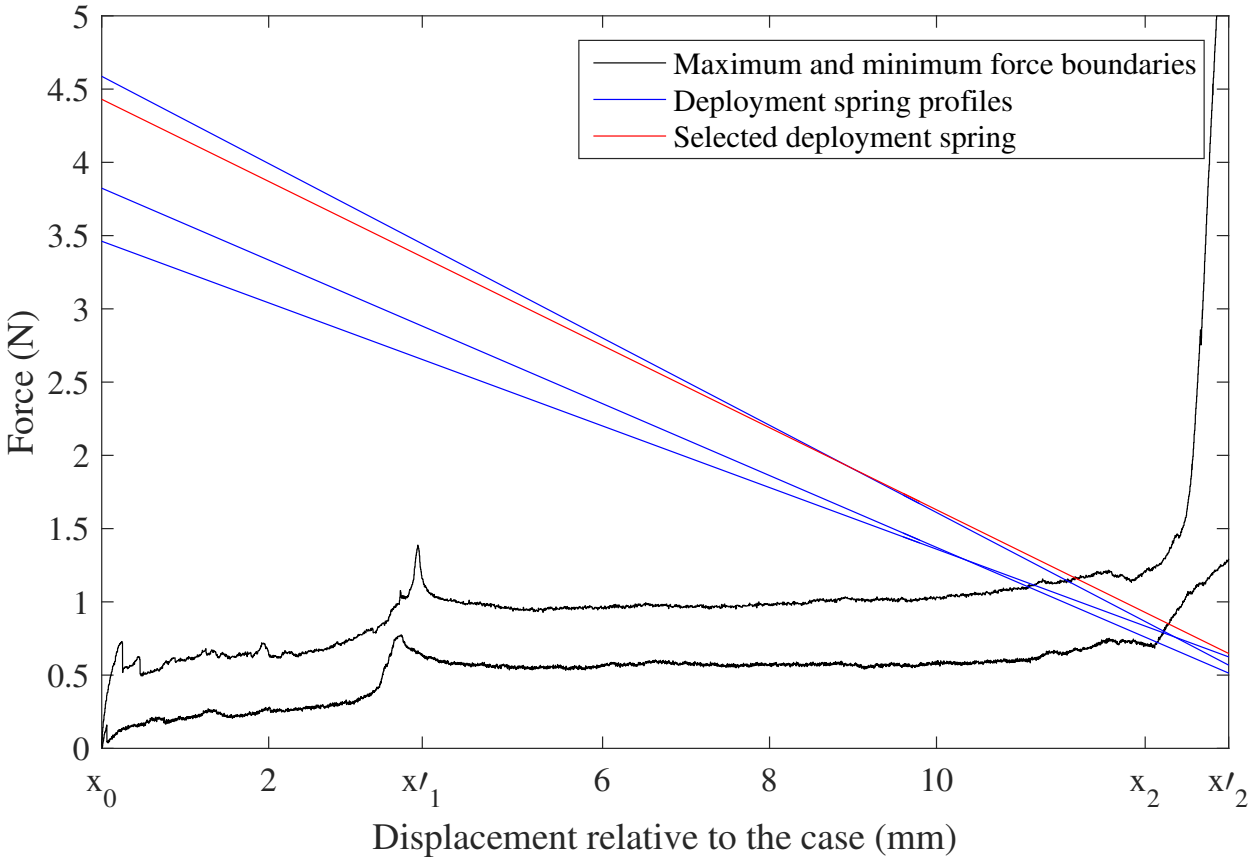

FIGURE 3.25: Plot of force versus piston displacement showing the theoretical force profiles of deployment springs from Table 3.7 (in blue), and the experimental piston force envelope (in black). The chosen spring (in red) is selected because it provides the highest force at the end of injection.

Retraction spring

The retraction spring should be capable of pushing the core back to its initial position, thus retracting the needles inside the case. The core needs to travel 3.8 mm backwards. This travel corresponds to x'_1, the maximum core-case displacement observed during needle deployment. The final core position after deployment is $x'_2 = 13.6$ mm, which corresponds to the designed piston travel distance. Translating this information into piston-case displacement, the piston needs to travel from $x'_2 = 13.6$ mm to $x_3 = 9.8$ mm, in order to fully retract the needles.

Three forces oppose needle retraction between x_2' and x_3: the core-case friction force F_{c-c}, the force due to the silicone rubber hinges F_h, and the force required to partially recompress the deployment spring. The profiles of hinge force and of core-case friction can be obtained using the simple model described during discussion. The deployment spring force corresponds to the theoretical force profile of the selected deployment spring between x_2' and x_3. The three forces add up to the *minimum retraction spring force boundary*, which is the minimum force the retraction spring should exert on the core in order to retract the needles.

Figure 3.26 shows the three force components and the minimum retraction spring boundary. The minimum force the retraction spring needs to exert corresponds to the maximum force required to complete retraction at x_3, $F_{ret.min} = 3.64$ N.

The size of the capsule imposes geometrical constraints on the retraction spring. The outer diameter D_o and compressed length x_c are the two parameters of interest, where D_o needs to be at most 12.7 mm, and x_c is desired to be as small as possible. Table 3.8 lists available off-the-shelf retraction springs from D.R. Templeman Co.® that meet the geometry specification. Spring 2 is selected, because it provides the lowest sufficient force to achieve needle retraction.

TABLE 3.8: Springs from D.R. Templeman Co.® that meet the geometrical requirements for the retraction spring. The selected retraction spring is in bold font.

Spring number	D_o [mm]	x_f [mm]	x_c [mm]	k [N/m]
1	6.2	10.9	2.9	665
2	**6.2**	**12.3**	**2.8**	**700**
3	8.1	10.5	2.9	1016
4	5.5	14.1	3.2	683
5	7.6	14.5	3.7	858

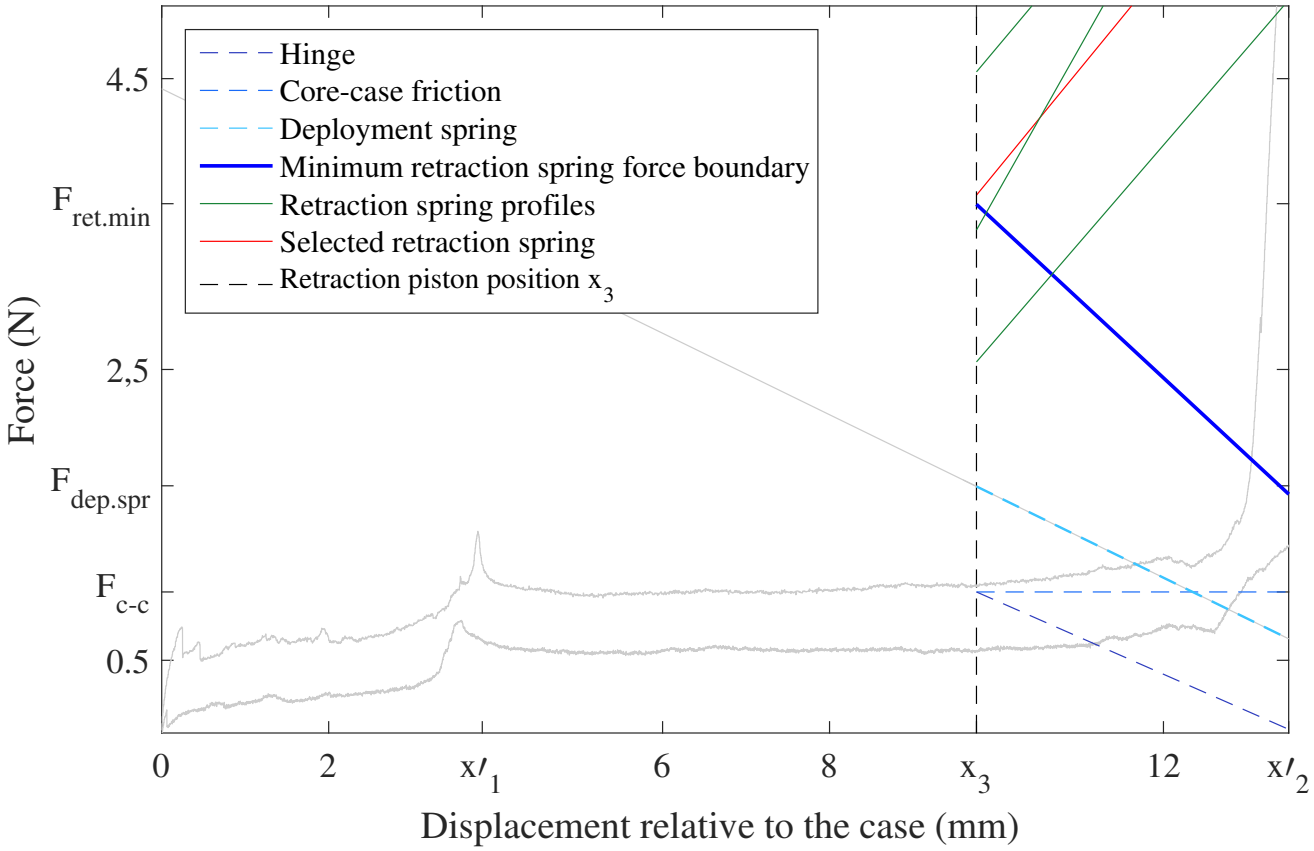

FIGURE 3.26: Plot of force versus piston displacement showing the theoretical force profiles of retraction springs from Table 3.8 (in green), and the minimum retraction spring force boundary (in blue). The minimum retraction spring force boundary is composed of the core-case friction force, the hinge force, and the resistance imposed by the deployment spring. Spring 2 (in red) is selected because it provides the smallest sufficient force at the end of retraction.

Chapter 4

Prototype and design assessment

4.1 Chapter overview

This chapter covers the assessment of the final Spanish newt capsule prototype and design. A final prototype test is performed, aiming to prove the concept and determine the prototype performance. This chapter is structured in four sections. Section 4.2 covers the details of the prototype test, Section 4.3 provides an assessment of the tested prototype and the Spanish newt design, and Section 4.4 covers the areas of improvement of the prototype.

4.2 Final prototype test

The objectives of the final prototype test are to show that the DISC prototype operates as expected and that it matches the requirements established in Chapter 2. The final prototype is the assembled capsule, equipped with the selected springs, and filled with tinted water. The test consists of triggering manually the deployment and retraction mechanism, and filming of the process for later analysis.

4.2.1 Test set-up

The set-up elements of the test consist of a clamping vice, a camera, a camera arm, and the final prototype, loaded with tinted water, and the compressed deployment and retraction

springs selected in Section 3.5.

The clamping vice holds the final prototype by the deployment and retraction caps, leaving the piston and retraction pusher shafts free to travel inside the capsule. Figure 4.1 shows a picture of the clamping vice-capsule set-up. Activation of the deployment and retraction mechanism consists of removing the pin that holds the corresponding spring in a compressed state. Deployment and retraction are triggered individually. Deployment is activated first, followed by retraction, once deployment and injection are completed. The camera used to record the test is a Panasonic® model No. DMC-FZ45 with 24x optical zoom and 14 Megapixels, set at a recording frequency of 24 frames per second.

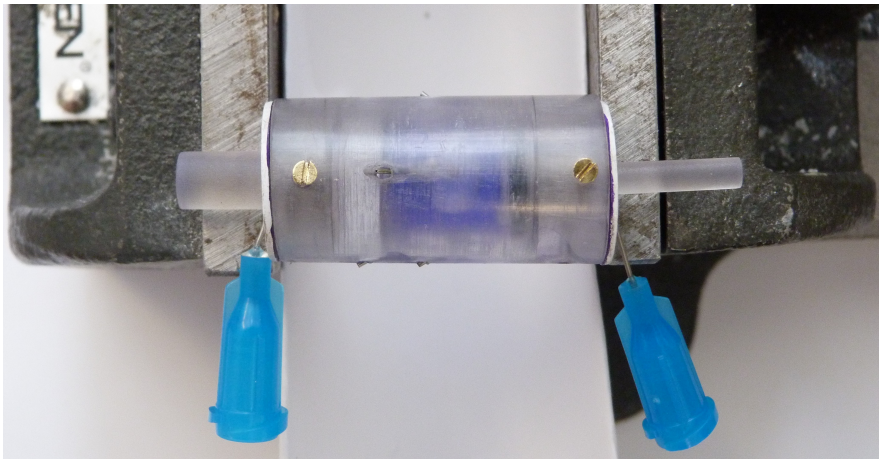

FIGURE 4.1: Image of the final prototype test set-up. The capsule is held by a clamping vice at its two extremes, the deployment and the retraction caps. The two pins, holding the deployment and retraction springs in place, are shown in light-blue. (Note that the prototype shown here is the older prototyped version with six needles).

The durations of deployment, injection, and retraction are obtained from analyzing the video of the tests. The number of frames between different events are counted and translated into seconds. The time between two frames corresponds to 1/24 s. Frame #0 is defined as the frame prior to the activation of deployment.

4.2.2 Results

The final prototype achieves deployment, injection, and retraction successfully. Figure 4.2 shows some frames extracted from the video of the test. The total time of capsule operation is under 1.5 s. Table 4.1 summarizes the number of frames and respective duration in which an event (deployment, injection, or retraction) is observed.

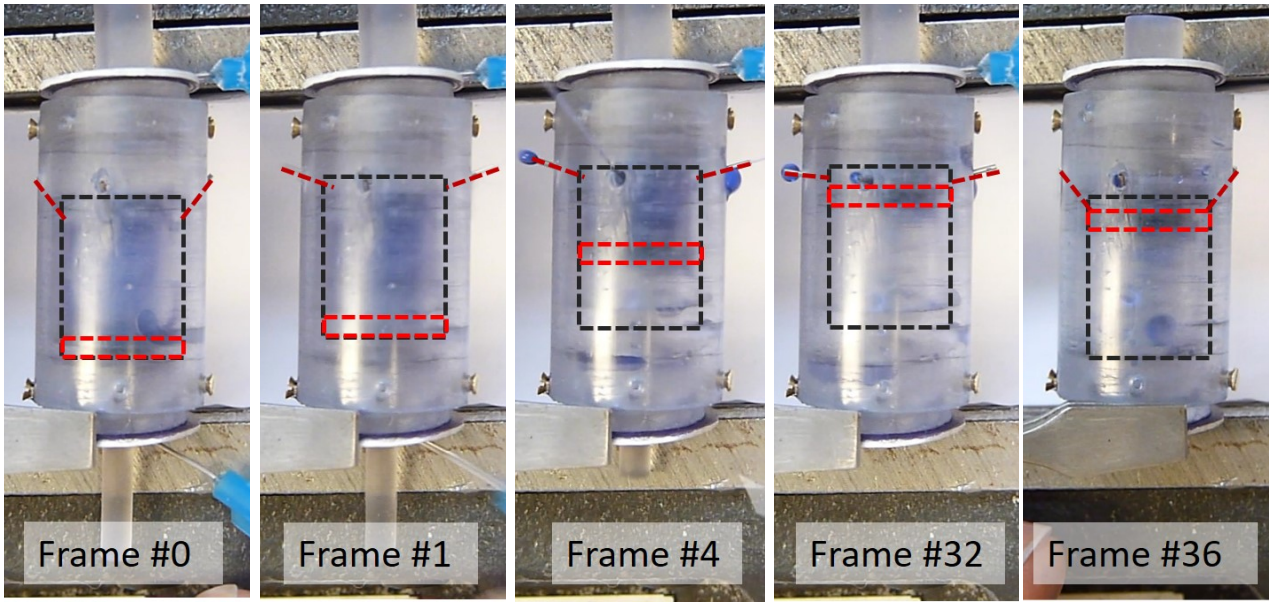

(A) Undeployed. (B) Deployed and injecting. (C) Injecting. (D) Fully injected. (E) Retracted.

FIGURE 4.2: Images of the relevant frames extracted from the final prototype test recording. The images are labeled with their respective frame number and show the prototype at different stages. Note that the core, piston, and needles, are traced in black, red, and burgundy dashed-lines, respectively, to better visualize their position at every stage.

TABLE 4.1: Time characterization of the final prototype.

Event	Number of frames	Duration (s)
Needle deployment	1	$t_{dep} \leq 0.04$
Injection	32	$1.29 \leq t_{inj} \leq 1.33$
Retraction	4	$t_{ret} \leq 0.17$
Total	36	$t_{tot} \leq 1.50$

Figure 4.3 shows an annotated version of Frame #4, with the needles deployed and injecting. The needles are deployed at an angle of 15 degrees (for reference, the designed angle is zero degrees). One possible reason for this discrepancy is the fitting of the retraction pusher (as shown in Figure 3.16c), which can prevent the full displacement of the core. The deployed needle length is measured to be 1.9 ± 0.5 mm (for reference, the designed length is 2 mm).

Water exits through all four needles during injection, indicating that the needles did not get blocked during assembly nor deployment.

The total injected volume was not measured. Only one leak was observed at the case-needle interface, as shown in Figure 4.3. A water drop formed on the case at the interface with the needle during injection, and as injection progressed, the drop increased in size. The source of this leak is attributed to the detachment of the silicone rubber hinge. Assembly of the needles onto the core is challenging; the silicone rubber hinges get pushed inside the core during needle installation, and sometimes detach from the wall of the core, providing an escape route for the fluid.

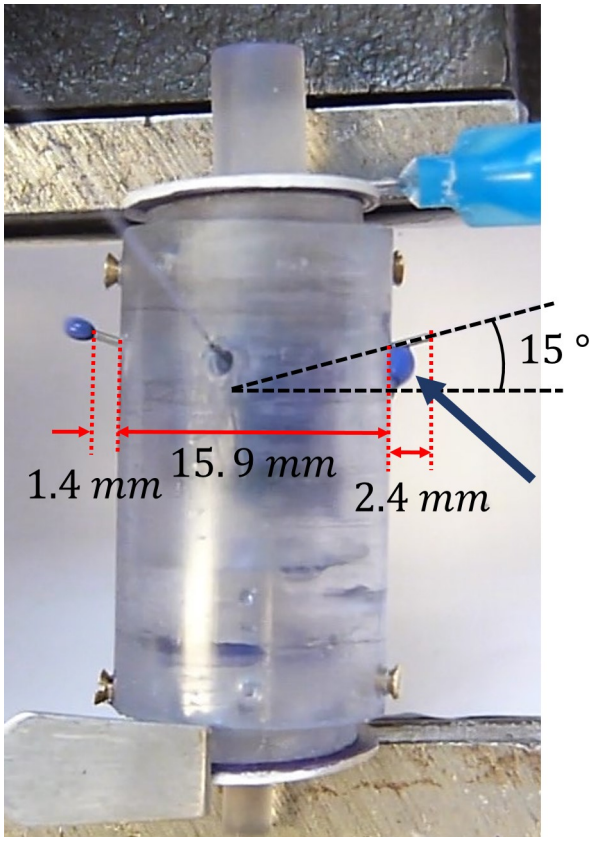

FIGURE 4.3: Image of the final prototype test at frame #4, fully deployed and injecting. The image shows the deployed needle length and angle. The blue arrow indicates the location of the observed leak.

4.3 Prototype and design assessment

The final capsule prototype measures 31.5 mm in length and 15.9 mm in diameter. It is capable of deploying needles by 1.9 ± 5 mm and at 15°, injecting water in less than 1.33 s (well below the maximum target time of 5 s), and fully retracting the needles. The minor leak observed at the case-needle interface is a product of manufacturing defects. The final prototype performance is compared to the mechanism requirements (see Section 2.2) in Table 4.2.

TABLE 4.2: Final prototype performance overview with respect to the mechanism requirements from Section 2.2.

Requirements	Prototype performance
Needles must be distributed radially	Achieved by design
Deployment angle $\alpha_{dep} = 0°$	$\alpha_{dep} = 0°$ in spring selection process test, $\alpha_{dep} = 15°$ in final prototype test
Needle deployment length of 1 - 2 mm	1.9 ± 0.5 mm
Fully retract the needles	Achieved
Inject $V_{drug} = 0.5$ mL	Loaded drug volume: 0.5 mL. Injected volume not measured
Injection time $t_{inj} \leq 5$ s	Achieved: $1.29 \leq t_{inj} \leq 1.33$
Must be watertight	Leak at core-needle attachment point
Maximum size: 35 mm in length by 20 mm in diameter	Capsule size: 31.5 mm in length by 15.9 mm in diameter
Must be easy to manufacture	Achieved by design

The prototype partially achieves the required needle deployment angle and length, and watertightness targets. Manufacturing capabilities and processes need to be improved to fully achieve those requirements. Aside from manufacturing problems, the final prototype is capable of deploying needles, injecting the drug, and retracting needles. The Spanish newt inspired mechanism has therefore proven itself a useful and relevant needle deployment and retraction mechanism design for drug injecting swallowable capsules.

4.4 Areas of improvement

There are three main areas of improvement of the Spanish newt design: manufacturing process, miniaturization opportunities, and including puncturing requirements into the design.

4.4.1 Manufacturing process

The machining methods used to build the Spanish newt prototype were sufficient for demonstrating the concept. However, the performance can be improved with the use of specialized manufacturing methods (such as industrial 3D printing and injection molding). Industrial

3D printers offer better resolution and a different build process, allowing them to achieve thin-walled precise prints, with no print supports that interfere with the parameters of interest of the capsule components. Moreover, specialized capsule manufacturing equipment can be used to make a custom capsule with particular specifications. The wall of a standard hard shell commercial capsules is about 0.1 mm thick, and a standard soft shell commercial capsules is about 0.4 mm thick. Such wall thicknesses should set the wall thickness target for future design iterations.

Finally, the needle-core assembly can be improved to avoid detaching the silicone rubber seal from the core, which causes leaks in the capsule. This can be achieved by investigating an alternative assembly method, custom needles, and new materials for the flexible hinge.

4.4.2 Miniaturization opportunity

The total capsule volume V_{total} of the prototype is 6.3 mL, which represents 12.6 times the loaded drug volume. The volume contribution of each component is given in Table 4.3, and the diagram showing their corresponding section in the capsule is shown in Figure 4.4.

TABLE 4.3: Absolute and relative volume contributions of the capsule components.

Component	Absolute volume contribution (mL)	Relative volume contribution (%)
Drug	0.5	8
Retraction	1.4	22
Case	1.4	22
Core	1.1	17
Piston	0.7	11
Deployment	1.3	20
Subtotal: empty capsule	6.2	92
Total	**6.7**	**100**

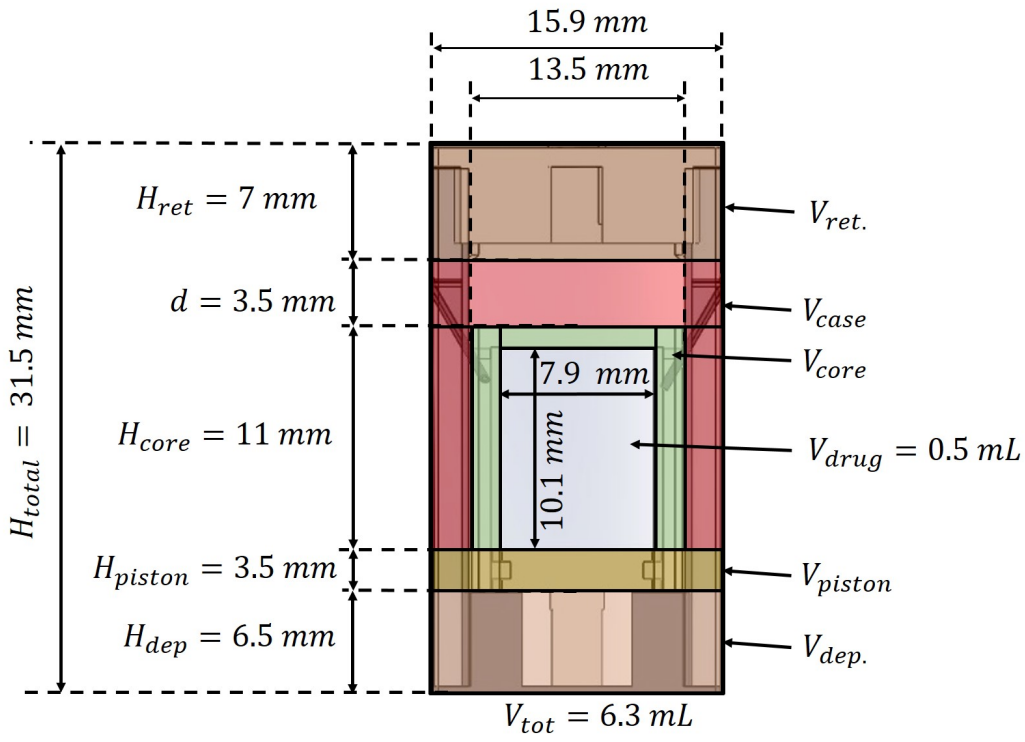

FIGURE 4.4: Diagram of the cross-section view of the capsule design. The volume contribution of each component is sectioned, labeled, and shown in a distinct color. The total volume of the capsule is 6.3 mL. Individual volume contributions of components are listed in Table 4.3.

Miniaturizing the capsule is possible by improving and changing the manufacturing methods used to build the capsule components. The three main miniaturizing opportunities consist of changing the capsule manufacturing method, using conical springs, and buying custom O-rings.

The case wall thickness t_{case} could reach an ideal minimum of 0.6 mm, equivalent to the minimum thickness of a hard gelatin capsule (0.1 mm) plus the needle diameter (0.5 mm), which needs to be contained within the body of the case. The core thickness t_{core} could reach an ideal minimum of 0.5 mm, corresponding to a hard capsule shell (0.1 mm) plus a soft capsule shell (0.4 mm), integrated one inside the other. The hard/soft capsule shell combination is done to obtain a structure analogous to the silicone rubber hinge.

Conical springs can also be designed so that their compressed length is equivalent to the thickness of the constitutive wire. Most common wire thicknesses of small springs are approximately 0.5 mm. The deployment and retraction components' height would then be $H_{dep} = H_{ret} = 0.6$ mm, which includes the wire thickness (0.5 mm) and the minimum thickness of the case wall (0.1 mm).

Additionally, the O-ring of the piston can be custom made to a minimum cross-section W of 0.2 mm. The piston head height H_{piston} can then reach a minimum dimension of 1.2 mm, assuming that the thickness of the piston flanges is 0.5 mm.

Improved volume contributions of all the components of the capsule were calculated considering the ideal capsule parameters: $t_{case} = 0.6$ mm, $t_{core} = 0.5$ mm, $H_{dep} = H_{ret} = 0.6$ mm, $H_{piston} = 1.2$ mm, and $d = 1.5$ mm (from Eq. (3.2) in Section 3.3.2). The calculated improved volume contributions are summarized in Table 4.4. The theoretical minimum total capsule volume of this design is 1.2 mL, equivalent to an 82% of volume reduction, and the drug volume would corresponds to 42% of the total capsule volume, compared to 8% in the prototyped design.

TABLE 4.4: Volume contribution of capsule prototype and ideal minimum volume contribution of the design.

Component	Volume contribution of prototype (mL)	Ideal minimum volume contribution (mL)	Volume reduction potential (%)
Drug	0.5	0.5	-
Retraction	1.4	0.1	93
Case	1.4	0.2	86
Core	1.1	0.2	82
Piston	0.7	0.1	83
Deployment	1.3	0.1	92
Subtotal: Empty capsule	6.2	0.7	89
Total	**6.7**	**1.2**	**82**

4.4.3 Puncturing requirement and intestine wall engagement

The *in situ* performance of the Spanish newt DISC should be assessed. This includes investigating puncturing requirements, studying how the needles engage into the intestine wall, and verifying the ability to inject the drug through the engaged needles.

In terms of puncturing, the needle attachment to the core needs to be designed so that the needles do not slide into or out of the core. Needle resistance to sliding should be at least 3.13 N (2.3 ± 0.83 N) [8], which is the force required to puncture soft tissue with a 1.3 mm outer diameter surgical needle with a bevel tip. The required puncturing force can be lowered by using a narrower needle with a different tip property. Nevertheless, the current silicone rubber hinges cannot bear such a force. To achieve a greater attachment strength, barbed needles, or needles with different head types–such as rings or legs–can be tested. Note that these needles would need to be custom-made since there are no such needles commercially available. Moreover, needles with different diameters and tip properties can be tested to reduce the needle puncturing force, therefore reducing the required needle resistance to sliding.

The DISC should be designed in such a way that all the needles engage in the intestine wall, otherwise only a partial dose of bio-therapeutic is delivered. The Spanish newt prototype should be tested *in vitro* in intestine models, and ultimately *in vivo*, to ensure the developed design is capable of engaging all needles into the wall of the intestine at deployment. The number and position of the needles, as well as the triggering strategy, are the main design variables to achieve a satisfactory needle engagement. The deployment should be triggered when the intestine is contracted, and in full contact with the capsule body, to maximize the chance of full needle engagement.

Chapter 5

Conclusion and future work

Drug Injecting Swallowable Capsules (DISCs) would enable a painless and convenient oral delivery of bio-therapeutics such as insulin. This thesis focused on the development of a needle deployment and retraction mechanism to implement into such capsules.

Chapter 1 provided the background of this work. First, the gastrointestinal tract (the working environment of DISCs) and its properties (pH profile, chyme transit times, dimensions, and modes of motility) were described. Then, a literature review of medical capsules was performed, covering the current state-of-the-art of medical capsules with different capabilities. The need to develop DISCs, and needle deployment and retraction mechanisms in particular, was identified and further studied.

Chapter 2 defined the design space of the needle mechanisms and proposed eleven novel mechanism designs. The design space was developed by considering the GI tract properties and precedent information of medical capsules. The three main mechanism requirements were to deploy needles radially to the capsule by 1 to 2 mm of length, to inject 0.5 mL of drug in less than 5 seconds, and to fully retract the needles after injection. The eleven novel mechanisms proposed were inspired by macroscale structures and biological systems, and derived from cross-component analysis. One design in particular, inspired by the defense mechanism of the Spanish newt, was selected for its simplicity, isolated injection motion, and distribution of needles around the capsule.

Chapter 3 further developed the Spanish newt inspired design. The development of this capsule was divided into four stages: analysis, embodiment, manufacturing, and spring selection.

The analysis allowed to determine needle and core dimensions, and investigated syringeability forces. The embodiment broke down the interactions of components into sub-modules, and determined the needle attachment type and piston dimensions. The manufacturing and assembly process of the capsule were then detailed. The main manufacturing challenges consisted of drilling V-shaped holes into cylindrical surfaces, manufacturing silicone rubber hinges and assembling the needles into them, handling small components (needles, piston, springs), and achieving high precision of small features with large manufacturing tools that experience vibrations and cutting tool deflections. Finally, the selection process of the springs involved performing mechanical tests to characterize the force required by the piston to complete deployment and injection. The selected springs were off-the-shelf models that met the geometry requirements, and provided the smallest sufficient force to complete their operation. The final manufactured prototype was equipped with four needles around the perimeter of the capsule, and measured 31.5 mm in length and 15.9 mm in diameter.

In Chapter 4, the manufactured prototype, assembled with the chosen springs, was tested *in vitro*. The prototype proved successful and demonstrated its ability to deploy the needles, inject 0.5 mL of drug in 1.33 s, and fully retract the needles. The deployed needles protruded by 1.9 ± 0.5 mm at an angle of 15° with respect to the capsule wall normal.

The development of this novel, bio-inspired needle deployment and retraction mechanism fosters the further development of DISCs. Future work can be segmented into two main areas: further improvement and testing of the prototyped mechanism (partially discussed in Section 4.4), and development of an activation mechanism for DISCs, as described below:

To Further improve and test the prototyped mechanism:

1. *Investigate needle engagement into the intestine wall* to ensure the drug is indeed injected inside the wall of the intestine, fulfilling the purpose of the capsule. To achieve this, *in vitro* tests in intestine models, and ultimately *in vivo* tests, should be performed to determine capsule parameters, such as: the number of needles and their distribution on the capsule, the shape of the capsule body, and the timing of deployment activation (to coordinate it with intestinal contractions).

2. *Include skin puncturing requirements* to ensure the needles are capable of piercing through the intestine wall. This involves ensuring the needle attachment resists the

loads introduced by puncturing the skin, preventing the needles from sliding in or out of the core. Design parameters include needle features at the connection point with the core, and alternatives to the silicone rubber hinge.

3. *Develop a single-actuation mechanism* to reduce the number of triggers to be developed, and simplify the design. The current design requires to be activated twice. One trigger controls deployment and injection, another controls retraction. Two methods can be investigated to achieve a single-actuation mechanism: (1) develop the Spanish-newt-flower hybrid design (Section 2.3) and (2) modify the Spanish newt mechanism to have a core with a two-step inner diameter and a back spring (see Figure 5.1). The modified core, which is pushed to the deployed position by the piston, features a larger diameter at its closed end. When the piston reaches the larger section, it no longer makes contact with the wall of the core, and the core is no longer held in the deployed position. The back spring then pushes the core back to its initial position, thereby retracting the needles. In contrast to the retraction spring in the prototyped design, the back spring is not preloaded before deployment. The development of this design requires careful design of the springs.

4. *Miniaturize the design* to obtain a capsule with a total volume of 1.2 mL. The prototyped capsule volume is 6.3 mL. Manufacturing improvements can be implemented (as discussed in Section 4.4.2), including using specialized manufacturing equipment and designing conical springs.

To Develop an activation mechanism for DISCs to complement the development of needle mechanisms and develop a fully functional DISC:

1. *An externally triggered activation system* can be integrated into the capsule. The thermo-mechanical activation system is widely used in prototyped capsules (discussed in Section 1.2), as well as in commercial capsules, such as the Enterion Capsule®. This system consists of melting a nylon wire, which holds a preloaded compression spring. Melting is achieved by generating an electrical current using external radio-frequencies or magnetic fields. The thermo-mechanical system can be implemented into the needle mechanism by replacing the pin, used to hold the preloaded spring, by a nylon wire.

2. *An autonomous activation system* would allow DISCs to self-trigger needle deployment,

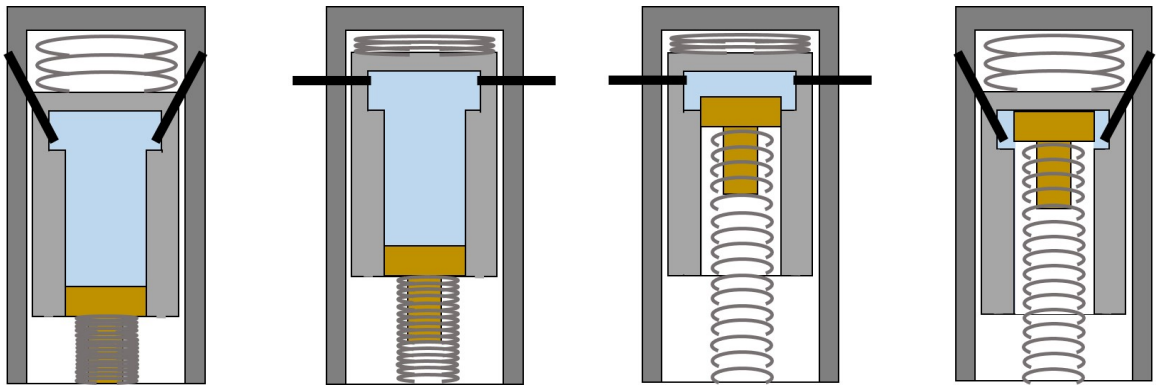

(A) Undeployed. (B) Deployed before injection. (C) Deployed after injection. (D) Retracted.

FIGURE 5.1: Schematic of the kinematics of the modified Spanish newt design with a single-actuation mechanism. The cross-section views show the capsule at four different stages. This design consists of having a two-step inner diameter core, and a back spring. When the piston is pushed by the deployment spring, it travels with the core in the case ((A) to (B)). When the core reaches the end of its displacement, the needles are deployed (B). The piston then continues traveling inside the core. When the piston reaches the wider diameter of the core (end of injection), it disengages from the core (C). The force of the back spring is then capable of pushing the core back to its initial position (D).

injection, and retraction. Autonomous activation mechanisms should trigger deployment and injection at the duodenum, and at the appropriate moment, ensuring drug delivery. Retraction should be triggered after injection, before the capsule evacuates the body. Autonomous activation could exploit the pH profile, temperature profile, and characteristic contractions of the intestine, using them as triggers. Synthetic absorbable sutures (instead of nylon wires) can be used to hold preloaded springs. The mechanism would be triggered when the suture dissolves once exposed to the alkaline environment of the duodenum. Synthetic absorbable sutures have been shown to (1) withstand loads of at least 5.4 N [76] (enough to hold the deployment spring of the prototype, which exerts a maximum force of 4.4 N when fully compressed), and (2) undergo hydrolytic degradation at different pH-dependent rates (3) during extended periods of time (4 or more weeks) [77]. Implementing these sutures into DISCs requires

the investigation of their chemical composition (i.e. glycolide or lactide based), architecture (i.e. braided or monofilament), size (USP designation: 9-0 to 4 [78]), and knot configurations. These investigations should focus on achieving a fast or instantaneous dissolution of sutures at desired pHs, which differ from current studies ([76], [77], [79], among others) that focus on achieving strong and durable sutures.

Appendix A

Concept selection via quantitative analysis

The following quantitative analysis has the purpose of identifying the design that best meets the design requirements determined in Section 2.2. This analysis uses the functional and non-functional requirements as evaluation criteria, that are then used to validate and obtain the total weighted score of each design. The best performing design is the one with the highest score.

Table A.1 classifies each requirement as an embodiment dependent or design intrinsic parameter, and gives each criterion an evaluating weight. The evaluating weight can be (yes/no) or a number (the numbers all criteria add up to 10).

Table A.2 illustrates the quantitative analysis. Two design are denominated best performing: the Spanish newt with longitudinal actuation and the flower inspired design.

TABLE A.1: Evaluation criteria

Requirement	Performance dependent on	Conformity check or Evaluation Weight
Functional Requirements		
Deploy needles (at least one) by 1 to 2 mm perpendicular to the capsule	embodiment	yes/no
Inject V_{drug} = 0.5 mL of drug in less than t_{inj} = 5 s	embodiment	yes/no
Fully retract the needles after injection	embodiment	yes/no
Non-Functional Requirements		
Needles must be distributed along the perimeter of the capsule	design	w= 3
Capsule must measure at most 35 mm in length and 20 mm in diameter	embodiment	-
Energy source should be sufficient, small, and originated from preloaded springs	embodiment	-
Drug reservoir must be watertight	embodiment	-
Needle mechanism should be as simple as possible	design	w=3
Capsule should not use motors or batteries	design	yes/no
Capsule should be easy to manufacture	design	w= 4

TABLE A.2: Concept evaluation

Requirement weight	Evaluation Criteria	Deployment and retraction mechanism body										
		Spiked	Portable hair brush	Multineedle syringe	Diamond-column-buckling	Porcupine-fish	Spanish newt long. act	Spanish newt rot. act	Flower inspired design	Spiked-porcupine-fish	Porcupine-fish-multineedle	Spanish-newt-flower
y/n	Deploy needles	y	y	y	y	DATUM	y	y	y	y	y	y
y/n	Inject drug	y	y	y	y		y	y	y	y	y	y
y/n	Retract needles	n	y	y	y		y	y	y	y	y	y
3	Needle distribution	0	-1	-2	0		0	0	0	0	0	0
3	Simple mechanism	2	1	1	0		1	1	1	0	0	1
y/n	No motor/batteries	y	y	y	y		y	y	y	y	y	y
4	Easy to manufacture	2	-1	1	-2		1	0	1	0	0	0
Total wighted score		X	-4	1	-8	0	7	3	7	0	0	3

Legend - X: Non-satisfactory design. Scores: -2,-1,0,+1,+2 relative to benchmark

Appendix B

Vertical piston force tests and results

B.1 Testing machine specifications

The vertical test apparatus is shown in Figure B.1; the vertical testing machine, like the horizontal one, works in conjunction with a PC-based controller and a computer. The vertical testing machine and the controller, are both manufactured by ADMET®. The vertical testing machine has a static and a moving base. The moving base is instrumented with a 25 lb load cell (ADMET® 500 Series Low Force), and it moves up and down, along the vertical axis of the machine, with a maximum moving speed of 8.4 mm/s. The controller and software are the same as the one used with the horizontal testing machine. Figure B.1 shows the experimental set-up of the tests with the vertical machine.

B.2 Experiments and results

The sampling rate of the experiments was set to 20 samples/second, and the testing speeds were 0.2 mm/s and 2 mm/s. Table B.1 summarizes the performed tests. Note that the number of test speeds per setup is not uniform since reassembly of the capsule was necessary before the scheduled number of test was finished. This was due to needle detachment from the capsule, after multiple deployment and retraction cycles, when the capsule is designed for a single deployment and retraction cycle only.

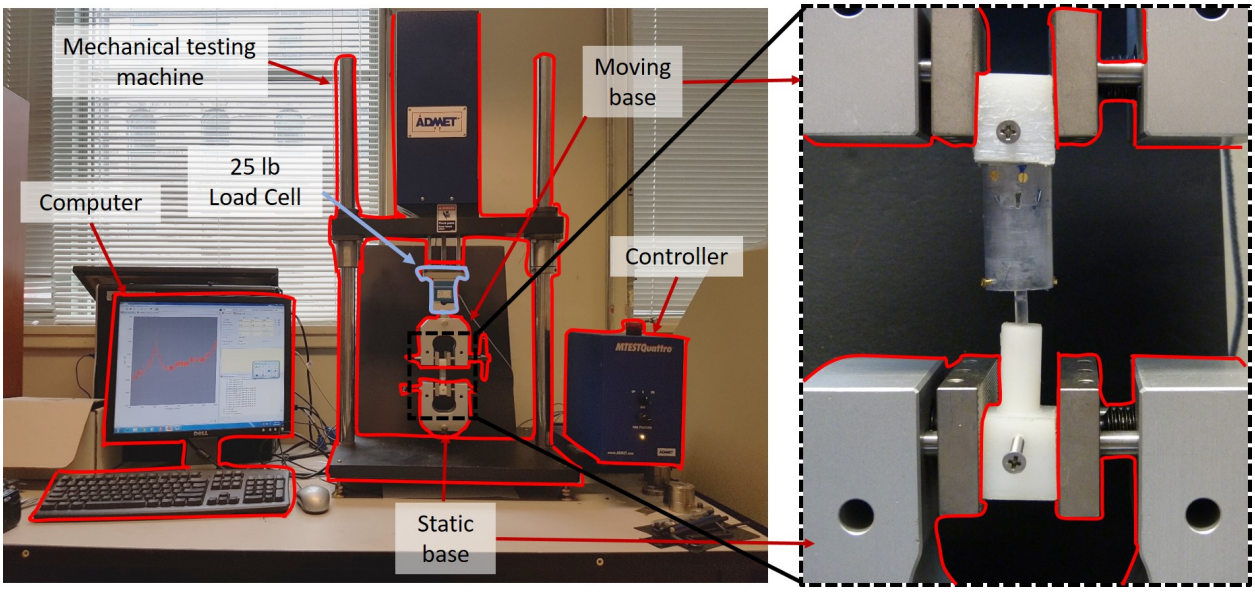

FIGURE B.1: Image of the vertical force measuring equipment. The image highlights the apparatus components (left), and zooms into the testing bed of the machine (right) to show the prototyped capsule body installed, with the testing widget, onto the moving and static base platforms of the machine. The testing widget, composed of the piston holder and the capsule holder, is tightened to the clamps of the testing machine. The capsule prototype is directly mounted onto the testing widget. The alignment of the capsule with the piston is calibrated before the test.

TABLE B.1: Piston force test matrix of the vertical tests.

Test number	Setup number	Speed (mm/s)
11	4	2
12	4	2
13	4	0.2
14	4	0.2
15	5	2
16	5	0.2
17	5	0.2

Figure B.2 shows the curves of the tests from Table B.1, colored by speed. One sample curve at speed 0.05 mm/s, and one at 0.1 mm/s, are plotted in this figure for trend and

magnitude reference to horizontal force test results. This information is complementary to the discussion of Section 3.5.

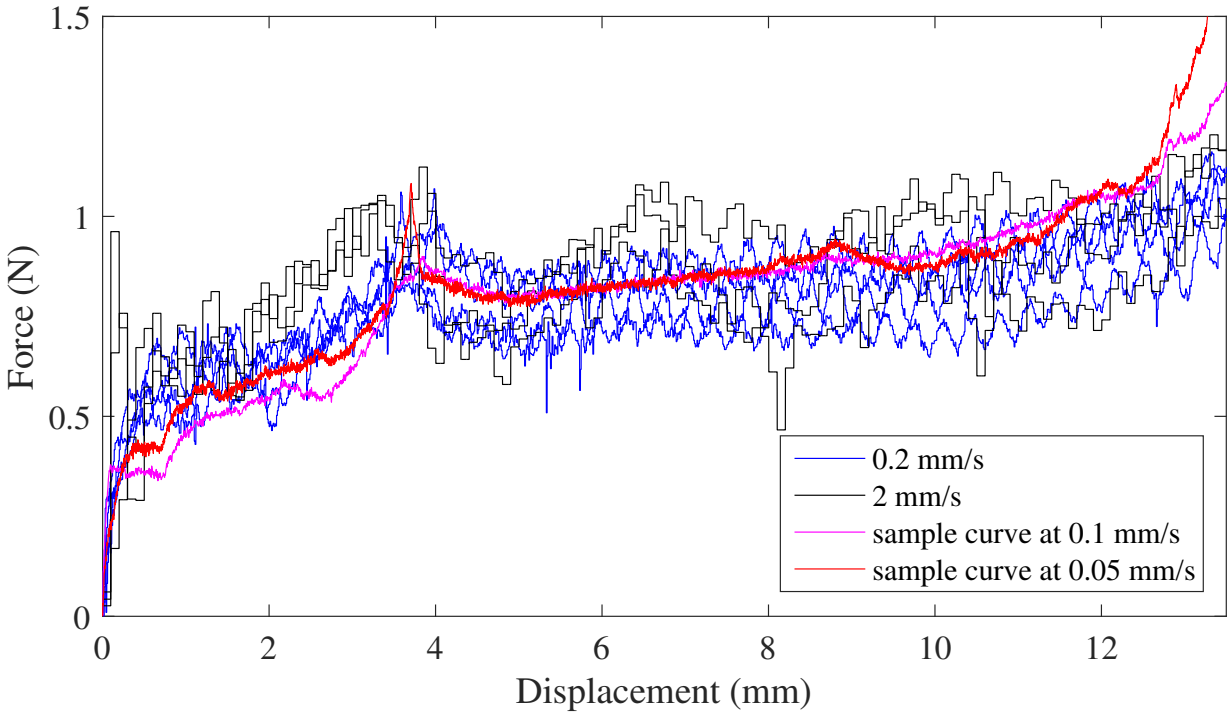

FIGURE B.2: Plot of experimental piston force versus displacement from tests listed in Table B.1 (speeds of 0.2 and 2 mm/s), colored by testing speed. Moreover, two sample force curves, from experiments performed in the horizontal testing machine at 0.05 mm/s and 0.1 mm/s, are also shown for reference.

Bibliography

[1] B. Jacobson and R. S. Mackay, "A pH-Endoradiosonde", *Lancet*, vol. 269, no. 6981, p. 1224, 1957. DOI: 10.1016/s0140-6736(57)91792-0.

[2] G. Iddan, G. Meron, A. Glukhovsky, and P. Swain, "Wireless capsule endoscopy", *Nature*, vol. 405, p. 417, 2000. DOI: http://dx.doi.org/10.1038/35013140.

[3] G. Traverso, C. M. Schoellhammer, A. Schroeder, R. Maa, G. Y. Lauwers, B. E. Polat, D. G. Anderson, D. Blankschtein, and R. Langer, "Microneedles for drug delivery via the gastrointestinal tract", *Journal of Pharmaceutical Sciences*, vol. 104, no. 2, pp. 362–367, 2015. DOI: 10.1002/jps.24182.

[4] N. Shalabi, "Ingestible sample collection device", Project Report, McGill University, 2011.

[5] J. G. Betts, P. Desaix, E. Johnson, J. E. Johnson, O. Korol, D. Kruse, B. Poe, J. A. Wise, M. Womble, and K. A. Young, *Anatomy and Physiology*. OpenStax, 2013, ch. 23.5 The Small and Large Intestines, pp. 1113–1122. [Online]. Available: https://cnx.org/contents/FPtK1zmh@8.107:Qw2OWvaZ@5/The-Small-and-Large-Intestines (visited on 03/03/2017).

[6] ThingLink.com. (2015). Digestive system, [Online]. Available: https://www.thinglink.com/scene/502867380259520512 (visited on 11/07/2017).

[7] P. Slawinski, D. Oleynikov, and B. S. Terry, "Intestinal biomechanics simulator for robotic capsule endoscope validation", *Journal of Medical Engineering and Technology*, vol. 39, pp. 54–59, 2014. DOI: 10.3109/03091902.2014.973619.

[8] A. M. Okamura, C. Simone, and M. D. O'leary, "Force modeling for needle insertion into soft tissue", *IEEE Transactions on Biomedical Engineering*, vol. 51, no. 10, pp. 1707–1716, 2004. DOI: 10.1109/tbme.2004.831542.

[9] S. P. Woods and T. G. Constandinou, "Wireless capsule endoscope for targeted drug delivery: Mechanics and design considerations", *IEEE Transactions on Biomedical Engineering*, vol. 60, no. 4, pp. 945–953, Apr. 2013. DOI: 10.1109/TBME.2012.2228647.

[10] S. P. Woods and T. G. Constandinou, "A compact targeted drug delivery mechanism for a next generation wireless capsule endoscope", *Journal of Micro-Bio Robotics*, vol. 11, no. 1-4, pp. 19–34, 2016. DOI: 10.1007/s12213-016-0088-9.

[11] R. Goffredo, D. Accoto, M. Santonico, G. Pennazza, and E. Guglielmelli, "A smart pill for drug delivery with sensing capabilities", in *37th Annual International Conference of the IEEE Engineering in Medicine and Biology Society*, 2015. DOI: 10.1109/embc.2015.7318621.

[12] C. McCaffrey, O. Chevalerias, C. O'Mathuna, and K. Twomey, "Swallowable-capsule technology", *IEEE Pervasive Computing*, vol. 7, pp. 23–29, 2008. DOI: 10.1109/mprv.2008.17.

[13] Y. Kimchy, R. Amrami, Y. Bouskila, U. Antebi, N. Sidorenko, G. Ben-David, and Y. Zilberstein, "Ingestible pill for diagnosing a gastrointestinal tract", 2011, US Patent 8,036,731 B2. [Online]. Available: https://www.google.com/patents/US8036731.

[14] NASA.gov. (2007). Ingestible thermometer pill helps athletes beat the heat, [Online]. Available: https://www.nasa.gov/vision/earth/technologies/thermometer_pill.html (visited on 02/03/2017).

[15] Actigraphy.com. (2014). Vitalsense, [Online]. Available: http://www.actigraphy.com/solutions/telemetry.html (visited on 02/03/2017).

[16] CDD.com. (2009). Small bowel capsule endoscopy, [Online]. Available: http://www.cdd.com.au/pages/procedures/capsule_endoscopy.html (visited on 02/03/2017).

[17] P. R. Slawinski, K. L. Obstein, and P. Valdastri, "Emerging issues and future developments in capsule endoscopy", *Techniques in Gastrointestinal Endoscopy*, vol. 17, no. 1, pp. 40–46, 2015. DOI: 10.1016/j.tgie.2015.02.006.

[18] GivenImaging.com. (2017). PillCam capsule endoscopy, [Online]. Available: http://www.givenimaging.com/en-int/Innovative-Solutions/Capsule-Endoscopy/Pages/default.aspx (visited on 07/20/2017).

[19] Jinshangroup.com. (2017). Omom capsule endoscopy, [Online]. Available: http://english.jinshangroup.com/capsuleendoscopy.html (visited on 07/20/2017).

[20] Medical.olympusamerica.com. (2017). Endocapsule 10, [Online]. Available: http://medical.olympusamerica.com/products/endocapsule (visited on 07/20/2017).

[21] Intromedic.com. (2017). Mirocam capsule endoscope, [Online]. Available: http://www.intromedic.com/eng/item/item_010100_view.asp?search_kind=&gotopage=1&no=3 (visited on 07/20/2017).

[22] Capsovision.com. (2017). Capsocam plus, [Online]. Available: http://www.capsovision.com/products/capsocam-plus (visited on 07/20/2017).

[23] G. Ciuti, R. Calio, D. Camboni, L. Neri, F. Bianchi, A. Arezzo, A. Koulaouzidis, S. Schostek, D. Stoyanov, C. M. Oddo, B. Magnani, A. Menciassi, M. Morino, M. O. Schurr, and P. Dario, "Frontiers of robotic endoscopic capsules: A review", *Journal of Micro-Bio Robotics*, vol. 11, no. 1, pp. 1–18, 2016. DOI: 10.1007/s12213-016-0087-x.

[24] H. Gu and H. L. Gu, "Intestinal fluid sampler", 1999, US Patent 5971942 A. [Online]. Available: https://www.google.com/patents/US5971942.

[25] V. W. D. Meindert, A. J. S. Jenneboer, A. J. Sprenkels, D. B. A. Van, and K. Venema, "Sampling device for *in vivo* sampling of liquids from the gastrointestinal tract, process for the production thereof and mould or mask for use in the production process", 2007, US Patent 20070161928 A1. [Online]. Available: https://www.google.com/patents/WO2007061305A3?cl=en.

[26] Y. Amoako-Tuffour, M. L. Jones, N. Shalabi, A. Labbe, S. Vengallatore, and S. Prakash, "Ingestible gastrointestinal sampling devices: State-of-the-art and future directions", *Critical Reviews in Biomedical Engineering*, vol. 42, no. 1, pp. 1–15, 2014.

[27] W. H. Crosby and H. Kugler, "Intraluminal biopsy of the small intestine", *The American Journal of Digestive Diseases*, vol. 2, no. 5, pp. 236–241, 1957. DOI: 10.1007/bf02231100.

[28] K. c. Kong, J. Cha, D. Jeon, and D. i. D. Cho, "A rotational micro biopsy device for the capsule endoscope", in *IEEE/RSJ International Conference on Intelligent Robots and Systems*, 2005, pp. 1839–1843. DOI: 10.1109/iros.2005.1545441.

[29] M. Simi, G. Gerboni, A. Menciassi, and P. Valdastri, "Magnetic torsion spring mechanism for a wireless biopsy capsule", *Journal of Medical Devices*, vol. 7, no. 4, art. no. 041 009 (9 pages), 2013. DOI: 10.1115/1.4025185.

[30] G. Ciuti, A. Menciassi, and P. Dario, "Capsule endoscopy: From current achievements to open challenges", *IEEE Reviews in Biomedical Engineering*, vol. 4, pp. 59–72, 2011. DOI: 10.1109/rbme.2011.2171182.

[31] A. Koulaouzidis, D. Iakovidis, A. Karargyris, and E. Rondonotti, "Wireless endoscopy in 2020: Will it still be a capsule?", *World Journal of Gastroenterology*, vol. 21, no. 17, pp. 5119–5130, 2015. DOI: 10.3748/wjg.v21.i17.5119.

[32] Z. Fireman and Y. Kopelman, "New frontiers in capsule endoscopy", *Journal of Gastroenterology and Hepatology*, vol. 22, no. 8, pp. 1174–1177, 2007. DOI: doi:10.1111/j.1440-1746.2007.04993.x.

[33] M. Quirini, A. Menciassi, S. Scapellato, C. Stefanini, and P. Dario, "Design and fabrication of a motor legged capsule for the active exploration of the gastrointestinal tract", *IEEE/ASME Transactions on Mechatronics*, vol. 13, no. 2, pp. 169–179, 2008. DOI: 10.1109/tmech.2008.918491.

[34] P. Valdastri, R. J. Webster, C. Quaglia, M. Quirini, A. Menciassi, and P. Dario, "A new mechanism for mesoscale legged locomotion in compliant tubular environments", *IEEE Transactions on Robotics*, vol. 25, no. 5, pp. 1047–1057, 2009. DOI: 10.1109/tro.2009.2014127.

[35] W. Chen, G. Yan, Z. Wang, P. Jiang, and H. Liu, "A wireless capsule robot with spiral legs for human intestine", *The International Journal of Medical Robotics and Computer Assisted Surgery*, vol. 10, no. 2, pp. 147–161, 2014. DOI: 10.1002/rcs.1520.

[36] G. Tortora, P. Valdastri, E. Susilo, A. Menciassi, P. Dario, F. Rieber, and M. O. Schurr, "Propeller-based wireless device for active capsular endoscopy in the gastric district", *Minimally Invasive Therapy and Allied Technologies*, vol. 18, no. 5, pp. 280–290, 2009. DOI: 10.1080/13645700903201167.

[37] E. Morita, N. Ohtsuka, Y. Shindo, S. Nouda, T. Kuramoto, T. Inoue, M. Murano, E. Umegaki, and K. Higuchi, "*In vivo* trial of a driving system for a self-propelling capsule endoscope using a magnetic field (with video)", *Gastrointestinal endoscopy*, vol. 72, no. 4, pp. 836–840, 2010. DOI: 10.1016/j.gie.2010.06.016.

[38] S. H. Woo, T. W. Kim, and J.-H. Cho, "Stopping mechanism for capsule endoscope using electrical stimulus", *Medical and Biological Engineering and Computing*, vol. 48, no. 1, p. 97, 2010. DOI: 10.1007/s11517-009-0553-x.

[39] A. Menciassi, C. Stefanini, S. Gorini, G. Pernorio, B. Kim, J. Park, and P. Dario, "Locomotion of a legged capsule in the gastrointestinal tract: Theoretical study and preliminary technological results", in *26th Annual International Conference of the IEEE Engineering in Medicine and Biology Society*, vol. 1, 2004, pp. 2767–2770. DOI: 10.1109/iembs.2004.1403791.

[40] P. R Slawinski, K. L. Obstein, and P. Valdastri, "Capsule endoscopy of the future: What's on the horizon?", *World Journal of Gastroenterology*, vol. 21, no. 37, pp. 10 528–10 541, 2015. DOI: DOI:10.3748/wjg.v21.i37.10528.

[41] M. E. Karagozler, E. Cheung, and J. Kwon, "Miniature endoscopic capsule robot using biomimetic micro-patterned adhesives", in *The First IEEE/RAS-EMBS International Conference on Biomedical Robotics and Biomechatronics*, 2006, pp. 105–111. DOI: 10.1109/biorob.2006.1639068.

[42] P. Glass, E. Cheung, and M. Sitti, "A legged anchoring mechanism for capsule endoscopes using micropatterned adhesives", *IEEE Transactions on Biomedical Engineering*, vol. 55, no. 12, pp. 2759–2767, 2008. DOI: 10.1109/tbme.2008.2002111.

[43] D. Dodou, P. Breedveld, and P. A. Wieringa, "Stick, unstick, restick sticky films in the colon", *Minimally Invasive Therapy and Allied Technologies*, vol. 15, no. 5, pp. 286–295, 2006. DOI: 10.1080/13645700600929144.

[44] S. Tognarelli, C. Quaglia, P. Valdastri, E. Susilo, A. Menciassi, and P. Dario, "Innovative stopping mechanism for esophageal wireless capsular endoscopy", *Procedia Chemistry*, vol. 1, no. 1, pp. 485–488, 2009. DOI: 10.1016/j.proche.2009.07.121.

[45] W. Lin and G. Yan, "A study on anchoring ability of three-leg micro intestinal robot", *Engineering*, vol. 4, no. 8, art. no. 22168 (7 pages), 2012. DOI: 10.4236/eng.2012.48062.

[46] W. Chen, G. Yan, S. He, Q. Ke, Z. Wang, H. Liu, and P. Jiang, "Wireless powered capsule endoscopy for colon diagnosis and treatment", *Physiological Measurement*, vol. 34, no. 11, p. 1545, 2013. DOI: 10.1088/0967-3334/34/11/1545.

[47] B. Kim, S. Lee, J. H. Park, and J.-O. Park, "Design and fabrication of a locomotive mechanism for capsule-type endoscopes using shape memory alloys (SMAs)", *IEEE/ASME Transactions On Mechatronics*, vol. 10, no. 1, pp. 77–86, 2005. DOI: 10.1109/tmech.2004.842222.

[48] H. M. Kim, S. Yang, J. Kim, S. Park, J. H. Cho, J. Y. Park, T. S. Kim, E.-S. Yoon, S. Y. Song, and S. Bang, "Active locomotion of a paddling-based capsule endoscope in

an *in vitro* and *in vivo* experiment (with videos)", *Gastrointestinal Endoscopy*, vol. 72, no. 2, pp. 381–387, 2010. DOI: 10.1016/j.gie.2009.12.058.

[49] G. Kósa, P. Jakab, and F. Jolesz, "Swimming capsule endoscope using static and RF magnetic field of MRI for propulsion", in *IEEE International Conference on Robotics and Automation*, 2008, pp. 2922–2927. DOI: 10.1109/robot.2008.4543653.

[50] G. Kósa, P. Jakab, G. Szekely, and N. Hata, "MRI driven magnetic microswimmers", *Biomedical Microdevices*, vol. 14, no. 1, pp. 165–178, 2012. DOI: 10.1007/s10544-011-9594-7.

[51] S. H. Woo, T. W. Kim, Z. Mohy-Ud-Din, Y. Park, and J.-H. Cho, "Small intestinal model for electrically propelled capsule endoscopy", *Biomedical Engineering Online*, vol. 10, no. 1, p. 108, 2011. DOI: 10.1186/1475-925x-10-108.

[52] K. Twomey and J. R. Marchesi, "Swallowable capsule technology: Current perspectives and future directions", *Endoscopy*, vol. 41, pp. 357–362, 2009. DOI: 10.1055/s-0028-1119640.

[53] H. M. Kim, J. S. Choi, and J. H. Cho, "A pilot trial of ambulatory monitoring of gastric motility using a modified magnetic capsule endoscope", *Journal of Neurogastroenterology and Motility*, vol. 20, no. 2, pp. 261–264, 2014. DOI: 10.5056/jnm.20.2.261.

[54] A. Lambert, F. Vaxman, F. Crenner, T. Wittmann, and J. F. Grenier, "Autonomous telemetric capsule to explore the small bowel", *Medical and Biological Engineering and Computing*, vol. 29, no. 2, pp. 191–196, 1991. DOI: 10.1007/bf02447107.

[55] I. Wilding, P. Hirst, and A. Connor, "Development of a new engineering-based capsule for human drug absorption studies", *Pharmaceutical Science and Technology Today*, vol. 3, no. 11, pp. 385–392, 2000. DOI: 10.1016/s1461-5347(00)00311-4.

[56] M. E. A. McGirr, S. M. McAllister, E. E. Peters, A. W. Vickers, A. F. Parr, and A. W. Basit, "The use of the InteliSite® Companion device to deliver mucoadhesive polymers to the dog colon", *European Journal of Pharmaceutical Sciences*, vol. 36, no. 4, pp. 386–391, 2009. DOI: 10.1016/j.ejps.2008.11.007.

[57] V. H. Le, H. L. Rodriguez, C. Lee, G. Go, J. Zhen, V. D. Nguyen, H. Choi, S. Y. Ko, J.-O. Park, and S. Park, "A soft-magnet-based drug-delivery module for active locomotiveintestinal capsule endoscopy using an electromagnetic actuation system", *Sensors and Actuators A: Physical*, vol. 243, pp. 81–89, 2016. DOI: 10.1016/j.sna.2016.03.020.

[58] R. Goffredo, A. Pecora, L. Maioli, A. Ferrone, E. Guglielmelli, and D. Accoto, "A swallowable smart pill for local drug delivery", *Journal of Microelectromechanical Systems*, vol. 25, no. 2, pp. 362–370, 2016. DOI: 10.1109/jmems.2016.2524542.

[59] Drug-dev.com. (2013). Advanced delivery devices - IntelliCap: An intelligent, electronic capsule for oral drug delivery and development, [Online]. Available: http://drug-dev.com/main/back-issues/advanced-delivery-devices-intellicap-an-intelligen-557.aspx (visited on 02/07/2017).

[60] S. P. Woods and T. G. Constandinou, "Engineering micromechanical systems for the next generation wireless capsule endoscopy", *Biomed Research International*, vol. 2015, 2015, art. no. 741867 (7 pages), 2015. DOI: 10.1155/2015/741867.

[61] M. Beccani, G. Aiello, N. Gkotsis, H. Tunc, A. Taddese, E. Susilo, P. Völgyesi, A. Lédeczi, E. De Momi, and P. Valdastri, "Component based design of a drug delivery capsule robot", *Sensors and Actuators A: Physical*, vol. 245, pp. 180–188, 2016. DOI: 10.1016/j.sna.2016.04.035.

[62] A. M. Bellinger, M. Jafari, T. M. Grant, S. Zhang, H. C. Slater, E. A. Wenger, S. Mo, Y.-A. L. Lee, H. Mazdiyasni, L. Kogan, R. Barman, C. Cleveland, L. Booth, T. Bensel, D. Minahan, H. M. Hurowitz, T. Tai, J. Daily, B. Nikolic, L. Wood, P. A. Eckhoff, R. Langer, and G. Traverso, "Oral, ultra-long-lasting drug delivery: Application toward malaria elimination goals", *Science Translational Medicine*, vol. 8, no. 365, pp. 1–12, 2016. DOI: 10.1126/scitranslmed.aag2374.

[63] M. Imran, "A novel approach to the oral delivery of biologics, peptides and antibodies", *ONdrugDelivery*, no. 69, pp. 18–19, 2016, Expert Review. [Online]. Available: https://issuu.com/guyfurness/docs/novel_oral_drug_delivery_systems_-_.

[64] Grand View Research, "Disposable syringes market analysis by type (conventional syringes, safety syringes), by application (immunization injections, therapeutic injections) by region (north america, europe, asia pacific, latin america, mea), and segment forecasts, 2013 - 2024", Grand View Research, Tech. Rep., 2016. [Online]. Available: http://www.grandviewresearch.com/industry-analysis/disposable-syringes-market.

[65] American Diabetes Association®. (2017). Statistics about diabetes, [Online]. Available: http://www.diabetes.org/diabetes-basics/statistics/?referrer=https://www.google.ca/ (visited on 01/31/2017).

[66] WHO.int. (2017). Diabetes, [Online]. Available: http://www.who.int/diabetes/en/ (visited on 07/23/2017).

[67] M. Imran, "Swallowable drug delivery device and methods of drug delivery", 2016, US Patent 9456988 B2. [Online]. Available: https://encrypted.google.com/patents/US9456988.

[68] J. A. Mayfield and R. D. White, "Insulin therapy for type 2 diabetes: Rescue, augmentation, and replacement of beta-cell function", *American Academy of Family Physicians*, vol. 70, no. 3, pp. 489–511, 2004. [Online]. Available: http://www.aafp.org/afp/2004/0801/p489.html.

[69] P. Lee, "Brush with attached mirror and sewing kit", 2006, US Patent 20060249169 A1. [Online]. Available: https://www.google.com/patents/US20060249169.

[70] Najecki Reproductions. (2017). Wire needle threader, [Online]. Available: http://www.najecki.com/repro/notions/NeedleThreader.html (visited on 08/05/2017).

[71] Q-files.com. (2017). Extraordinary fish, [Online]. Available: https://www.q-files.com/life/fish/extraordinary-fish/ (visited on 04/30/2017).

[72] E. Heiss, N. Natchev, D. Salaberger, M. Gumpenberger, A. Rabanser, and J. Weisgram, "Hurt yourself to hurt your enemy: New insights on the function of the bizarre antipredator mechanism in the salamandrid *Pleurodeles waltl*", *Journal of Zoology*, vol. 280, no. 2, pp. 156–162, 2010. DOI: 10.1111/j.1469-7998.2009.00631.x.

[73] FiftyFlowers. (2017). Lilies, [Online]. Available: https://www.fiftyflowers.com/flowers/lilies_47.htm (visited on 07/31/2017).

[74] C. G. Caro, T. J. Pedley, and R. C. S. ad W. A. Seed, "The mechanics of the circulation", in, 2nd ed. Cambridge University Press, 2012, ch. 5. Flow in pipes and around objects, pp. 45–79.

[75] E. Oberg, F. D. Jones, H. L. Horton, and H. H. Ryffel, "Machinery's handbook", in, C. J. McCauley, Ed., 29th. Industrial Press, 2012, ch. Machine elements: O-rings, pp. 2587–2592.

[76] D. Abellán, J. Nart, A. Pascual, R. E. Cohen, and J. D. Sanz-Moliner, "Physical and mechanical evaluation of five suture materials on three knot configurations: An *in vitro* study", *Polymers*, vol. 8, no. 4, pp. 147–155, 2016. DOI: 10.3390/polym8040147.

[77] K. Tomihata, M. Suzuki, and Y. Ikada, "The pH dependence of monofilament sutures on hydrolytic degradation", *Journal of Biomedical Materials Research Part A*, vol. 58, no. 5, pp. 511–518, 2001. DOI: 10.1002/jbm.1048.

[78] Pharmacopeia.cn. (2007). USP monographs: Absorbable surgical suture, [Online]. Available: http://www.pharmacopeia.cn/v29240/usp29nf24s0_m80190.html (visited on 08/15/2017).

[79] C. Chu, "A comparison of the effect of pH on the biodegradation of two synthetic absorbable sutures.", *Annals of surgery*, vol. 195, no. 1, pp. 55–59, 1982. DOI: 10.1097/00000658-198201001-00009.